Shear Analysis of Non-Prismatic Concrete Beams

Shubham Toshniwal

Shear Analysis of Non-Prismatic Concrete Beams

by

Shubham Toshniwal

In partial fulfilment to obtain the degree of
Masters of Science from Delft University of Technology,
defended publicly on 16th September 2019 at 9:00 am

An electronic version of this thesis is available at https://repository.tudelft.nl

Acknowledgement

Shubham Toshniwal
Delft, August 2019

Abstract

The governing load in long concrete bridges is the dead weight, as the span is long. In order to minimize the weight, non-prismatic beams, where the height of the beam varies along the length, are used, which ensures the reduction in weight and provides sufficient strength. Due to the alteration in height, the centroidal axis of a non-prismatic beam has a non-linear layout when compared to a prismatic beam. Therefore, in case of a non-prismatic beam, the vertical cross-section cut, on which cross-sectional analysis from the codes are performed, is no longer perpendicular to the centroidal axis, as is the case in a prismatic beam. Moreover, due to the geometry, these concrete beams are quite prone to shear failure even after providing sufficient amount of stirrups. This failure is mainly due to the vertical component of the inclined cross-section forces. The main focus of this study is to compare the cross-section results obtained on an inclined and vertical cross-section cut and also to validate the inclusion of the vertical component of the inclined cross-section forces in the shear capacity equation.

Performing inclined cross-sectional analysis in a prismatic beam is comparable to executing vertical cross-section analysis in non-prismatic beam. Different approaches and methods are proposed to calculate the cross-section results on an inclined cross-section cut, with the internal forces in the global (horizontal and vertical direction) as well as in the local direction (perpendicular and parallel direction of the cut). From the procedure it was seen that in a prismatic beam, subjected to a four point bending test, the analysis performed in a constant bending moment zone on an inclined cut and vertical cut gives the same result. However, in case of non-prismatic beams, the bending moment resistance obtained on an inclined cut, which is perpendicular to the centroidal axis with the forces in the local direction, is greater than that obtained on a vertical cross-section cut. Therefore to be conservative it is recommended to perform cross-section analysis on a vertical cross-section cut in a non-prismatic beam, which also ensures that an adequate amount of tensile reinforcement is provided.

A procedure to calculate the shear capacity of non-prismatic beam is determined in this study. First, the shear resistance contributed by concrete and stirrups are calculated at the assumed critical section. Then the inclined cross-section forces are determined for each load case and the capacity of the beam is either reduced or increased by the vertical component. This capacity is compared with the applied loading and is checked for failure. Since the shear capacity is influenced by the applied loading, failure of the beam is defined as the load for which the determined capacity is lower than the applied loading. The results obtained from this procedure are in good agreement with the limited experimental data available. Therefore, it can be concluded that the vertical component of the inclined cross-section forces should be considered in the shear capacity equation.

When a cross-sectional analysis is performed in a prestressed non-prismatic beam, the prestressing force P_∞ should be applied horizontally and at the centroidal axis level. Moreover the applied bending moment equation is changed by an amount equal to the prestressing force P_∞ multiplied with the eccentricity. This eccentricity is due to the variation of centroidal axis along the length of the beam.

Finally, the errors made in practice while performing cross-sectional analysis on non-prismatic bridge decks are studied. Due to the non-linear layout of the non-prismatic bridge decks, engineers find it difficult to perform cross-sectional analysis on these types of beams. Therefore, the cross-section of the bridge deck is modified such that the centroidal axis has a linear layout and the volume of concrete in use is equal to the original non-prismatic deck. From the analysis, it was seen that the results determined on a modified deck are approximately equal to the one obtained from the original deck. A common error engineers make is ignoring the inclination of the cross-section forces, which, in most cases, leads to underestimation of the shear capacity. This study shows that the vertical component of the inclined cross-section forces, which is considered in the shear capacity equation, should be

determined based on the bending moment obtained for the load combination in which the applied shear force is governing. Bending Moment envelopes obtained from different load combinations should be disregarded.

List of Symbols

Symbol	Description
x_u	Compressive zone (mm)
N_{cu}	Concrete compressive force (kN)
f_{ck}	Charachteristic cylinder compressive strength (MPa)
f_{cm}	Mean cylinder compressive strength (MPa)
f_{cd}	Design cylinder compressive strength (MPa)
F_{sb}	Steel force due to bottom reinforcement (kN)
A_{sb}	Area of bottom reinforcement (mm^2)
f_{yd}	Design yield strength of steel reinforcement (MPa)
F_{st}	Steel force due to top reinforcement (kN)
A_{st}	Area of top reinforcement (mm^2)
V_{Rd}	Shear resistance (kN)
$V_{Rd,c}$	Shear resistance contributed by concrete (kN)
$V_{Rd,s}$	Shear resistance contributed by stirrups (kN)
z	Lever arm (mm)
ρ_l	Reinforcement ratio
d / d_{eff}	Effective depth at that section (mm)
A_{sv}	Area of shear reinforcement (mm^2)
s	Spacing (mm)
V_{Ed}	Applied shear force (kN)
M_{Ed}	Applied bending moment (kN-m)
M_{Rd}	Bending moment resistance (kN-m)
a	Shear span (mm)
E_c	Young's modulus of concrete (MPa)
E_s	Young's modulus of steel (MPa)
α	Angle of inclination (degrees)
f_{yvd}	Design yield strength of shear reinforcement (MPa)

All the dimensions are in 'mm', unless specified otherwise.

Table of Contents

List of Figures

List of Tables

1 Introduction

This chapter summaries the main objectives of this study and the methodology adapted to answer the research questions.

1.1 Background

Beams are structural elements that transfer load mainly by bending action whilst sometimes supported over column. In reinforced concrete buildings, generally, slabs transfer the load to beams via the distribution of forces, based on the type of slab i.e. one way or two way slab. The loads transferred on the beam results in reaction forces which are taken up by columns, on which the beam is supported, and eventually transferred to the foundation of the building. In precast bridges, beams are laid in the longitudinal as well as in the transverse direction and a deck is then placed on top. In general, the longitudinal beams are precast whereas the transversal beams are cast in-situ. The longitudinal beams are placed on capping beams, which are supported on piers. Another option for cast-in situ bridges with longer spans is box girder bridges. In incrementally launched and cable-stray bridges, each box girder segment has constant dimensions whereas, in the cantilever balanced method, each segment varies in height. This would indicate that the height of the concrete bridge varies along the length i.e. non-prismatic beams. Sometimes capping beams are also non-prismatic as shown in Figure 1.

Figure 1 Haunched capping beam

It is clear that beams are a vital part of a structure. To distinguish between different types of beams, several classifications are possible. Some of them are mentioned below,

1. Type of material used can be made – Concrete, Steel or Timber. The use of material depends on the structure that is under construction, availability of materials, local expenses etc.
2. In reinforced concrete beams, the amount of reinforcement used – under-reinforced, over-reinforced and neutral. Therefore while designing, cross-section analysis is performed to calculate the amount of reinforcement that is required to resist the applied load. The amount of reinforcement dictates the type of failure i.e. either yielding of steel or crushing of concrete, provided sufficient amount of shear reinforcement is present.
3. Type of support – simply supported, cantilever, fixed, continuous, overhanging etc.
4. Cross-section of the beam – Rectangular, Circular, I-shaped, T-shaped, C-shaped etc.
5. Variation of height along the length of the beam – prismatic and non-prismatic beam.

In this study, the focus is on the cross-section analysis of concrete prismatic and non-prismatic beams.

1.1.1 Prismatic and Non-Prismatic beams

Prismatic beams are the beams where the cross-section remains constant along the length of the beam whereas in non-prismatic beam the cross-section varies along the length of the beam. Recently, the use of non-prismatic beams has increased in the construction industry mainly because the material is applied more efficiently. Moreover, these beams are economical, aesthetically pleasing and provide easement in placement of different equipment's, especially in buildings. Another benefit of non-prismatic beam is the reduction of

self-weight which is the governing load for long concrete bridges. Non-prismatic beams can be further classified based on the variation of height – tapered or haunched beams, curved beams and twisted beams.

Tapered beams or Haunched beams are the beams where the cross–section varies linearly along the length of the beam as shown in Figure 2. Mostly, tapered beams have greater depth near the support, enough to resist the applied shear forces, and less depth at the center, enough to resist the applied bending moment. The depth at the center may increase if the applied load is high or the amount of reinforcement used is less. Haunched beams have a wide range of application such as in framed buildings, cantilever retaining wall, simply supported and continuous bridges for economic and aesthetic purposes. Generally, the angle of the haunch or the angle of taper varies from -12° to 12°. This restriction is due to construction complication and aesthetic view.
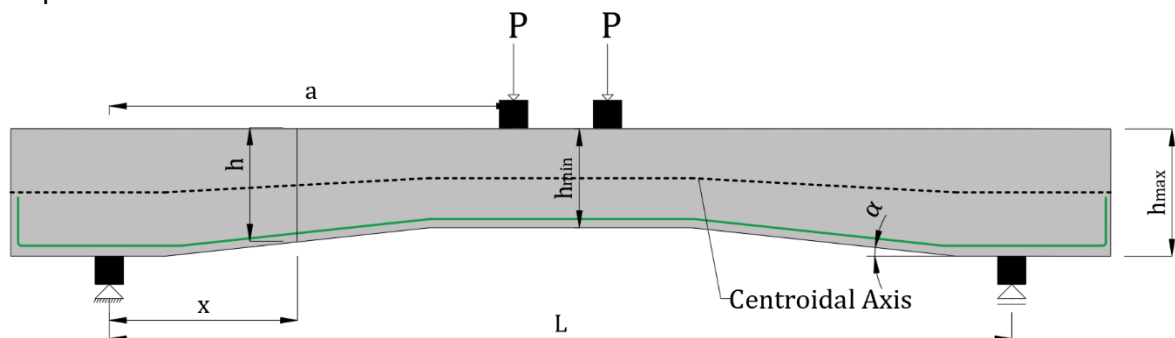
Figure 2 Negatively haunched beam

Curved beams are the beams where the cross-section varies in a parabolic or in a curvilinear manner along the length. This variation might be in the horizontal or vertical plane. As mentioned previously, the cantilever balanced method uses box girder segments to construct curved beams, with spans ranging from 90-200 m as shown in Figure 3. As the box girder segments are used, these beams have the structural advantage of carrying torsional moments.

Figure 3 Bridge with a curvilinear centroidal axis

Twisted beams are the beams where the cross-section varies along the length of the beam such that the cross-section rotates around the centroidal axis. Due to their complicated shape these beams are rarely used and are ignored in this study.

1.2 Scope and Objectives of Research

With the change in the cross-section along the length of the beam, non-prismatic beams behave differently compared to prismatic beams. When a cross-section analysis is performed at the critical section of the beam, which is in the haunched part, the resulting steel force or the concrete compressive force acts at an angle, due to the geometry. A cross-sectional analysis is performed at a distance 'x' from the support in the haunched beam shown in Figure 2. This analysis is performed at the Ultimate Limit State (ULS). As the steel reinforcement is

placed at an angle of taper (α), the steel force (F_{sb}) also acts at the given angle. This force is further decomposed in the horizontal ($F_{sb}.\cos(\alpha)$) and the vertical component ($F_{sb}.\sin(\alpha)$) as shown in Figure 4. Because of the vertical component of the inclined steel force, these non-prismatic beams are difficult to analyze.
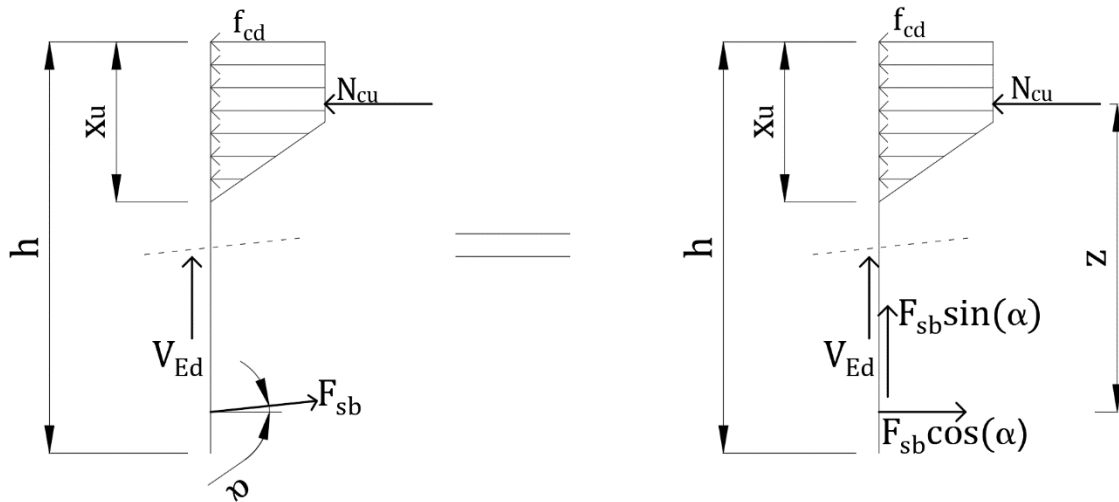
Figure 4 Cross-Sectional analysis in the haunch side of the beam shown in Figure 2

The vertical component is also seen in prestressed prismatic beams with parabolic tendon layout or with a tendon layout that varies linearly along the length of the beam as shown in Figure 5. In this beam, irrespective of where the cross-section analysis is performed, the prestressed force (ΔP) always acts at an angle. Decomposition of this force would also result in a horizontal and a vertical component.
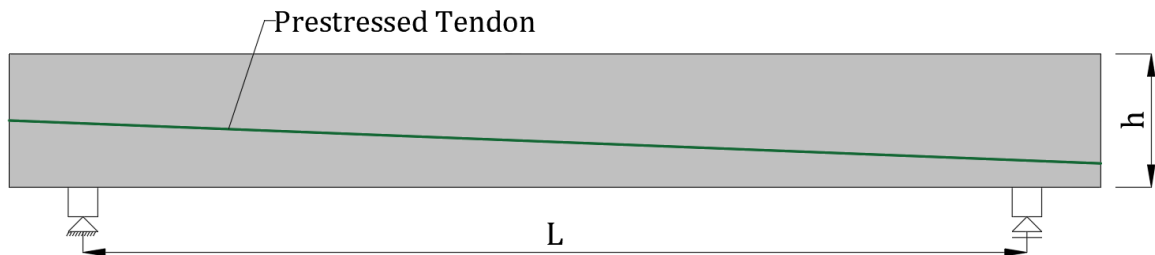
Figure 5 Concrete beam with linearly varying prestressed tendon

Codes around the world suggests that this force should be considered in the shear resistance (V_{Rd}) or the applied shear force (V_{Ed}) of the beam. Few researchers have performed shear tests on non-prismatic beams and have proposed different formulae to predict the shear capacity of these beams. Few authors suggest that, the vertical component should be considered in the shear resistance of the beam whereas others suggest that it should be left out of the shear capacity equation. This might seem conservative but one might overestimate the shear capacity of these non-prismatic beams leading to brittle shear failures. Furthermore, this vertical component might significantly change the shear capacity of long non-prismatic beams, where heavy prestressing is applied. In this study, experimental data will be used to check the existence of the vertical component in tapered beams and its effect on the shear capacity.

In prismatic beams, as the cross-section is constant along the length of the beam, the centroidal axis is also straight. Performing a vertical cross-sectional analysis in a prismatic beam would indicate that the cross-section cut is perpendicular to the centroidal axis. On the other hand, in non-prismatic beams the cross-section (height) varies along the length and hence the centroidal axis has a non-linear layout as shown in Figure 2. When a cross-sectional analysis is performed in non-prismatic beams, the vertical cross-section cut is no longer perpendicular to the centroidal axis unlike prismatic beams. Hence the cross-section cut which is perpendicular to the centroidal axis will be investigated in this study. Different approaches

are proposed to perform cross-section analysis of non–prismatic beam and the cross-section results are further analyzed.

1.3 Research Hypothesis

The research hypothesis for the above mentioned scope and objectives is as follows:

"According to Structural Mechanics, the cross-section results for any beam should remain constant, irrespective of the angle of the cross-section cut. Also the vertical component of the inclined internal compression chord or tensile tie should be taken into account by the shear capacity of the beam."

1.3.1 Research Question and Methodology

Based on the scope, objective and the hypothesis the following research questions are determined.

1. *In prismatic beams, does the cross-section results change when the cross-section cut is made at different angles with respect to the centroidal axis?*
2. *In non-prismatic beams, does the cross-section results change when the cross-section analysis is performed on a vertical cut and on a cut that is perpendicular to the centroidal axis?*
3. *What should be the procedure to predict the shear capacity of non-prismatic beams?*
4. *What are the different errors that an engineer might commit while analyzing non-prismatic bridge decks?*

The first research question answers whether the cross-section results, viz. Moment Resistance and Shear Resistance, in a prismatic beams are dependent on how the cross-section cut is made. Performing a cross-section analysis in a prismatic beam on a cross-section cut which is at an angle of '90+α', with respect to the centroidal axis, is not different than performing a vertical cross-section cut in the tapered or curved zone of a non-prismatic beam. Cross-section results will be checked for different angle of inclination and the error will be notified. For this study, prismatic beams that are subjected to four point bending test will be used. These beams will be designed for a given load and modelled in DIANA. Once the results are obtained, different approaches would be hypothesized and checked.

The second research question answers whether the cross-section results in a non-prismatic beams depends on how a cross-section cut is made or not. The approaches that were hypothesized in the previous research question are used here to further analyze non-prismatic reinforced and prestressed concrete beams.

The third research question focuses on the shear capacity of non-prismatic beams. This research question highlights on whether the vertical component of the inclined compression strut or tensile tie should be included to the shear capacity of the beam or not. Different authors have performed tests on non-prismatic beams (mainly subjected to four point bending test) and the experimental data will be used to compare the analytically obtained results.

The fourth research question lays emphasis on different types of error an engineer might commit in practice while analyzing non-prismatic bridges. Due to the non-linear layout of centroidal axis in non-prismatic bridges, performing cross-sectional analysis is complicated. Hence engineers modify the cross-section or ignore the inclination of the cross-section forces, which might change the shear resistance and the bending moment resistance envelope. The amount and different types of error will be addressed in this research question.

2   Literature Review

Concrete beams are susceptible to shear failure but more so in non-prismatic beams. Many authors and codes believe that this failure is due to the vertical component of the inclined force, which is because of the geometry of the beam. The following state of art gives more insight in this regard. Experiments performed on non-prismatic beams by different authors are also discussed in this chapter.

2.1 Codes and Standards

In this section, different codes are discussed for the inclined cross-section forces and different formulas regarding this are mentioned.

2.1.1 Eurocode 1992-1-1

In the Eurocode 1992-1-1 [1], clause 6.2.1(2) gives the following formula for inclined forces.

$$V_{Rd} = V_{Rd,s} + V_{ccd} + V_{td} \ldots\ldots\ldots\ldots(2.01)$$

where,

$V_{Rd,s}$ = shear resistance offered by the shear reinforcement

V_{ccd} = vertical component of the inclined compression chord

V_{td} = vertical component of the inclined tensile tie
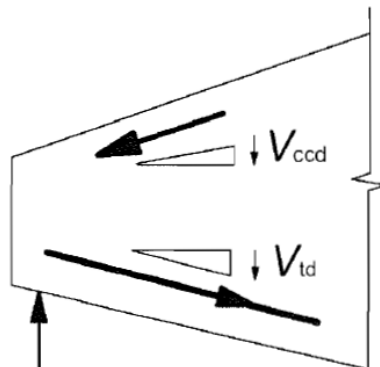
Figure 6 Vertical component of the inclined forces according to Euro Code [1]

The above formula states that if the compression chord or the tensile ties are inclined, the vertical component of this force either increases or decreases the shear capacity of the beam, depending on the direction of the forces as shown in Figure 6. According to the above formula, the vertical components are only combined with the shear capacity contributed by stirrups. A possible contribution of shear capacity due to concrete ($V_{Rd,c}$) is neglected in this regard. In long non-prismatic beams, the forces in the inclined chords are high and the vertical component of this force would significantly change the shear capacity of the beam, which is uncertain.

2.1.2 ACI 318-05

In ACI 318-05 Building code requirement for Structural Concrete and Commentary [2], clause 11.1.1.2 states that "In a member of variable depth, the internal shear at any section is increased or decreased by the vertical component of the inclined flexural stresses". ACI code also includes the vertical component to the shear capacity of the beam. The nominal shear strength (V_n) is calculated according to the following formula

$$V_n = V_c + V_s \ldots\ldots\ldots\ldots(2.02)$$

where V_c is the shear strength provided by concrete and V_s is the shear strength provided by shear reinforcement, formulae of which differ for every other situation. The vertical component of the inclined flexural stresses are added or subtracted from the equation 2.02. The general equation of the shear capacity of concrete and stirrups is given below. Note that these might be subjected to changes with different situation.

$$V_c = 2\left(1 + \frac{2000N}{A_c}\right)\cdot\sqrt{f_{ck}}\cdot b_w\cdot d \ldots\ldots\ldots\ldots(2.03)$$

$$V_s = \frac{A_{sv}\cdot f_{yvd}\cdot(\sin(\alpha) + \cos(\alpha))\cdot d}{s} \ldots\ldots\ldots\ldots(2.04)$$

where,

N = Axial force

A_c = Cross sectional area of structure

α = Angle of inclination of stirrups

$\dfrac{N}{A_c}, f_{ck}, f_{yvd}$ is in psi

b_w, d, s is in inches

A_v, A_c is in inches^2

2.1.3 Fib Model Code 2010

In the fib-Model Code 2010 for concrete structures [3], the clause 7.3.3.1 states that for determining the effective applied shear force (V_{Ed}), in case of inclined forces, the shear force from the sectional analysis (V_{Ed0}) may be decreased by positive influence of the inclined tension tie (V_{Etd}) or inclined compression chords (V_{Ecd}) or prestressing tendons (V_{Epd}). On the other hand, any negative influence from these inclined forces should be added to the shear force (V_{Ed0}). The vertical component of these inclined forces are added or subtracted from the applied shear force. The Model Code is flexible with the favourable contributions whereas unfavourable contribution should be considered in the applied shear force. This is taken into account for all the level of approximation and the shear resistance due to concrete is also considered to calculate the capacity of a beam or deck.
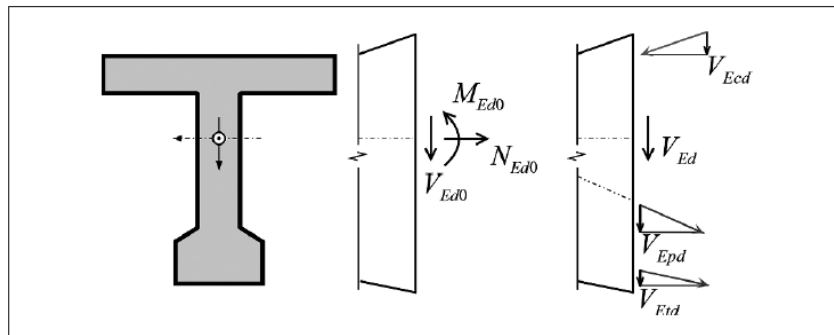
Figure 7 Vertical component of the inclined forces according to Model Code [3]

2.2 Cross-section assumptions

Few assumptions to determine the ultimate bending moment resistance of reinforced and prestressed concrete cross-sections are given as follows:

a. Plane section remains plane.
b. Tensile strength of the concrete after cracking is ignored.
c. Stresses in concrete and reinforcement are derived from the constitutive relation that these materials are assigned.
d. The strain in bonded reinforcement is same as that of the surrounding concrete.

2.3 Arch action in beams

From the experiments performed on non-prismatic beams, it was seen that arch action is present in almost every other beam. This arch action is not due to the horizontal restrained at the ends but due to loss of bond between steel reinforcement and the surrounding concrete. This mechanism is enhanced in short non-prismatic beams.

Daejoong Kim et al. [4] studied the arch action in reinforced concrete prismatic beams. The author states that the internal shear resistance in a reinforced concrete beam without stirrups is expressed as a contribution from two actions – beam action and arch action.

When the internal moment arm/lever arm remains constant, pure beam action is obtained whereas when there is a loss of bond between reinforcement and the surrounding concrete,

arch action occurs. However, the combined resistance of these two mechanisms results in the shear resistance of the reinforced concrete beam as the bond force cannot be developed completely due to cracking and bond slip. The extent of contribution of each mechanism depends on the shear span to the depth ratio (a/d). If $\frac{a}{d}$ > 2.5 i.e. in a slender beam, beam action governs and if $\frac{a}{d}$ < 2.5 i.e. for short beams, arch action governs.

To check the hypothesis, the authors conducted tests on 8 prismatic beams without shear reinforcement which were subjected to four point bending test. The steel force was analytically calculated along the length of the beam and was checked against the experimental results. It was seen that in the zone of constant bending moment, steel force obtained from the analytical calculation predicts quite well with the experimental results. On the contrary, in the shear span the experimental steel force was greater than the steel force which was calculated analytically using the beam theory. This was because of the assumption of constant lever arm throughout the length of the beam. Near the support, the actual moment arm length is shorter than the calculated moment arm. This leads to an increase in the steel force. The author states that the measured steel force is given as

$$T_m = T_a + T_b..............(2.05)$$

where

T_a = Steel Force due to the arch action

T_b = Steel Force due to the beam action

The author believed that the reduction in the lever arm was due to the loss of bond between the steel reinforcement and the surrounding concrete leading to the arch action. Formulae for the Ultimate Shear Strength of reinforced concrete prismatic beam without web reinforcements were proposed, which takes into account the contribution of arch action as well. The formulae was in good agreement with other test results.

2.4 Experiments on Non-Prismatic beams

In this section the experiments conducted on non-prismatic beams are discussed and different formulas are proposed by authors that predicts the shear capacity of non-prismatic beam which considers the vertical component of inclined forces as well. The concrete strength mentioned in all the beam specimens is the cylindrical concrete compressive strength.

2.4.1 Behaviour and Strength of Reinforced Concrete Haunched Beams in Shear – S. Y. Debaiky et al. [5]

S. Y. Debaiky et al. [5] conducted extensive research on non-prismatic beams back in 1982. The authors performed four point bending test on 33 different reinforced concrete beams to investigate the behaviour and shear strength. The beam depth vary linearly along the shear span and remain constant in the constant bending moment zone as shown in Figure 8 and Figure 9. 33 beams were divided into 6 different series. Series A and B differ in shear span length. Series C and A differ in concrete compressive strength, Series C and D differs in the amount of shear reinforcement present, Series E has different amount of longitudinal reinforcement compared to Series C and D. Series E also had different arrangement of longitudinal reinforcement and hence is ignored in this study. Series F and Series A differ in the percentage of longitudinal reinforcement. The point loads are applied at the vertex of the haunch, except in series B, and are 600 mm apart. Range of parameters for different series is given in Table 1.
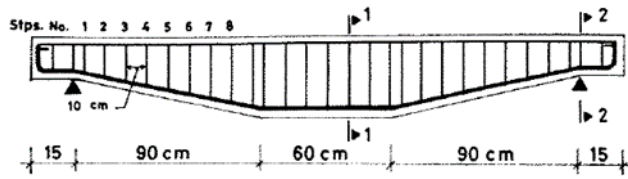
Figure 8 Dimensions of the negatively haunched beam tested by Debaiky et al. [5]
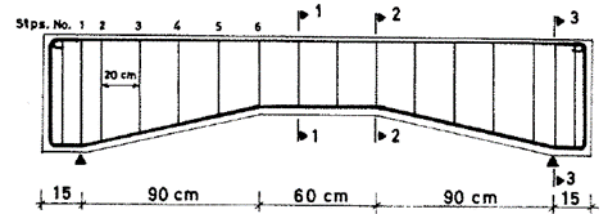
Figure 9 Dimensions of the positively haunched beam tested by Debaiky et al. [5]

Table 1 Comparison of different Series with the given range for a particular parameter [5]

Parameters	Series				
	A	B	C	D	F
Concrete Strength (MPa)	17 - 25	17 - 25	27 – 31	27 - 32	20 - 21
Longitudinal Reinforcement Ratio	0.03	0.03	0.03	0.03	0.019-0.024
Stirrup Reinforcement Ratio (x 10^{-3})	1.98	1.98	1.98	3.96-4.19	4.19
Shear Span (mm)	900	500 - 700	900	900	900

Table 2 Details of specimen tested by Debaiky et al. [5]

Specimen	Height at support (mm)	Concrete Strength (MPa)	Angle (α) (degrees)	Shear Span (mm)	Stirrup Diameter (mm)	Spacing Stirrup (mm)	Bottom Reinforce-ment
A1	300	25	0	900	5.5	200	3 bars-20 mm
A2	150	20	+9.46	900	5.5	200	
A3	225	17.8	+4.76	900	5.5	200	
A4	375	22	-4.76	900	5.5	200	
A5	450	22.5	-9.46	900	5.5	200	
B1	300	25	0	700	5.5	200	
B2	300	17.6	0	500	5.5	200	
B3	150	18.9	+12.1	700	5.5	200	
B4	150	21	+16.7	500	5.5	200	
B5	450	20.6	-12.1	700	5.5	200	
B6	450	20.4	-16.7	500	5.5	200	
C1	300	28.6	0	900	5.5	200	
C2	150	28.2	+9.46	900	5.5	200	
C3	225	27.8	+4.76	900	5.5	200	
C4	450	31.1	-9.46	900	5.5	200	
C5	375	31.4	-4.76	900	5.5	200	
D1	300	30.4	0	900	5.5	100	
D2	300	31.2	0	900	8	200	
D3	150	29.6	+9.46	900	5.5	100	
D4	150	27.5	+9.46	900	8	200	
D5	450	28.9	-9.46	900	5.5	100	
D6	450	32.2	-9.46	900	8	200	
F1	450	21.1	-9.46	900	6	200	3 bars-16 mm
F2	450	20.8	-9.46	900	6	200	3 bars-18 mm
F3	150	21.5	+9.46	900	6	200	3 bars-16 mm
F4	150	21	+9.46	900	6	200	3 bars-18 mm
F5	300	20.6	0	900	6	200	3 bars-18 mm
F6	300	20.9	0	900	6	200	3 bars-16 mm

Prismatic beams, negatively haunched beam – where the vertical component of the inclined forces has a negative effect on the shear capacity as shown in Figure 8 and positively haunched beam – where the vertical component of the inclined forces has a positive effect on the shear capacity as shown in Figure 9, were tested by authors. Most of the negatively haunched beams failed in shear compression and almost all of the positively haunched beam had instability shear failure. The length and width of all the beams was 2.4 m and 120 mm respectively. The height of the beam at the centre was 300 mm and was constant for all the beams. Beam description with the corresponding concrete strength is given in Table 2.

Table 3 Critical Load and failure type for different specimens tested by Debaiky et al. [5] SC- Shear Compression, DT – Diagonal Tension, IS- Instability Shear

Specimen	Type of Beam	Shear Crack Angle (degrees)	Initial Crack (kN)	Major Crack (kN)	Failure Load (kN)	Failure Type
A1	Prismatic	48	25	45	73.5	SC
A2	Positively Haunched beam	36	35	37.5	58	DT
A3	Positively Haunched beam	34	25	35	78.5	SC
A4	Negatively Haunched beam	49	25	30	51.3	SC
A5	Negatively Haunched beam	50	25	35	57	SC
B1	Prismatic	34	25	40	68.8	SC
B2	Prismatic	37	25	40	82.5	SC
B3	Positively Haunched beam	28	25	40	65.5	SC
B4	Positively Haunched beam	16	25	35	101.5	SC
B5	Negatively Haunched beam	39	25	40	78.5	SC
B6	Negatively Haunched beam	50	20	40	103.5	DT
C1	Prismatic	36	27.5	43.75	72.5	SC
C2	Positively Haunched beam	15	25	35	72	IS
C3	Positively Haunched beam	23	20	37.5	52	SC
C4	Negatively Haunched beam	42	27.5	35	61	SC
C5	Negatively Haunched beam	47	25	35	57.5	SC
D1	Prismatic	42	22.5	38.5	83.5	SC
D2	Prismatic	29	27.5	40	75	SC
D3	Positively Haunched beam	22	17.5	37.5	69	IS
D4	Positively Haunched beam	24	22.5	27.5	58.5	IS
D5	Negatively Haunched beam	40	10	25	65	SC
D6	Negatively Haunched beam	40	20	37.5	75	SC
F1	Negatively Haunched beam	34	25	42.5	67	SC
F3	Positively Haunched beam	16	25	34	44	SC
F4	Positively Haunched beam	15	10	27.5	45.5	DT
F5	Prismatic beam	24	20	32.5	67.5	SC
F6	Prismatic	25	25	37.5	62.5	DT

From the experiments it was seen that the number of cracks increases for higher depth at the support i.e. negatively haunched beam and decreases for smaller depth at the support i.e. positively haunched beam. The position of major cracking was also different for negatively and positively haunched beams. For the positively haunched beam, cracks occurred near the support whereas for negatively haunched beam, the cracks moved towards the loading position. This observation was as expected, as cracking occurs at the position of the weakest

section in the beam. For the negatively haunched beam, this section is near the vertex of the haunch, near the loading point, as the height is minimum with the vertical component of the inclined tensile tie further reducing the capacity. Whereas for the positively haunched beam, this section is near to the support as the height is small and the magnitude of the vertical component of the inclined tensile tie, which has a favourable contribution, is relatively low. The authors presented three different forces for each beam viz. Initial cracking, Major Cracking and Failure load as shown in Table 3.

From Table 3, it can be observed that the force required to produce initial cracking is almost same for all the studied samples. Major cracking load and the failure load have quite a variation for prismatic and non-prismatic beam. Due to the stirrups present the major cracking load and the failure load for the prismatic beam is different. From the experiments it was seen that in positively haunched beam, the major cracking, near the support, forms a weak strut action. Whereas in negatively haunched beam, the crack, joining the line from the loading point to the support, creates a strong strut action which is capable of resisting more load. From the results the author concluded that the strength of positively haunched beam did not reduce much when compared to the prismatic beams and the ultimate strength of the negatively haunched beam did not increase compared to the prismatic beams. This, according to the author, is due to the vertical component of the inclined steel force that contributes to the shear capacity of the beam.

The authors proposed a formula to calculate the nominal shear stress of reinforced concrete haunched beams which is given as,

$$\frac{V_{Rd}}{bd_s} = \left[v_c' \cdot \left(1 + 1.7 \cdot \tan(\alpha)\right) + \rho_v \cdot f_{yvd} + 0.25 \cdot \rho_l \cdot f_{yd} \cdot \sin(\alpha) \right] \dots\dots\dots\dots(2.06)$$

where,

$$\rho_l = \frac{A_{sb}}{bd_f} \text{ and } \rho_v = \frac{A_{sv}}{b.s}$$

$A_{sb} = $ Area of tensile longitudinal reinforcement

$A_{sv} = $ Area of stirrup

$b = $ width

$d_s = $ effective depth at the support

$d_f = $ effective depth at the flexural section

$\alpha = $ angle of inclination

$v_c' = $ Shear strength of concrete given in ACI code

f_{yd} and $f_{yvd} = $ Yield strength of longitudinal reinforcement and stirrups

The critical section at which the shear capacity is calculated is considered at a distance of $d_{cr} = d_s \cdot \left(1 + 1.7 * \tan(\alpha)\right)$ from the support. According to the author, the last term of the equation i.e. $0.25 \cdot \rho_l f_{yd} \sin(\alpha) \cdot b \cdot d_s$ is to account for the dowel action.

2.4.2 Shear Strength of Haunched Beams without Shear Reinforcement – I. A. Macleod et al. [6]

I.A. Macleod et al. [6] describes a technique to predict the shear strength of tapered reinforced beam without shear reinforcement. In practice, haunched beams are present in bridges as shown in Figure 10. A test specimen is shown in Figure 11. The depth of the beam near the support is increased in order to resist the applied shear force. The authors only considered the haunch part and subjected it to four point bending test as shown in Figure 13 and Figure 15.

Figure 10 Intermediate haunched section

Figure 11 Test specimen

The authors focused on the concept of critical section in this paper. Equations were formulated to predict the critical section of the beam which were validated with the experiments. The width of all these beams was 150 mm. Table 4 gives the specimen detailing with the respective experimental shear strength. When a sectional analysis is performed in the tapered zone, the vertical component of the inclined compression chord increases the shear capacity of the beam and therefore these non-prismatic beams are termed as positively haunched.

Table 4 Description of the beams tested by Macleod et al. [6]

Specimen	Maximum Height (mm)	Minimum Height (mm)	Concrete Strength (MPa)	Angle of inclination (degrees)	Shear Strength (kN)
Beam 2	250	200	33	4.74	36.4
Beam 3	250	250	33	0	30.9
Beam 4	300	200	28	6.34	38
Beam 5R	250	170	28	7.57	41
Beam 6	250	140	28	10.37	42

Figure 12 Reinforcement cross-section

Figure 13 All the specimen dimensions except Beam 4 [6]

14

Figure 14 Reinforcement detailing for all the beams
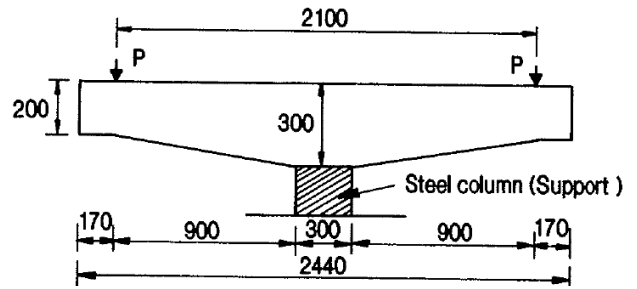
Figure 15 Beam 4 dimensions [6]

Cracking was observed with the increase in the load. Initially cracks appeared at the top side of the beam and then tended towards the support. When these diagonal cracks moved down to the compression zone, the propagation of the diagonal crack encountered resistance, which increased as the angle of haunch increases. This resistance was offered by the inclined compression zone and additional load was required to produce shear failure in the haunched beams as seen from Table 4. The failure pattern of all the beams was shear compression near the support as seen from Figure 16. From the experiments, it was seen that the failure of the prismatic specimen Beam 3 was brittle whereas the positively haunched beams had significant stand-in strength after the formation of the crack.
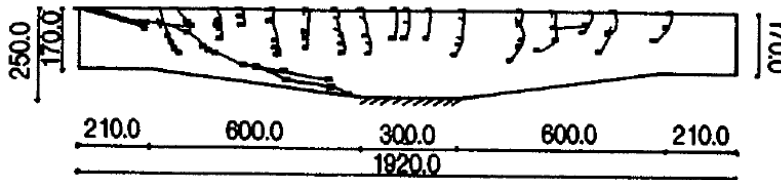
Figure 16 Cracking pattern in the specimen Beam 5 [6]

The positively haunched beams has a less amount of concrete when compared to the prismatic beam and yet the shear strength of the haunched beam is greater than the prismatic one. This, according to the author, is due to the compression zone present in the beam. Figure 17 and Figure 18 shows the compression zone in prismatic beam and positively haunched beam respectively. In the prismatic beam, compression path moves away from the loading point to eventually become horizontal near the support. While in the haunch beam, the compression path is straight/angled, which creates an inclined strut action near the support. With increase in the haunch angle, this strut action becomes straighter. Therefore the diagonal cracks encounter more resistance to propagate further down to the support and hence require additional load to produce failure.

The authors also proposed a formula to predict the shear capacity of the beam which is given as follows,

$$V_{Rd} = \left(V_{Rd,c} + \frac{M}{d_{cr}}.F.\tan(\alpha) \right) \dots\dots\dots\dots(2.07)$$

where,

d_{cr} = effective depth at the critical section

$V_{Rd,c}$ = shear strength of concrete in the prismatic zone according to BS 8110

M = Bending Moment at the critical section

α = Angle of haunch

F = factor = $0.27.(1+\tan(\alpha))^{10}$

15
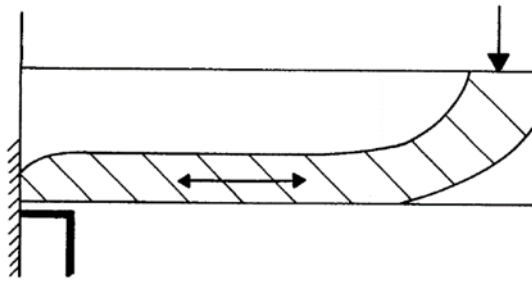
Figure 17 Compression zone in primsatic beam [6]
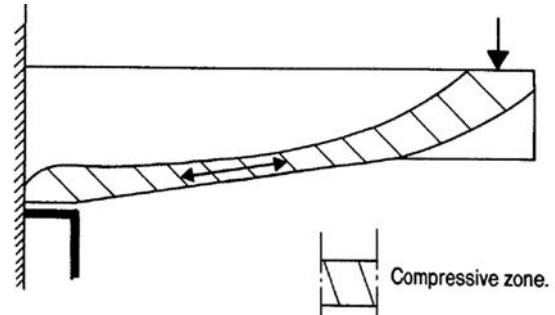
Figure 18 Compression zone in tapered beams [6]

The author assumed that the critical section is at a distance of 2 times the effective depth of the prismatic section which is measured from the point of contra flexure. The factor F is applicable only for haunches that have a slope in the range of 0.083-0.183 (4.74-10.3 degrees).

2.4.3 Shear Resistance of Reinforced Concrete Beams with Non-Prismatic Sections – G. D. Stefanou [7]

G. D. Stefanou [7] performed three point bending tests on varying depth beams to investigate the shear behaviour of reinforced concrete beam with non-prismatic sections and compared it with prismatic beams. The author proposed complicated formulae, to predict the shear capacity of non-prismatic beams, based on different type of cracking viz. Shear cracking of regions cracked in flexure (Flexural Shear Failure), Shear cracking in regions free from flexural cracks (Tensile Shear Failure) and Shear resistance following shear cracking. Two different types of beams were used which were subjected to three point bending test as shown in Figure 19. The critical section for the Type A beams was considered at a distance of minimum effective depth (d_{min}) from the support. Whereas for Type B beams the critical section was considered at a distance of $\dfrac{d_{min}}{\left(1 - 1.5 * \tan(\beta)\right)}$ from the support, where 'β' is the angle of taper. Specimen Detailing is given in Table 5.

The length and width of all these beams was 1.52 m and 150 mm respectively. The data present in the paper was limited. The diameter of shear reinforcement used was not mentioned in the paper. Therefore only the beams without shear reinforcement are discussed in this study.
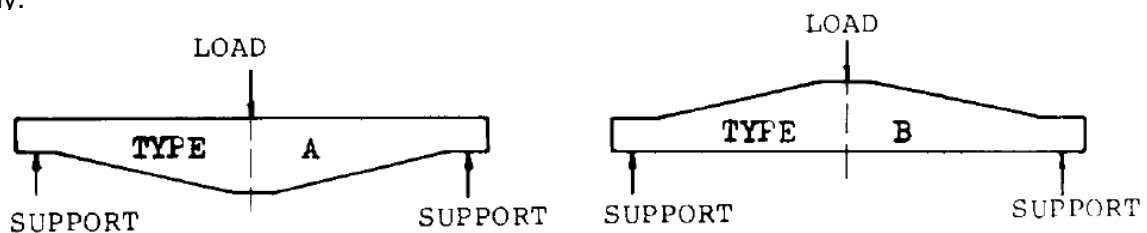
Figure 19 Types of beams tested by Stefanou [7]

Table 5 Description of beams tested by Stefanou [7]

Specimen	Type	h,max (mm)	h,min (mm)	Concrete Strength (MPa)	Angle of inclination (degrees)	Shear Capacity (KN)
B1	A	200	75	33.44	13.5	15.8
B2	A	200	125	33.44	7.96	26.5
B3	B	200	75	28.27	13.5	27.5
B4	B	200	125	28.27	7.96	26.5

The proposed formulae was validated using the experimental data that was present. The author considered the shear capacity of concrete, shear capacity of stirrups and also the inclusion of the vertical component of the inclined forces in the formulation.

2.4.4 Shear Failure Mechanism of Reinforced Concrete Haunched Beams – Chenwei HOU et al. [8]

Chenwei HOU et al. [8] studied the shear failure mechanism of reinforced concrete haunched beams. The authors performed four point bending tests on 10 haunched beam which differed in four different parameters viz. position of point loads with respect to the vertex of the haunch, thickness of concrete cover, area of stirrups and arrangement of the bottom reinforcement. The influence of these four parameters on the debonding cracks along the bottom reinforcement, which is responsible for the strut action and increase in the shear capacity, was investigated. Specimen details and material properties are given in Table 6. The beams are divided in 4 different series shown in Figure 20, Figure 21, Figure 22 and Figure 23. The number in the name of the specimen indicates the distance between the point load and the end of the haunch for example the specimen H-100 means that the point load is applied at a distance of 100 mm from the vertex of the haunch.

The depth of all the beams at the support is 300 mm and at the centre is 250 mm, providing a constant angle of haunch of 11.3°. The concrete cover of the beam is 50 mm, except in Series III. The span of the beam is 1500 mm. Two bars of 25.4 mm diameter and yield strength of 411 MPa were used as tensile longitudinal reinforcement bars. Two bars of 6 mm diameter were used compression reinforcement with a yield strength of 328 MPa. Shear reinforcement with 6.35 mm diameter, spaced at 200 mm, and yield strength of 322 MPa were used in the non-test shear span of the beams in Series I, II and IV. In Series III the non-test shear span was reinforced with 9.52 mm diameter, spaced at 120 mm while in the test shear span, shear reinforcement of 6.35 mm diameter is placed at spacing of 120 mm.

Table 6 Descripiton of beams tested by Chenwei HOU et al. [8]

Series	Specimen	f_c' (MPa)	Shear Span (a) (mm)	b (mm)	c (mm)	e (mm)
	H-0	33.0		0		400
	H-100	33.6		100		300
I	H-200	29.6		200		200
	H-300	36.7		300		100
II	HN-200	28.6		200		200
	HS-0	33.5	650	0	250	400
III	HS-100	28.0		100		300
	HS-300	34.4		300		100
IV	HD-100	34.0		100		300
	HD-300	37.4		300		100
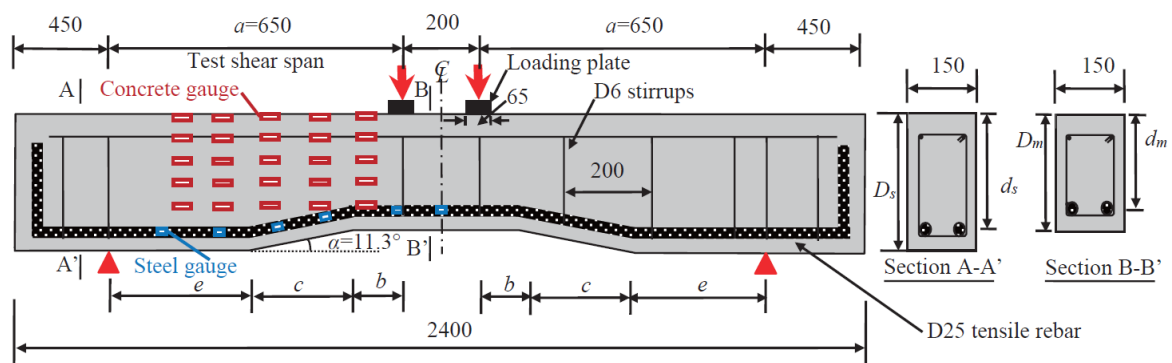
Figure 20 Beam specimen of Series-I [8]
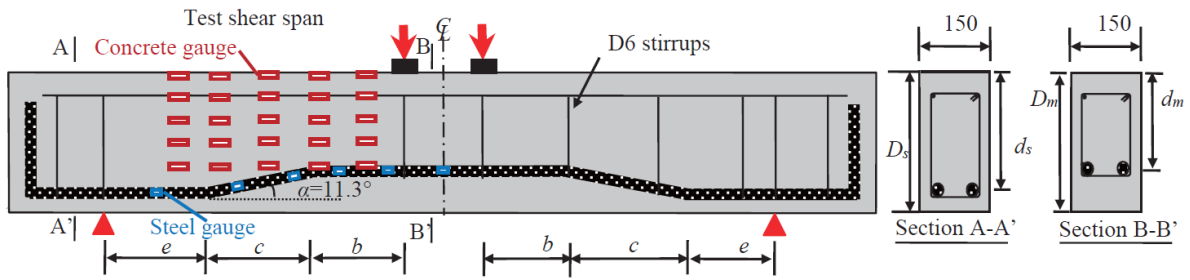
Figure 21 Beam specimen of Series II [8]
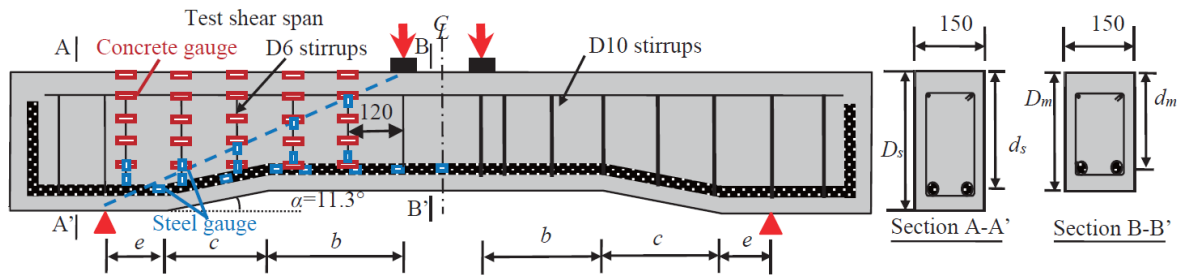
Figure 22 Beam specimen of Series III [8]
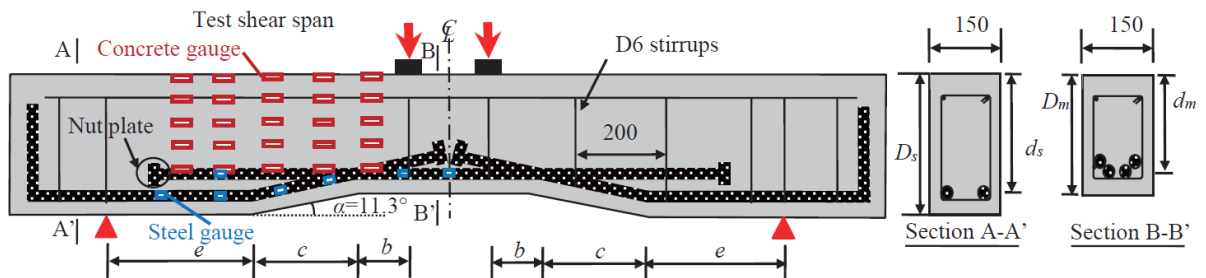
Figure 23 Beam specimen of Series IV [8]

The crack pattern observed in all the beams proved the existence of strut action. In Series I, once the flexural cracks are developed, the main diagonal crack starts from the vertex of the haunch near the loading point and further propagates in two direction – towards the loading point and along the inclined tensile rebar as can be seen in Figure 26. This is because of the stress concentration at the end of the haunch. All the beams failed in Shear Compression. For the beams in Series II, the crack originated at the middle part of the haunch and propagated both ways – first the loading point and then along the tensile rebar. The crack pattern for the beams in Series III was similar to those of Series I, with more shear and flexural cracks, due to the presence of stirrups.

The load-displacement graph of all the beams were plotted. It was seen that as the distance between the point load and the end of the haunch decreases, there is a drastic increase in the peak load mainly due to the strut action. Load-Displacement graph for beams of series I is given in Figure 24. The peak load and the shear capacity of all the beams are given in Table 7.
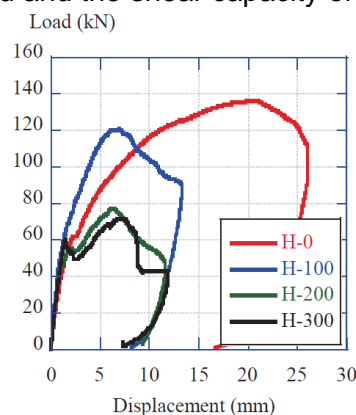
Figure 24 Load-Displacement curve for all the beams of Series I [8]

18

Table 7 Peak Load and Shear Capacity of all the specimens tested by Chenwei HOU et al. [8]

Specimen	Peak Load (kN)	Shear Capacity (kN)
H-0	136.2	68.1
H-100	120.5	60.3
H-200	77.1	38.5
H-300	71.9	36.0
HN-200	73.3	36.5
HS-0	154.7	77.4
HS-100	146.6	73.3
HS-300	137	68.5
HD-100	129.6	64.8
HD-300	157.6	78.8

The material parameters and the amount of reinforcement, in a particular series, were similar but still the shear capacity changes due to the position of point load with respect to the end of the haunch. The shear capacity of H-0 and H-100 is much higher compared to H-200 and H-300. This significant difference between the shear capacities resulted from the different contribution of strut action and also due to the debonding cracks. Debonding cracks was formed due to the stress concentration at the bending position which made the bent tensile rebar straighten and push over the concrete cover. This reduces the bond, which increases the capacity [4].

Table 8 Compressive zone in all the beams of Series I [8]
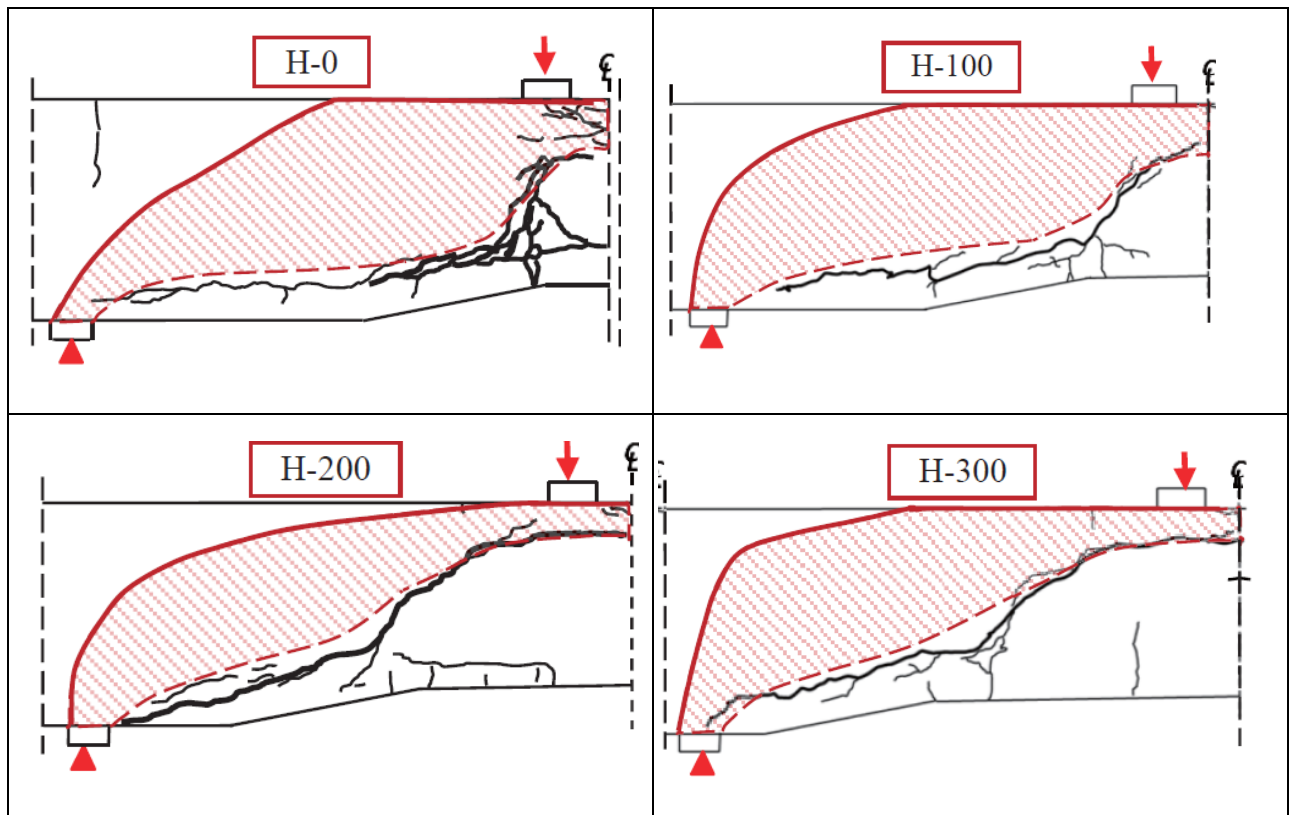
Table 8 shows the compression zone for all the beams of Series I just before the peak load. The use of concrete gauge was made to derive the strut zone in all these beams. The proof of bond loss, for the beam specimen H-0, is shown in Figure 25. At smaller loads, the strain

distribution in bottom reinforcement started from zero at the support and then increased proportional to the bending moment, meaning a good bond exist. But at the peak load, the strain distribution started at around 1200μ whereas the strains in the shear span became flat, leading to a partial loss of bond. This loss of bond with the presence of compression zone is responsible for the increase in the shear capacities. The extent of strut action in beam H-200 and H-300 is less when compared to H-0 and H-100, which can be seen from the minimal difference between the shear capacities for these two beams.
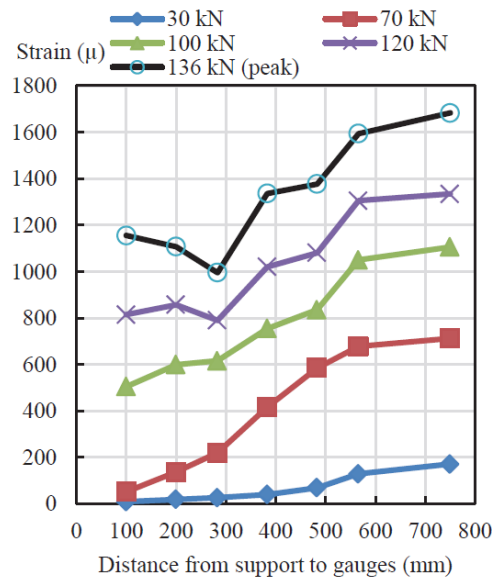
Figure 25 Strains in the reinforcement vs Distance from the support, for the beam H-0 for different load level [8]

The shear capacity of the beam is equal to the shear capacity of concrete and stirrups.

$$V_{Rd} = V_{Rd,c} + V_{Rd,s} \dots\dots\dots\dots (2.08)$$

As the dimensions and the longitudinal reinforcements are the same for the beams in Series I and Series III, $V_{Rd,c}$ for the beams of Series I and Series III were assumed to be the same and the shear capacity contributed by stirrups was calculated and cross-checked with the experimental results.

The authors modelled the beams of Series I, II and IV in DIANA system (version 9.4.4) to get a better understanding of shear resistance mechanism of the haunched beams. The load-displacement graph obtained from DIANA showed good coherence with the experimental graph. Figure 26 shows the principal tensile strain and the principal compressive stress for the beam H-100 just before the peak. The contour plot shows the debonding cracks along the tensile rebar and the strong compression zone, leading to strut action in the beam H-100.
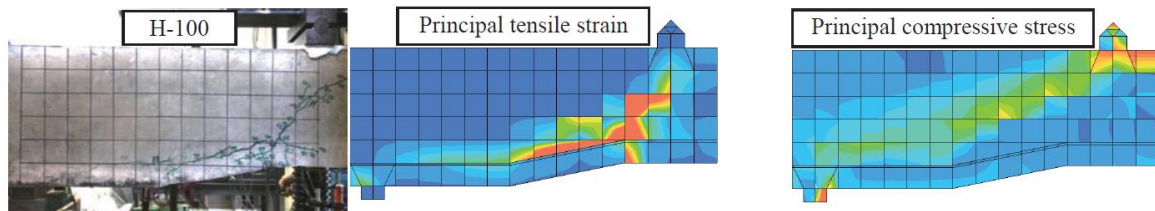
Figure 26 Comparison between experimental and DIANA results for the beam H-100 [8]

One of the conclusion of the author was that the bent tensile rebar has a negative effect to the shear resistance of the haunched beam but the strut action eventually increases the capacity or nullifies the effect of the vertical component. However the extent of this mechanism varies according to the crack pattern and the area of compression zones. In all these experiments,

the length of the beam was very short (1.5 m) and in practice, the length of non – prismatic beam is considerably long. Therefore, in reality, the probability of occurrence of such type of strong strut mechanism is less.

2.4.5 Shear Design of Straight and Haunched Beams – Vu Hong Nghiep [9]

Vu Hong Nghiep [9] worked on the "Shear Design of Straight and Haunched Concrete Beams without Stirrups" as a PhD topic. The beams that are tested in this study are chosen from the bridge slab deck. The haunch part of these beams are under compression as is the case in the intermediate support of a bridge deck. In this study, the haunch beams are subjected to three point bending test. The height of all these beams are kept constant at the centre which is equal to 340 mm. The beams were reinforced with three longitudinal bars of 20 mm diameter. The width of these beams was 120 mm. Material Properties for all the beam is mentioned in Table 9. In the first set (L-series), the ratio of the shear span to the effective depth (a/d) is 5 whereas in the second set (K-series) the ratio is 3.

Specimen 4L1-4L2 and 5L1-5L2 were reinforced with extra stirrups as shown in Figure 27. These specimens failed in flexure whereas all the other 14 specimens failed in shear. Table 9 gives the failure region with corresponding concrete strength and shear capacity. The load-deformation graph for the 4 specimens, which failed in flexure, showed ductile behaviour. The beams were capable to resist the load until the longitudinal reinforcements are yielded or the compressive strength of the concrete has reached.

The other 14 specimens failed in shear. The author divided the shear failure process in three phases:

i. Phase 1 – Flexural behaviour till half the peak load. At the midspan, where the bending moment is maximum, first vertical flexural crack appeared and as the load increases, other vertical flexural cracks originate.

ii. Phase 2 – Flexural-shear behaviour occurred with loading of $0.5F_u$-$0.9F_u$. The flexural cracks at the mid-span stays the same, but other cracks grow up. These cracks are no more vertical and tends to be inclined with respect to the neutral axis of the beam. These cracks are termed as flexural-shear cracks.

iii. Phase 3 – Shear failure occurred between $0.9F_u$-F_u. At this point of loading, the flexural shear crack doesn't grow anymore, however a pure diagonal shear crack appeared in the web of the beam as soon as the peak load is reached. Hence the failure pattern of these beams was the diagonal shear failure and brittle collapse occurred.
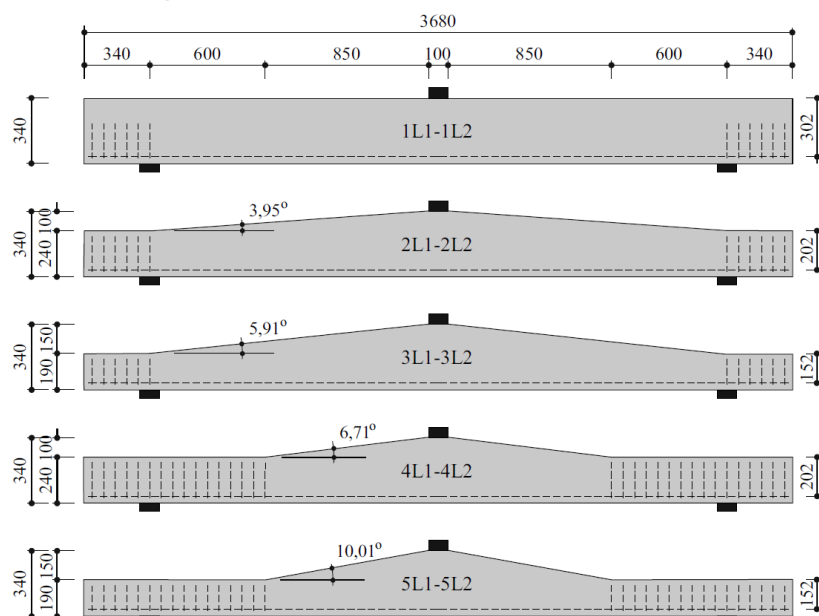
Figure 27 Dimensions of all the beams in Series L [9]

21

Specimen	Height at the support (mm)	Concrete strength (MPa)	Angle of inclination (α) (degrees)	Failure Region	Shear Capacity (kN)
1L1	340	48.11	0	Load Position	75.44
1L2	340	49.24	0	Load Position	79.21
2L1	240	49.45	3.95	Support	75.18
2L2	240	49.99	3.95	Support	74.6
3L1	190	50.21	5.91	Support	66.47
3L2	190	50.98	5.91	Support	69.3
4L1	240	52.21	6.71	Flexural Failure	-
4L2	240	52.44	6.71		-
5L1	190	53.13	10.01		-
5L2	190	53.25	10.01		-
1K1	340	53.83	0	Load Position	75.63
1K2	340	53.95	0	Load Position	69.31
2K1	281	54.18	3.95	Support	83.53
2K2	281	54.22	3.95	Support	85
3K1	240	54.26	6.71	Support	79.34
3K2	240	54.31	6.71	Support	79.93
4K1	190	54.78	10.01	Support	84.74
4K2	190	54.82	10.01	Support	83.88

The specimens failed in shear will be discussed in this study. Failure type of all the haunched beam was diagonal shear failure. Interestingly, the load-deflection graph of these beams showed brittle failure once the peak load was reached. According to the DIN 1045-01 (German code), the vertical component of the inclined concrete force (V_{ccd}) increases the shear strength of the beam, provided it follows the same sign convention. This is seen in the K-series, where the shear span to effective depth (a/d) ratio is 3. Shear capacity of the beam with an inclination of 10° was around 18% higher than the prismatic beam. But this trend was not seen in the L-series with the shear span to the effective depth of 3. In this case, the shear strength of 3L beams was around 16% lower than that of prismatic beams. The author states that this conclusion is in contrast to the one mentioned in the German code.
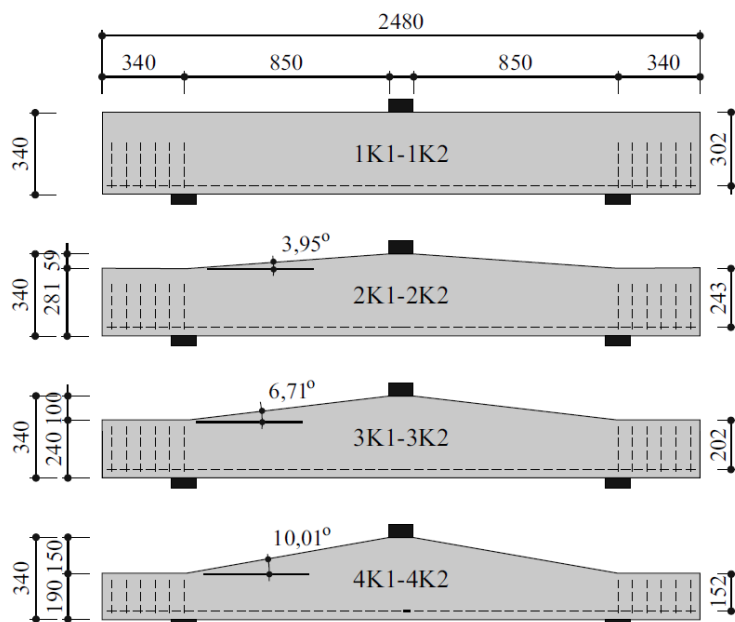
Figure 28 Dimensions of all the beams in Series K [9]

All these haunch beams were analysed in the Non-Linear FEM package – ABAQAS 6.9. 3-D beam models are analysed and the results are validated with the experimental values. The load-deflection graph of all the beams obtained from ABAQAS showed good coherence to the experimental graphs as shown in Figure 29, which is an example for the beam specimen 2L-2. The crack pattern, crack spacing and location, and inclination of shear cracks obtained from numerical analysis also showed good agreement with the experimental results, but not exact due to the heterogeneous nature of concrete. However, the failure type of all these beams was exactly predicted in ABAQAS.
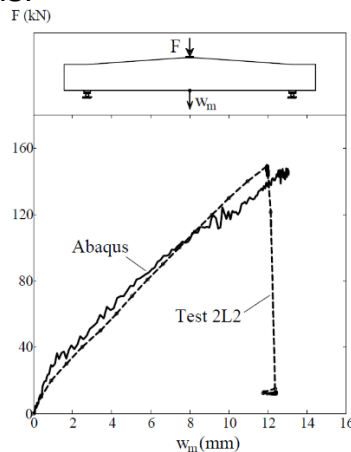
Figure 29 Load - Deformation graph for the beam Specimen 2L-2 [9]

Figure 30 and Figure 31 shows the different failure position for the prismatic and non-prismatic beam. It was also seen that the shear strength distribution of haunched beams is totally different than the prismatic beam. In straight beams, parabolic shear stress distribution was observed with maximum at the centre but in the positively haunched beams, the shear stress distribution was half parabola with maximum at the top part of the beam as shown in Figure 32. Figure 32 also shows that in non-prismatic beam the shear stress distribution near the support resembles to the prismatic beam i.e. parabolic distribution with maximum at the centre but when the section is closer to the loading point, the distribution takes the shape of half parabola with the maximum value at the top surface of the beam.
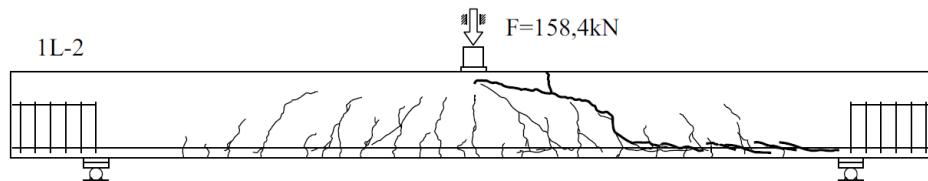
Figure 30 Cracking pattern at failure for test specimen 1L-2 [9]
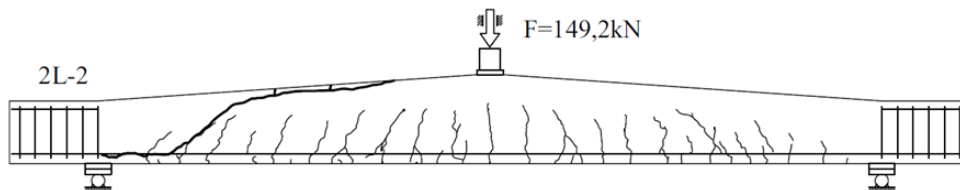
Figure 31 Cracking pattern at failure for test specimen 2L-2 [9]
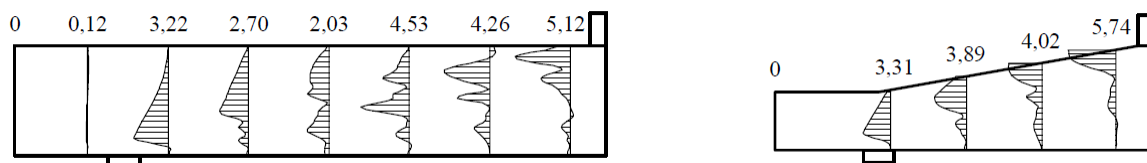
Figure 32 Shear stress distribution in prismatic and positively haunched beam [9]

The author also stated that the shear capacity of reinforced concrete beam without stirrups is due to the compression zone and the uncracked concrete part in the tension zone and this contribution is equal to 95% of the total shear force. Other shear resistance mechanism such

as aggregate interlock, dowel action etc. provides the remaining 5% of the total shear force. Based on the experimental results and data present, the author proposed following formulas to calculate the shear capacity of beams.

1. For prismatic beam

$$V_{Rd} = 2.\left(\frac{4d_1}{a}\right)^{\frac{1}{4}}.\left(\frac{250}{d_1}\right)^{\frac{1}{4}}.\left(f_{ck}\right)^{\frac{1}{4}}.\rho_l^{\frac{1}{3}}.b.d_1$$

$$V_{Rd} = 11.25\left(\frac{f_{ck}}{a}\right)^{\frac{1}{4}}.\rho_l^{\frac{1}{3}}.b.d_1 ....(2.09)$$

2. For non-prismatic beam

$$V_{Rd} = 2.\left(\frac{4d_2}{a}\right)^{\frac{1}{4}}.\left(\frac{250}{d_2}\right)^{\frac{1}{4}}.\left(f_{ck}\right)^{\frac{1}{4}}.\rho_l^{\frac{1}{3}}.\left(1+\tan\left(\alpha\right)\right).b.d_2$$

$$V_{Rd} = 11.25\left(\frac{f_{ck}}{a}\right)^{\frac{1}{4}}.\rho_l^{\frac{1}{3}}.\left(1+\tan\left(\alpha\right)\right).b.d_2 ....(2.10)$$

where,

$f_{ck} =$ Charachteristic cylinder compressive strength

$a =$ Shear Span

$b =$ Width of the beam

$\rho_l =$ Reinforcement ratio

$d_1 =$ Effective depth of prismatic beam at a distance

$d_2 =$ Effective depth of tapered beam at a distance of $1.3*d_{min}$ from the support

$d_{min} =$ Minimum effective depth

The equation of prismatic beam was validated using 878 experimental results and the mean value, for the ratio between the experimental values to the analytical ones, is equal to 1.0086 with a standard deviation of 0.1379. The equation of haunched beam was compared to the 14 available test data set and the mean was 1.013, with a standard deviation of 0.063. The shear resistance of prismatic beam can be predicted using the above given equation but more dataset is required to validate the equation which predicts the shear resistance of non-prismatic beam. For a conservative approach, the author proposed that whenever the vertical component of the inclined tensile tie or compression chord provides favourable contribution to the shear capacity i.e. in a positively haunched beam, only 50% of this component should be considered in the shear capacity or the applied shear force equation.

$$V_{ed}^{'} = V_{ed} - 0.5V_{ccd} ....(2.11)$$

where,

$V_{ccd} =$ Vertical component of the inclined compression chord

2.4.6 Behaviour of concrete haunched beams subjected to static shear loading – Arturo Tena Colunga et al. [10]

Arturo Tena-Colunga et al. [10] studied the behaviour of reinforced concrete haunched beams subjected to static and cyclic shear loading. In this study the results of static shear loading will be discussed. Five beams (one prismatic and four haunched) where tested without shear reinforcement and five beams (one prismatic and four haunched) with the minimum shear

24

reinforcement according to the norms of Mexico's Federal District Code. All these beams where subjected to four point bending test. Figure 33 shows the static scheme and dimensions for the specimens (TASC αi-Rj). Table 10 shows the specimen dimensions and the concrete strength.
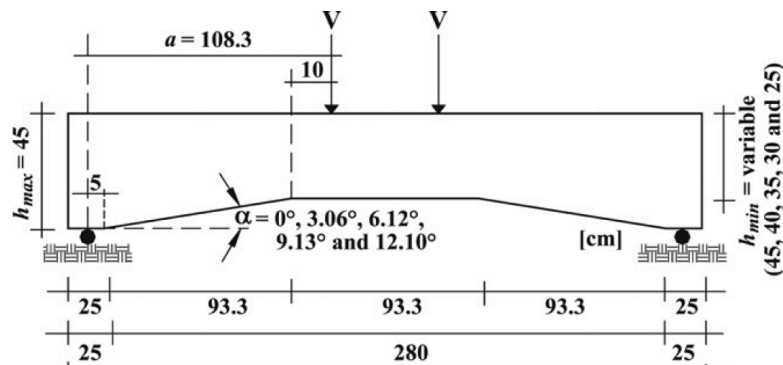
Figure 33 Dimensions of the beam tested by Arturo et al. [10] (in cm)

The first letter in the specimen indicates the angle of inclination i.e. i = 0 = 0°, i = 1 = 3.07°, i = 2 = 6.12°, i = 3 = 9.13°, i = 4 = 12.1°, whereas the second letter indicates the presence of stirrups, j = 0 = no shear reinforcement, j = 1 = Minimum shear reinforcement. 4 bars of 25.4 mm in diameter (A_{st}=2026.83 mm²) were used as bottom reinforcement whereas 3 bars of 25.4 mm diameter (A_{sb}=1520.12 mm²) were used as top reinforcement. All these bars are placed in a width of 220 mm. The shear reinforcement used is 8 mm in dimeter with a spacing of 185 mm. An example for the specimen TASC α4-R1 specimen is shown in Figure 34.

Table 10 Specimen dimensions and material properties tested by Arturo et al. [10]

Specimen (TASC αi- Rj)	Height at support (mm)	Height at centre (mm)	Concrete Strength (MPa)	Angle of inclination (degrees)
TASC α0-R0		450	33.4	0
TASC α1-R0		400	32.1	3.07
TASC α2-R0		350	29.5	6.12
TASC α3-R0		300	23.6	9.13
TASC α4-R0		250	28.1	12.1
TASC α0-R1	450	450	31.5	0
TASC α1-R1		400	26.9	3.07
TASC α2-R1		350	29.2	6.12
TASC α3-R1		300	28.8	9.13
TASC α4-R1		250	21.2	12.1

Figure 34 Specimen detailing of TASC α4-R1 [10] (Beam Dimensions in cm)

Table 11 shows the experimental shear forces for all the specimen. Critical shear force is the force where the first diagonal crack occurred. The ultimate shear force is the ultimate capacity of the beam whereas the collapse load is the force associated with the collapse of the beam. The cracking pattern at the ultimate load and collapse load for the beam specimen TASC α3-R1 is given in Figure 35. One would expect the ultimate shear force and the collapse load to

be the same as is the case in the prismatic beam. But in non-prismatic beam, this is not the situation as can be seen from Table 11

Table 11 Critical Forces for all the specimens tested by Arturo et al. [10]

Specimen	Critical Shear Crack Angle (degrees)	Critical Shear Force (kN)	Ultimate Shear Force (kN)	Collapse Load (kN)
TASC α0-R0	51	45	75	75
TASC α1-R0	43	57.5	67.5	87.5
TASC α2-R0	41	50	60	65
TASC α3-R0	35	27.5	37.5	80
TASC α4-R0	33	25	30	40
TASC α0-R1	38	70	250	255
TASC α1-R1	40	110	200	210
TASC α2-R1	33	87.5	170	170
TASC α3-R1	36	40	120	140
TASC α4-R1	29	40	80	80

(a) (b)
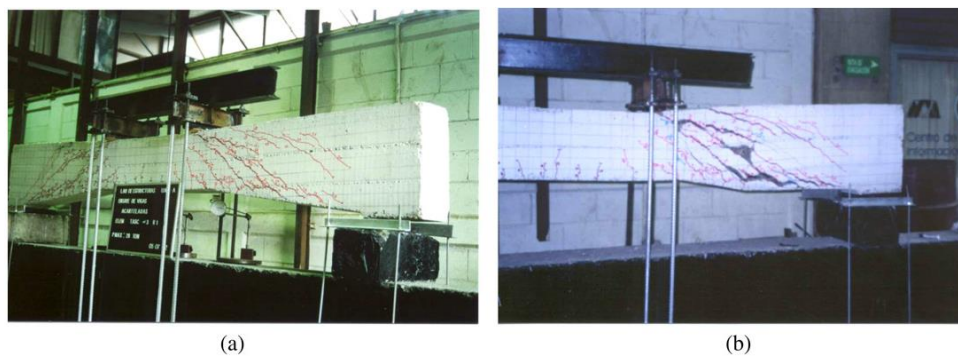
Figure 35 Cracking pattern in TASCα3-R1 a) at ultimate shear b) at collapse load [10]

From the load-deformation graph of all the specimens, it was seen that prismatic beam collapsed as soon as the ultimate load was reached. However non-prismatic beam showed some deformation capacity after reaching the ultimate shear force as is evident from Table 11 and Figure 36. The ultimate shear force of the haunched beam were smaller than the prismatic beam but the deformation capacity showed reverse trend. The author believes that such ductile behaviour of reinforced concrete haunched beam is due to the redistribution of cracking.
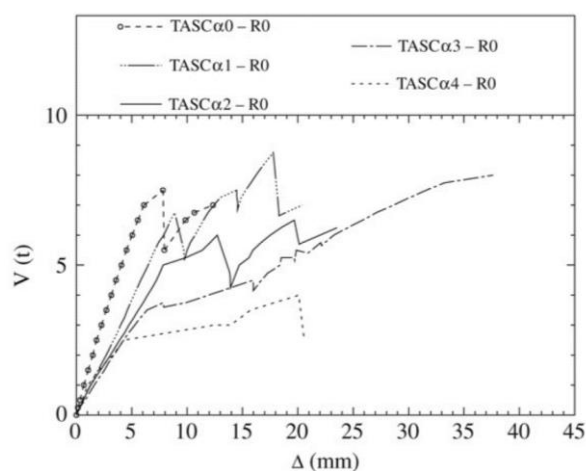
Figure 36 Load-Displacement curve for all the beams, without shear reinforcement, tested by Arturo et al. [10]

The cracking pattern proved the existence of strut action in reinforced haunched beams. Compression struts, generally, formed between the loading point and at the mid-point of the

26

haunch length as can be seen in Figure 37. For the specimens with minimum shear reinforcement, placing stirrups at the vertex did not allow the cracking to propagate in the prismatic section and no local fault was observed at the vertex. Another trend was seen with the shear crack angle and the angle of haunch. As the angle of haunch increases the shear crack angle further decreases.
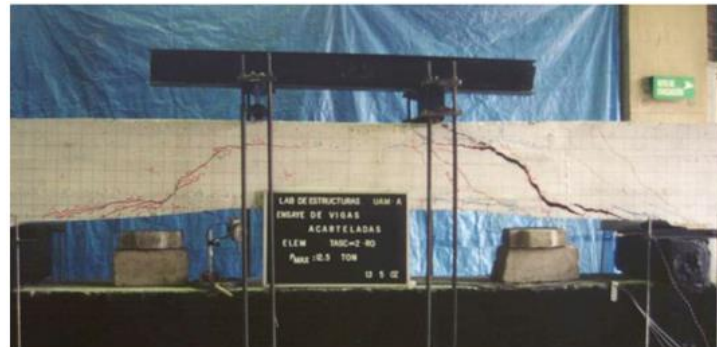
Figure 37 Cracking pattern in the beam specimen TASCα2-R0 [10]

Strains in the longitudinal reinforcement, for the specimens without shear reinforcement, are much smaller than the yield strain of reinforcement, whereas for the beams with shear reinforcement, the peak strain is greater than the yield strain. For the haunched beams with shear reinforcement, the peak strain of the stirrups located at the vertex was greater than the yield strain of reinforcement. The author states that this is due to the vertical component of the inclined steel force.

Based on all the test results, the authors compared the formulas proposed by Debaiky et al. [5] and Macleod et al. [6]. The author also discussed the shortcomings of the formulas. Shortcomings for the formulation proposed by Debaiky et al. [5] are

I.   The moment term was accounted indirectly for the dowel action, which was assumed to be constant. This was not clear and realistic, especially in case of haunched beams with shear reinforcement.

II.   The contribution of shear reinforcement was assumed to be the same as for the prismatic beam, despite the fact that the shear crack angle varies with the angle of the haunch.

Shortcomings for the equation proposed by Macleod et al. [6] are

I.   The factor *F* increases exponentially as the angle of haunch increases, which might overestimate the second term of the equation

II.   Nothing was mentioned about the shear capacity contributed by stirrups

III. The critical depth d_{cr} was not bounded – sometimes the numerical value is greater than the maximum effective depth.

To overcome these shortcomings, Arturo Tena – Colunga et al. [10] proposed an equation which was based on the experimental results conducted on all the non-prismatic beam. All these test data were checked according to the ACI code. To calculate the effective depth at the critical section, graph was plotted between $\dfrac{V_c}{\sqrt{f_{ck}}.b.d_{min}}$ against the tangent of the angle of inclination. A proposed linear regression led to the critical depth formula as shown below

$$d_{cr} = d_{min}.\left(1+1.35\tan\left(\alpha\right)\right) \leq \left[\left(\frac{h_{max}.h_{min}-h_{max}^{2}}{2l_{h}}+h_{max}\right)-c\right]\ldots\ldots\ldots\ldots(2.12)$$

where,

27

V_c = Shear capacity contributed by concrete calculated according to ACI Code

f_{ck} = Concrete cylinder compressive strength

b = width

d_{min} = minimum effective depth

d_{cr} = effective equivalent depth at the critical section

h_{max} = Maximum height

h_{min} = Minimum height

l_h = Haunch length

c = Concrete cover

The limiting value of the formulated effective equivalent depth is to assure that a realistic value is considered, so that the numerically obtained value of the effective depth should not be greater than the maximum effective depth. The shear capacity formulation for the haunched beam is given by

$$V_{Rd} = V_c + V_s - \frac{M_{cr}}{d_{cr}}\tan(\alpha)..............(2.13)$$

where,

$M_{cr} = 0.15.M_n.(1 - 2.5\tan(\alpha))..........$(For beams without shear reinforcement)

$M_{cr} = 0.5.M_n.(1 - 1.6\tan(\alpha))........$(For beams with shear reinforcement)

M_n = Nominal Bending Moment at that section as if the beam were to fail in flexure

$$V_s = \frac{A_{sv}.f_{yvd}.d_{cr}}{s.\tan(45 - \alpha)}$$

The critical bending moment depends on the nominal bending moment which is calculated such that the beam would fail in flexure. This can be done by using the equivalent stress block mentioned in ACI 318-05 [2]. The exact equation to calculate M_n was not mentioned in the article published by the authors. The equation for the contribution of stirrups by the shear capacity is different as compared to the prismatic section. The author assumed that the shear crack angle θ is equal to 45-α. This was done for practical purposes and for consistency with the design of prismatic sections. This assumption might not be true in some cases. It was seen in the beam models tested by Debaiky et al. [5] that the shear crack angle for positively haunched beam could be as low as 15º and the assumption mentioned by authors would not reach such a small value. Nevertheless, the authors checked the above formula with the limited experimental data and the results are quite satisfactory. The mean and the standard deviation for the reinforced concrete haunched beam with shear reinforcement, for the ratio between the analytical to experimental result, is 0.887 and 0.17 respectively and for the haunched beam without shear reinforcement it is 0.879 and 0.286 respectively.

2.4.7 Shear Behaviour of Non – Prismatic Steel Reinforced Concrete Beams – John J. Orr et al. [11]

John J. Orr et al. [11] studied the shear behaviour of non-prismatic steel reinforced concrete beams. The authors designed non-prismatic beams based on different model – Truss Model or the Eurocode model (EC2), the compressive force path (CFP) model and the strut and tie model (STM).

The Eurocode model states that when the cross-section forces are inclined, the vertical component of the 'yielded' inclined tensile tie or inclined compression chord should be

considered in the shear resistance of the beam. 4 positively haunched beams were designed and constructed using this concept as shown in Figure 39.

The compressive force path method (CFP) was first invented for prismatic beams and is applied by considering two failure modes – ductile flexural failure and the brittle flexural-shear failure. For shear failure, the equation of the moment resistance and the shear capacity is known which depends on the effective depth. For non-prismatic members, the beam is divided into different sections and the effective depth is calculated, using the plain section theory, as the design shear force is known. Once the effective depth is known, the bending moment resistance, corresponding to the shear failure, and the shear capacity can be calculated. The point where the shear capacity is greater than the applied shear force, the iteration can be stopped and the effective depth will be obtained at that particular section. By doing so, a graph of the applied moment and the shear force, the moment and the shear force corresponding to flexural failure and the moment and the shear force corresponding to shear failure is plotted. Using this, curved beams were designed with shear failure and flexural failure as shown in Figure 40.

The Strut and tie model (STM) is differentiated from the EC2 model as it does not require the steel reinforcement to be yielded in the tapered section, unless the tapered area is in the maximum bending moment zone. The effective depth, at the point of maximum bending moment zone, is calculated that will ensure that the area of longitudinal steel reinforcement is yielded in this location. Tensile tie is formed at each point by joining the adjacent nodes. Using the equilibrium at each node, the vertical component of the inclined tensile reinforcement is calculated and hence the beams are designed as shown in Figure 41.

11 non-prismatic beams – 4 beams of EC2 model, 4 of CFP model and 3 of STM model were tested 19 times such that one side with the flexural failure and the other side with the shear failure as shown in Figure 38. The beam dimensions are given in Table 12. The width of all the beams was equal to 110 mm. Two high yield U-bars of 10mm diameter were used as bottom reinforcement and two 3mm diameter were used as top reinforcement. The mean concrete cylinder strength was 43.9 MPa with a standard deviation of 3.8 MPa. The characteristic yield strength is 500 MPa and the mean yield strength is 562 MPa. The length of all the specimen was equal to 2000 mm. The beams designed using CFP are curved beams as can be seen from Figure 40. Table 13 gives the design load, the load achieved in tests and the failure mode for all the specimen. Note that all the beams, except 1-EC2 and 1-CFP, were subjected to two test setups – one that fails in shear and the other that fails in flexure.

Table 12 Descripiton of beams tested by John J Orr et al. [11]

Specimen	Height at the support (mm)	Height at the centre (mm)	Angle of inclination (degrees)
Beam 1-EC2	60	220	9.09
Beam 2-EC2	60	198	15.43
Beam 3-EC2	60	129	12.95
Beam 4-EC2	60	82	8.34
Beam 1-CFP	70	220	8.53
Beam 2-CFP	70	214	-
Beam 3-CFP	70	181	-
Beam 4-CFP	70	158	-
Beam STM	70	208	15.43
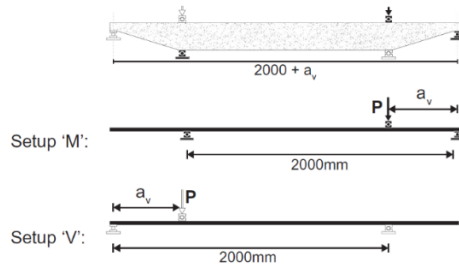
Figure 38 Flexural (M) and Shear(V) failure setup respectively [11]
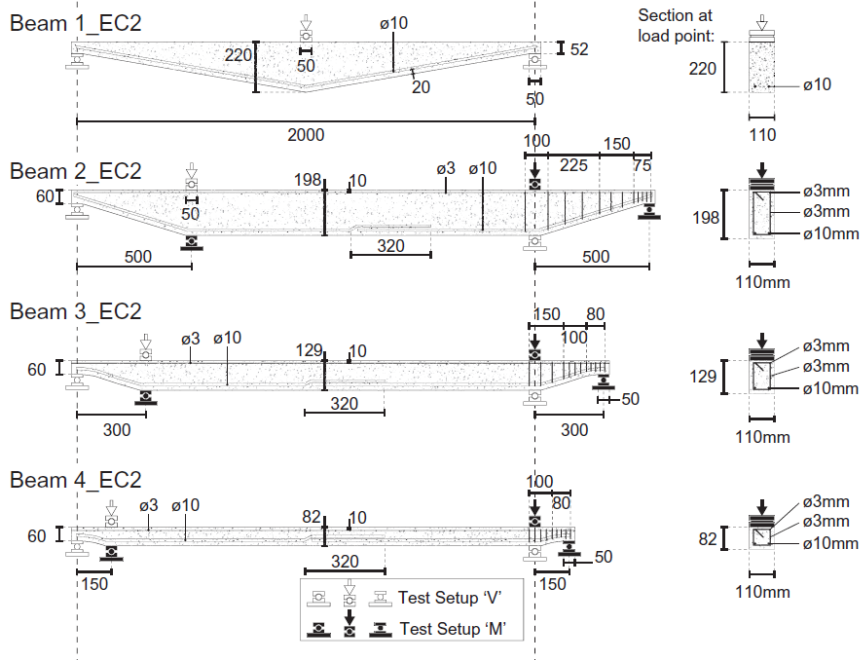
Figure 39 EC2 beam specification tested by John J. Orr et al. [11]
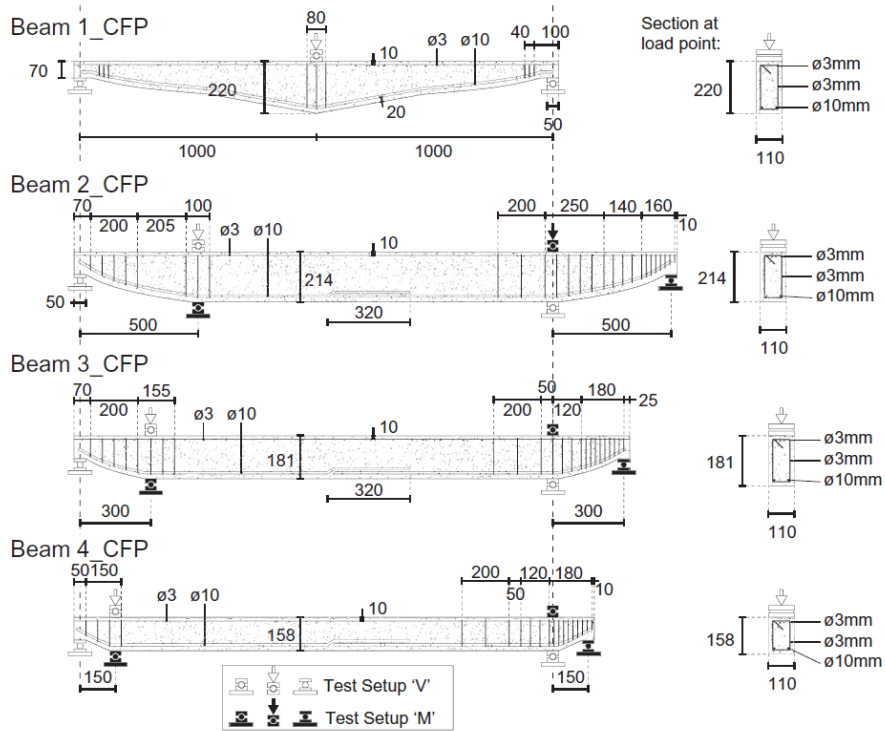
Figure 40 CFP beam specification tested by John J. Orr et al. [11]
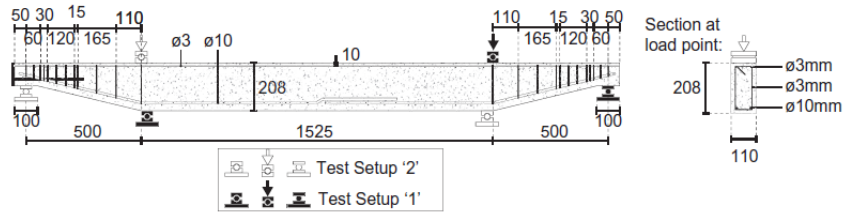
Figure 41 STM beam specification tested by John J. Orr et al. [11]

Table 13 Maximum Load and Faliure mode of all the specimens tested by John J. Orr et al. [11]

Specimen	Percentage of Shear Reinforcement (%)	Design Maximum Load (kN)	Maximum Load achieved (kN)	Failure Mode
1-EC2-V	0.00	32	19	Shear
2-EC2-V	0.00	36	28.2	Shear
2-EC2-M	0.28	36	32.1	Shear
3-EC2-V	0.00	31.8	17.1	Shear
3-EC2-M	0.47	31.8	18.8	Shear
4-EC2-V	0.00	29.2	26.1	Shear
4-EC2-M	0.69	29.2	9.6	Anchorage
1-CFP-V	0.06	32	29.6	Shear
2-CFP-V	0.18	36	46.9	Flexure
2-CFP-M	0.41	36	48.6	Flexure
3-CFP-V	0.26	31.8	43.8	Shear
3-CFP-M	0.56	31.8	31.5	-
4-CFP-M	0.77	29.2	28.7	-
STM_1(i)	0.31	36	41.8	Shear/Flexure
STM_2 (i)	0.31	36	41.5	Shear/Flexure
STM_1 (ii)	0.31	36	38.7	Flexure
STM_2 (iii)	0.31	36	37.9	Flexure
STM_1 (iii)	0.31	36	37.4	Flexure
STM_2 (iii)	0.31	36	40.6	Flexure

From Table 13 it can be seen that the beams designed using the EC2 concept are not conservative, with a mean value of the ratio between the load achieved in tests to the design load to be 0.66. Whereas the non-prismatic beams designed using the CFP and STM method has a mean value of 1.16 and 1.1 respectively, which proves that designing the beam using these two concept leads to conservative results. The load deflection graph for all the beams was also plotted. It was seen that the beams designed using EC2 concept failed in a brittle manner whereas the beams designed using the concept of CFP and STM method showed ductility in their behaviour as shown in Figure 42, Figure 43 and Figure 44 respectively.
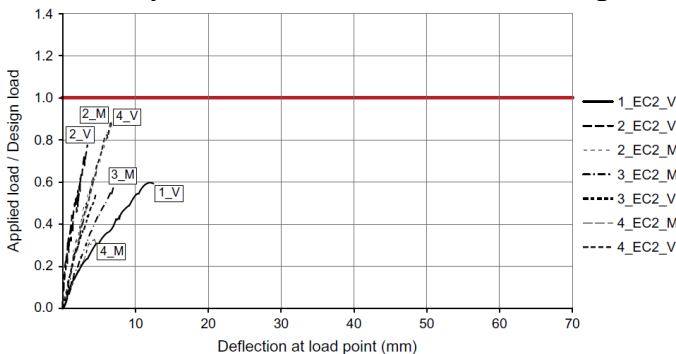
Figure 42 Load-Deflection curve for EC2 beams [11]
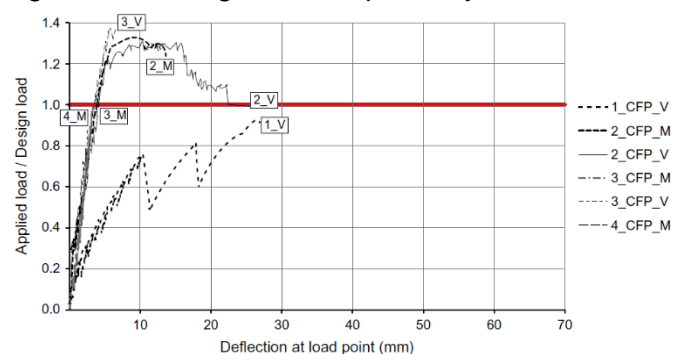
Figure 43 Load - Delfection curve for CFP beams [11]
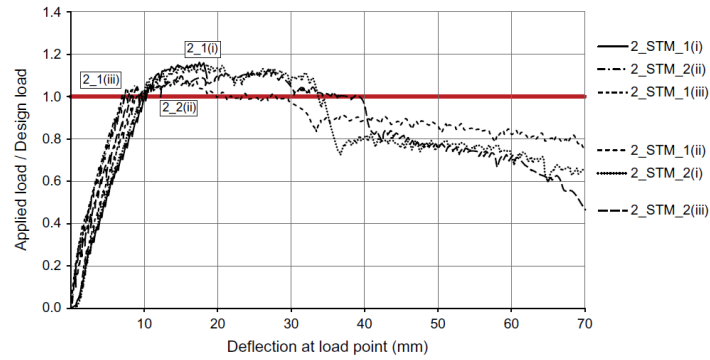
Figure 44 Load - Deflection curve for STM beams [11]

Digital Image Correlation (DIC) was used in all the beams to check the strain distribution and the cracking pattern. The EC2 beams cracked initially at the support, where the principal strain ε_1 was higher, and then propagated towards the point of application of load. In the Strut and tie model, cracking starts at the midpoint of the tapered section and spread across the loading point. In the beams designed using CFP method, the cracking started beneath the loading point and advanced across the tapered zone. In both the CFP and the STM model the area of tension zone moved towards the loading point, unlike the EC2 model and this was also seen from the strain distributions over the tapered area.

The reason behind the brittle, unstable and the shear critical design of EC2 model is because it was proposed that the inclined longitudinal reinforcement will carry both the entire shear force as well as the bending moment. From the results, it was seen the shear capacity of the beam did not increase even after providing transverse reinforcement in the specimens that where designed to fail in flexural. Also the difference between the maximum load achieved for the shear type of failure and the flexural type of failure is negligible for the same specimen as can be seen from Table 13.

On the contrary, the beams designed using the strut and tie model showed good coherence to the experimental data. Strut and tie model, unlike the EC2 model, does not consider the longitudinal reinforcement to be yielded everywhere in the beam but considers the actual force in the inclined longitudinal reinforcement in the tapered zone. Moreover all the STM specimens failed in flexure, leading to a ductile behaviour and less shear dominant design. But from the experiments the author concluded that the STM beams failed close to the brittle manner and that CFP was the ideal way for a conservative and a better ductile failure.

2.4.8 Remarks on the current theory of Shear Strength of Variable Depth Beams – A. Pagletti et al. [12]

A. Pagletti et al. [12] studied on the remarks on the current theory of shear strength of variable depth beams. The author explains the theory of shear stress in prismatic and non-prismatic beams and explains the origin. According to the ACI 318-05 [2], the vertical component of the inclined flexural stresses increases or decreases the shear strength of the beam. The author suggests that this in fact should not be the case and presents few paradoxes to prove this.

    I.   Paradox – 1

Consider the cantilevered beams shown in Figure 45, where Figure 45(a) is the cantilevered tapered beam whereas Figure 45(b) is a prismatic beam, such that the maximum depth of both the beams is the same. Let $\bar{P}_u$ and P_u denote the loading capacity of the tapered and the prismatic beam respectively. The beam will fail in shear if the applied load is greater than load capacity. Now according to the codes present worldwide, it can be concluded that the load required to produce a shear failure in the tapered beam $\bar{P}_u$ will be greater than the load

required to produce a shear failure in the prismatic beam P_u. However the prismatic beam is constructed by adding material to the non-prismatic beam as can be seen from the dotted area in Figure 45(b). This means that the amount of material used in the prismatic beam is greater than the non-prismatic beam and therefore the ultimate load of the former should not be less than that of the latter. The author states that this is both common sense and also the consequence of the lower bound theorem of limit analysis which states that "The collapse load cannot be decreased by increasing the strength of any part of the beam". But if the concept of effective shear force is used, it can be seen that the vertical component of the inclined compression chord increases the shear capacity of the cantilevered tapered beam and therefore it is capable of resisting higher load than the prismatic beam, which, according to the author, should not be the case.
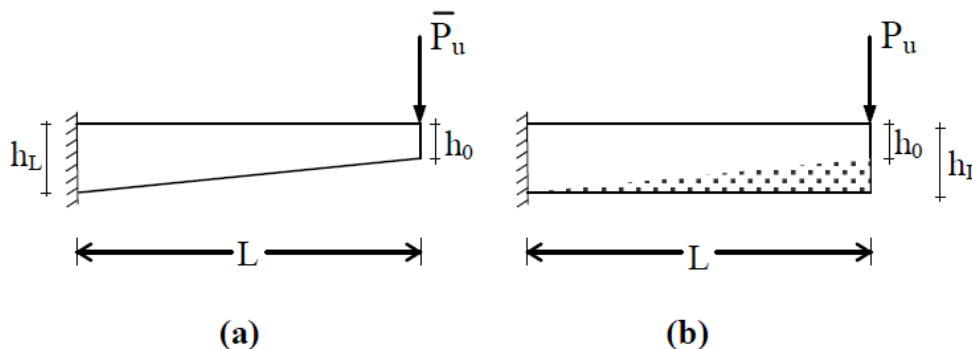
Figure 45 Comparison of non-prismatic and prismatic cantilevered beam [12]

II.   Paradox – 2

Consider the simply supported tapered beam shown in Figure 46. Figure 46 also shows the shear force diagram for the beam obtained due to the applied load (P), where R_A and R_B are the reaction forces at the two supports. The author states that after considering the vertical component of the inclined tensile tie, the effective shearing force V* would be greater or lesser than applied shear force V_s, as it depends on which side the cross-section analysis is performed. Moreover the shear force diagram will be changed even though there is no applied load other than 'P', which violates the equilibrium of the beam.
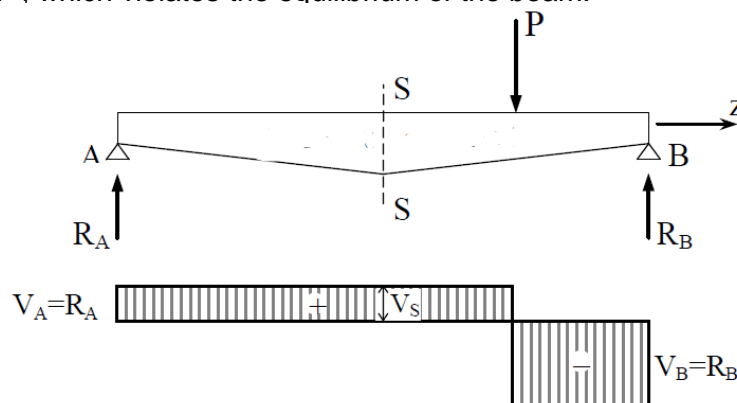
Figure 46 Shear force diagram of positively haunched beam [12]

III.   Paradox-3

Consider the cantilever non-prismatic beam shown in Figure 47. θ' is the angle of taper and C' is the force in the compression chord. Consider the cross-section S-S at the midpoint of the beam. When forces from the left side of the beam are considered, the vertical component, acting in the upward direction, of the inclined compression chord (C'), $\Delta V = C'.\tan(\theta)$, would increase the shear force. But according to the author, the vertical component of the inclined compression chord (-C') from the right side of the beam, which is acting in the downward direction, would negate this force and no net reduction in the applied shear force will be seen.

33
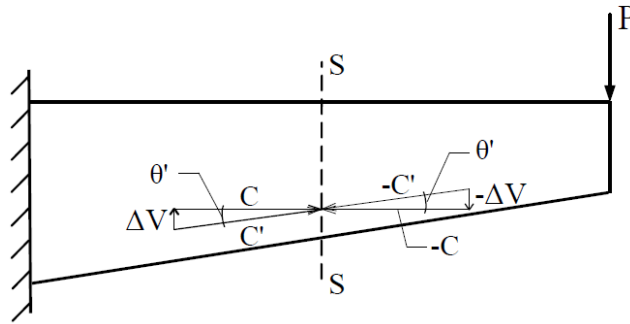
Figure 47 Non-Prismatic cantilevered beam with cross-sectional analysis [12]

IV.   Paradox – 4

This paradox is similar to the first paradox. Consider the constant depth beam and the non-prismatic beam shown in Figure 48 which are subjected to uniformly varying load, such that the ultimate shear strength of the beam is achieved. If the concept of effective shear force is valid, then the load bearing capacity of the beam would certainly increase by reducing the material and providing haunch near the support i.e. Figure 48(b) would have a higher load carrying capacity than Figure 48(a). According to the author this is completely unrealistic and is also the consequence of the lower bound theory of the limit analysis as stated previously.
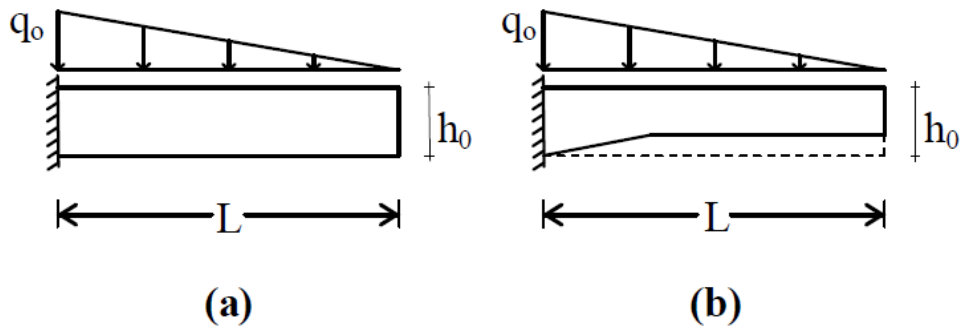
Figure 48 Prismatic and non-prismatic beam subjected to uniformly varying load [12]

3 Cross – Sectional Analysis of Prismatic Beam

This chapter studies different approaches to perform cross-section analysis on an inclined cut that can be applied on prismatic beams which is subjected to four point bending test. Prismatic beams are then modelled in DIANA and the cross-section results on inclined cuts are calculated and further discussed.

3.1 General Procedure
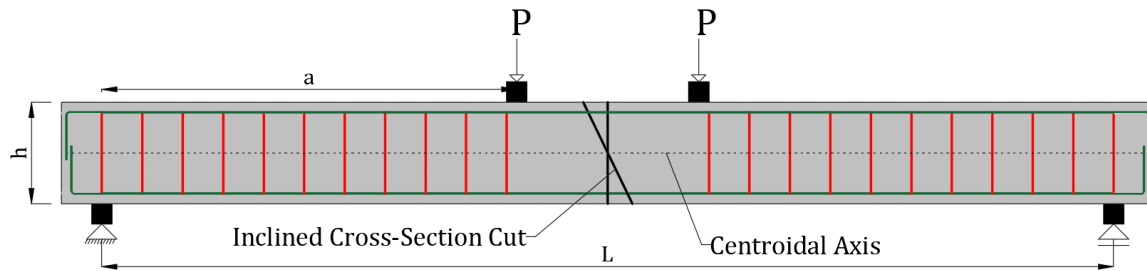
Figure 49 Prismatic beam subjected to four point bending test

Consider the prismatic beam shown in Figure 49 with length L and height h, subjected to four point bending test, with the point loads applied at a distance 'a' from the support. Top and bottom reinforcement are placed over the width 'b' of the beam. Stirrups are provided in the shear span of the beam. The cross-sectional analysis is performed at the point of maximum bending moment i.e. at the centre. This analysis is performed, assuming that sufficient shear reinforcement is provided to avoid shear failure and also the applied load produces a ductile flexural behaviour in the beam. To perform the cross-sectional analysis, a vertical cross section cut is made at the centre of the beam and the normal forces acting on this section are shown in Figure 50. Note that a bi-linear constitutive model is used for concrete as given in Figure 3.4 of the Eurocode 1992-1-1 [1].
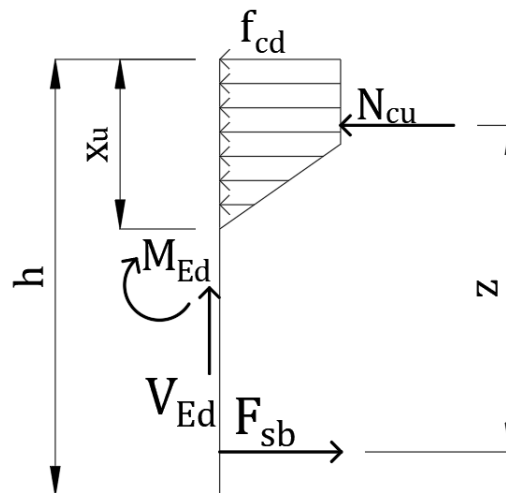
Figure 50 Cross-Sectional analysis in the zone of maximum bending moment

where,

x_u = height of the compression zone.

h = Height of the beam

z = Lever arm

V_{ed} = Applied Shear Force = 0 in this case

f_{cd} = Design concrete compressive strength

N_{cu} = Concrete Compressive force

F_{sb} = Steel force due to bottom reinforcement = $A_{sb}.f_{yd}$

A_{sb} = Area of bottom reinforcement

f_{yd} = Yield Strength of the reinforcement present

M_{Ed} = Applied Bending Moment = $P.a$

The top reinforcement is placed to hold the stirrups in position. Steel force due to the reinforcement placed in the compression side provides negligible contribution to the bending moment resistance and hence is neglected. If the point of application of the concrete force is known, the bending moment resistance can be calculated. The two horizontal forces acting in the cross-section cut are the steel force F_{sb} and the concrete compressive force N_{cu}. Considering the horizontal equilibrium for the above mentioned cross-section cut,

$$\sum H = 0$$
$$F_{sb} = N_{cu} ....(3.01)$$

The definition of the concrete compressive force is the area of the cross-section cut under which the compressive stresses are acting, multiplied with the design concrete compressive strength. From the stress block,

$$N_{cu} = \frac{3.f_{cd}.b.x_u}{4} ....(3.02)$$

The equation for the horizontal equilibrium can be rewritten as,

$$A_{sb}.f_{yd} = \frac{3.f_{cd}.b.x_u}{4}$$
$$x_u = \frac{4.A_{sb}.f_{yd}}{3.f_{cd}.b} = \frac{4.F_{sb}}{3.f_{cd}.b} ....(3.03)$$

When two equal forces acts in the opposite direction, a moment is produced which is equal to the magnitude of force multiplied by the distance between the two forces. Similarly, in this case also a moment is generated which is given as,

$$M_{Rd} = \text{bending moment resistance} = F_{sb}.z = M_{Ed}$$
$$M_{Rd} = A_{sb}.f_{yd}.z$$
$$z = \text{Lever arm} = \left(h - c - \phi_{stirrup} - \frac{\phi_{bot}}{2} - \frac{7.x_u}{18} \right) = \left(d_{eff} - \frac{7.x_u}{18} \right) = \left(d_{eff} - \frac{14.F_{sb}}{27.f_{cd}.b} \right)$$
$$M_{Rd} = A_{sb}.f_{yd}.\left(d_{eff} - \frac{14.F_{sb}}{27.f_{cd}.b} \right) ....(3.04)$$

where,

$c = $ Concrete cover

$\phi_{bot} = $ Diameter of bottom reinforcement

$\phi_{stirrup} = $ Diameter of stirrups

The term $\frac{7.x_u}{18}$ in the lever arm is the point of application of the concrete compressive force from the top part of the section. As the height of the concrete compressive zone is known, the bending moment resistance can be calculated. None of the internal forces are acting at an angle to the cross-section cut and hence the equation of shear resistance is unaffected. Note that in this case a vertical cross section cut is made to calculate the bending moment resistance .Now, the cross-section cut is made at an angle (α) as shown in Figure 49. According to structural mechanics, the cross-section results should not change irrespective of how a cross-section cut is projected on the beam. Also the beam does not know how the cross-section cut is made and therefore the results should remain the same.

3.2   Approaches for Cross-Sectional Analysis of Prismatic beam

Initially, different approaches were proposed for an inclined cross-section cut where the applied shear force was also taken into account by the moment resistance of the beam. All these approaches did not sound convincing as the bending moment resistance changed with the increase in the inclination of the cut as shown in Appendix A. However, the following approaches shows promising outcome and will be discussed further.

3.2.1 Approach 1 – Vertical Compressive zone with Forces in Global direction

Figure 51 shows the stress distribution and forces acting on an angled cut. The concrete compressive force is defined as the area, under which the compressive stresses are acting, multiplied with the concrete compressive strength. Note that here, the concrete compressive zone $x_{u,1}$ is considered in the vertical direction. According to the definition, the equation of compressive force $N_{cu,1}$ is given as,

$$N_{cu,1} = \frac{3.f_{cd}.b.x_{u,1}}{4.\cos(\alpha)}........(3.05)$$
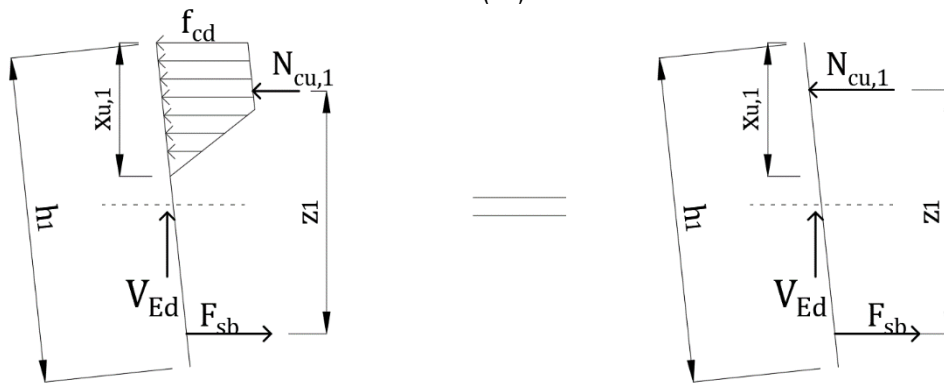
Figure 51 Stress distribution and forces in the global direction on an angled cut with vertical compression zone in prismatic beam

The vertical compression zone $x_{u,1}$ is decomposed in the inclined direction, as the stresses are acting on this angled length, and the force is further calculated. As these inclined cuts are performed in the constant bending moment zone of the prismatic beam shown in Figure 49, the concrete compressive force (or the compressive zone) should be constant. But this is not the case as the equation of $N_{cu,1}$ (equation 3.05) is not the same as that of N_{cu} (equation 3.02). This leads to violation of the horizontal equilibrium , as the steel force (F_{sb}) is constant but the compressive force obtained in this case ($N_{cu,1}$) is greater than that obtained when the cross-section cut was vertical (N_{cu}) i.e. $N_{cu,1} > F_{sb}/ N_{cu}$. This inconsistency is due to the definition of

the compressive force and the inclined compression zone $\dfrac{x_{u,1}}{\cos(\alpha)}$ .In order to take into

account the increased length of the concrete compressive zone, $N_{cu,1}$ is multiplied with the cosine of the angle of inclination and the analysis is then performed as shown in Figure 52.
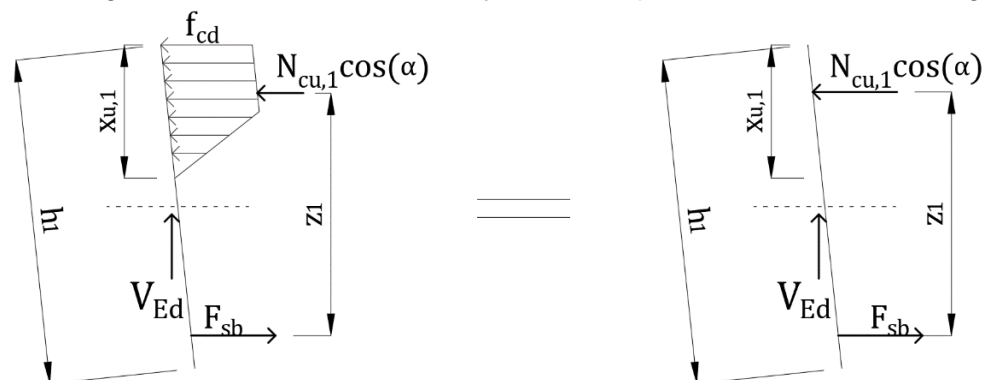
Figure 52 Revised stress distribution and forces in the global direction on an angled cut with vertical compression zone in prismatic

Horizontal Equilibrium for the angled cross-section cut, shown in Figure 52, is

$$\sum H = 0$$

$$N_{cu,1}.\cos(\alpha) = F_{sb}........(3.06)$$

The equation of the compressive force and vertical compressive zone is given as

$$N_{cu,1} = \frac{3.f_{cd}.x_{u,1}.b}{4.\cos(\alpha)}$$

$$x_{u,1} = \frac{4.F_{sb}}{3.f_{cd}.b} = x_u........(3.07)$$

The bending moment resistance is equal to the steel force multiplied with the lever arm as,

$$M_{Rd} = F_{sb}.z_1$$

$$z_1 = d_{eff} - \frac{7.x_{u,1}}{18} = d_{eff} - \frac{14.F_{sb}}{27.f_{cd}b}$$

$$M_{Rd} = F_{sb}.\left(d_{eff} - \frac{14.F_{sb}}{27.f_{cd}.b}\right)........(3.08)$$

The equation of bending moment resistance (equation 3.08), when the analysis is performed on an inclined cut (α), with a vertical compressive zone, is similar to that obtained when the analysis is performed on a vertical cut as shown in equation 3.04. The concrete compressive force is reduced by the cosine of angle of inclination which takes into account the increased length of the compression zone, keeping the force, bending moment resistance and the horizontal equilibrium in check. Also the equation of the vertical compression zone (equation 3.07) using this approach is constant and equal to that shown in general procedure (Section 3.1, equation 3.03).

3.2.2 Approach 2 – Inclined Compression Zone with Forces in Global direction

The stress distribution and the cross-section forces in this approach are similar to the one shown in Figure 52. The only difference is the definition of the compressive zone – in this case the compression zone $x_{u,2}$ is inclined as seen from Figure 53. However the lever arm is considered in the vertical direction (z_2). In this case as well, the compressive force is reduced by the cosine of the angle of inclination, to negate the increase in the length of the cross-section cut.

The procedure to calculate the bending moment resistance is applied in this case

$$M_{Rd} = F_{sb}.z_2$$

$$z_2 = d_{eff} - \frac{7.x_{u,2}.\cos(\alpha)}{18}$$

$$\sum H = 0$$

$$N_{cu,2}.\cos(\alpha) = F_{sb}$$
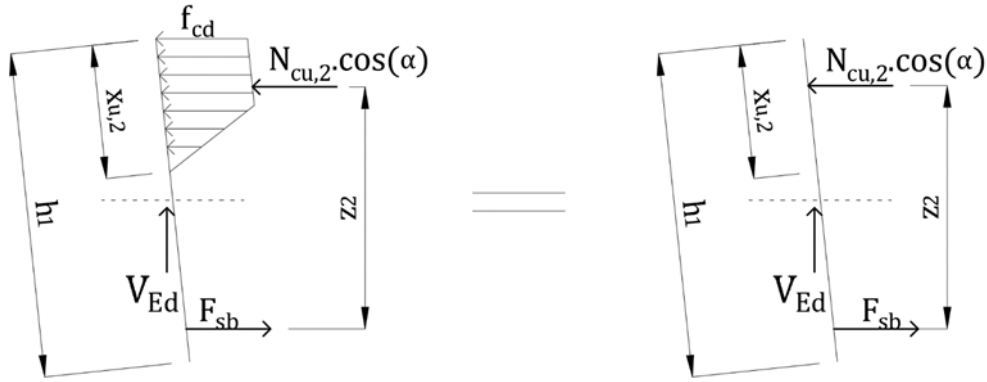
Figure 53 Stress distribution and forces in the global direction in an angled cut with inclined compression zone in prismatic beam

$$N_{cu,2} = \frac{3.f_{cd}.b.x_{u,2}}{4} \quad........(3.09)$$

$$x_{u,2} = \frac{4.F_{sb}}{3.f_{cd}.b.\cos(\alpha)} \quad........(3.10)$$

$$M_{Rd} = F_{sb}.\left(d_{eff} - \frac{7.x_{u,2}.\cos(\alpha)}{18} \right)$$

The equation of the vertical distance of this inclined compressive zone ($x_{u,2}.\cos(\alpha)$), obtained from the horizontal equilibrium, is similar to the equation of the vertical compressive zone (equation 3.03 and 3.07) calculated in Section 3.1 and Section 3.2.1. To calculate the point of application of concrete compressive force, and subsequently the lever arm, the inclined compressive zone is first decomposed in the vertical direction, by multiplying with the cosine of the angle of inclination, and then the factor of $\frac{7}{18}$ is applied. After substituting the equation of compressive zone in the bending moment equation, the following is obtained.

$$M_{Rd} = F_{sb}.\left(d_{eff} - \frac{14.F_{sb}}{27.f_{cd}.b} \right) ....(3.11)$$

Here also it can be seen that the equation of bending moment resistance for an angled cut with inclined compressive zone is similar to that obtained from the vertical cross-section cut.

3.2.3 Approach 3 – Inclined Compression Zone with Forces in Local direction

In this approach, the forces present in Figure 53 are decomposed such that one component is in the perpendicular direction, while the other is aligned in the parallel direction of the cross-section cut as shown in Figure 54. Equilibrium is checked in the direction perpendicular to the cross-section cut and the component, which is decomposed in the parallel direction, is considered in the shear capacity or the applied shear force. The lever arm and the compressive zone both are inclined as seen in Figure 54.

$$M_{Rd} = F_{sb}.\cos(\alpha).z_3$$

$$z_3 = \frac{d_{eff}}{\cos(\alpha)} - \frac{7.x_{u,3}}{18}$$
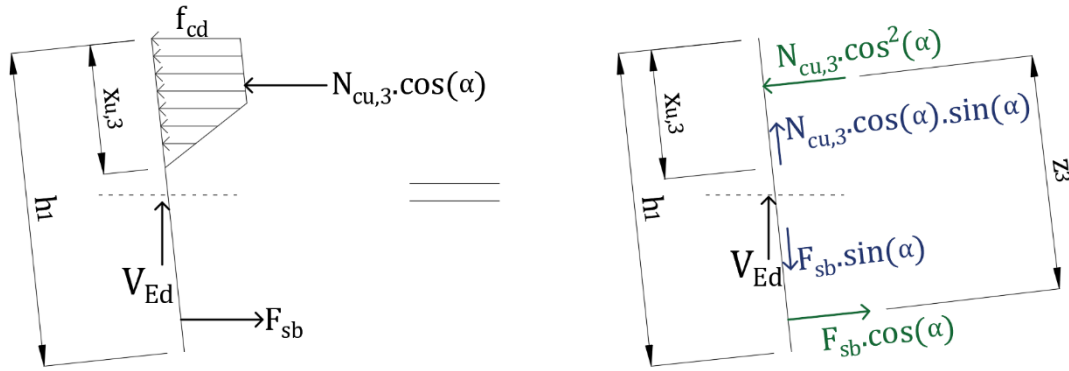
Figure 54 Stress distribution and forces in the local direction on an angled cut with inclined compression zone in prismatic beam

$$\sum H_{perpendicular} = 0$$

$$N_{cu,3}.\cos^2(\alpha) = F_{sb}.\cos(\alpha)$$

$$N_{cu,3} = \frac{3.f_{cd}.b.x_{u,3}}{4} \quad ....(3.12)$$

$$x_{u,3} = \frac{4.F_{sb}}{3.f_{cd}.b.\cos(\alpha)} \quad ....(3.13)$$

$$M_{Rd} = F_{sb}.\cos(\alpha).\left(\frac{d_{eff}}{\cos(\alpha)} - \frac{7.x_{u,3}}{18}\right)$$

$$M_{Rd} = F_{sb}.\cos(\alpha).\left(\frac{d_{eff}}{\cos(\alpha)} - \frac{14.F_{sb}}{27.f_{cd}.b.\cos(\alpha)}\right)$$

$$M_{Rd} = F_{sb}.\left(d_{eff} - \frac{14.F_{sb}}{27.f_{cd}.b}\right) \quad ....(3.14)$$

The forces in the parallel direction are given as,

$$C = \text{resultant force in the parallel direction} = F_{sb}.\sin(\alpha) - N_{cu}.\cos(\alpha).\sin(\alpha)$$

$$C = F_{sb}.\sin(\alpha) - F_{sb}.\sin(\alpha) = 0 \text{....as } N_{cu}.\cos(\alpha) = F_{sb}$$

From the above calculation it can be seen that there is no shear force in the direction parallel to the cross-section cut. Also the equation of the inclined compressive zone (equation 3.13) is similar to that obtained from the previous approach (equation 3.10). Moreover, in this approach, the steel force is reduced and the lever arm is increased, by the same amount, and therefore the equation of bending moment resistance remains same.

3.3   DIANA Models
The use of DIANA was made to validate the outcome of all the above three approaches. Beams are designed using hand calculations and are then analysed in DIANA. Models are then examined for different angle of inclination with the stresses directed in the local (perpendicular and parallel direction) as well as in the global direction. The beams analysed are subjected to four point bending test and cross-section analysis is performed at the centre of the beam.

3.3.1 Model – 1
Beam description for the 1st Model is given in Table 14. The material description for the same model is given in Table 15.

Table 14 Beam Description for DIANA Model-1

Description	Value	Unit
Length	6400	mm
Span (L)	6000	mm
Height (h)	350	mm
Width (b)	200	mm
Concrete cover (c)	35	mm
Diameter of two legged stirrup ($\varphi_{stirrup}$)	8	mm
Spacing of two legged stirrup (s)	250	mm
Diameter of bottom reinforcement (φ_{bot})	12	mm
Area of bottom reinforcement (A_{sb})	452.39	mm^2
Shear span (a)	2000	mm
Effective depth(d_{eff})	301	mm

Table 15 Material Description for DIANA Model-1

Description	Value	Unit
Characteristic concrete compressive strength (f_{ck})	20	MPa
Design concrete compressive strength (f_{cd})	13.33	MPa
Design concrete tensile strength (f_{ctd})	1.03	MPa
Design yield strength of steel (f_{yd})	411	MPa
Young's Modulus of concrete (E_c)	23663.8	MPa

As the amount of reinforcement and the yield strength of the steel is known, the steel force due to bottom reinforcement can be calculated. By using the procedure and the formulations mentioned in Section 3.1, the load bearing capacity of the beam can be determined by performing cross-section analysis, on a vertical cut, at the centre of the beam. The stress distribution and forces are similar to the one shown in Figure 50. All the symbols are mentioned in Section 3.1.
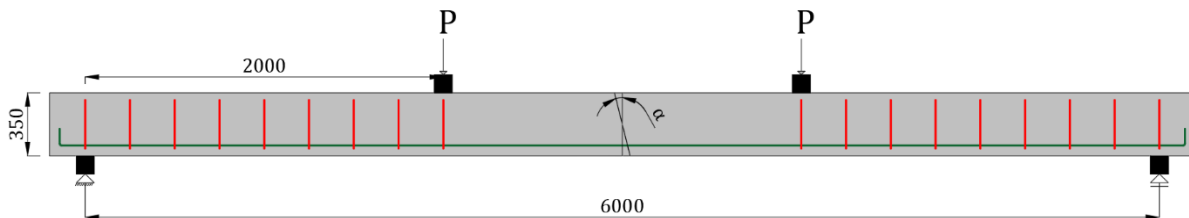
Figure 55 Beam dimensions for DIANA model-1

Steel Force $F_{sb} = A_{sb}.f_{yd} = 185.93$ kN

Now, $\sum H = 0$

$N_{cu} = F_{sb} = 185.93$ kN

$x_u = 92.96$ mm

$M_{Rd} = F_{sb}.\left(d_{eff} - \frac{7.x_u}{18} \right) = 48.49$ kNm

Design load $= \dfrac{M_{Rd}}{a} = 24.25$ kN

Now, the beam is modelled in DIANA with the given specifications. The concrete constitutive model used in the analysis is shown in Figure 56 and Figure 57.
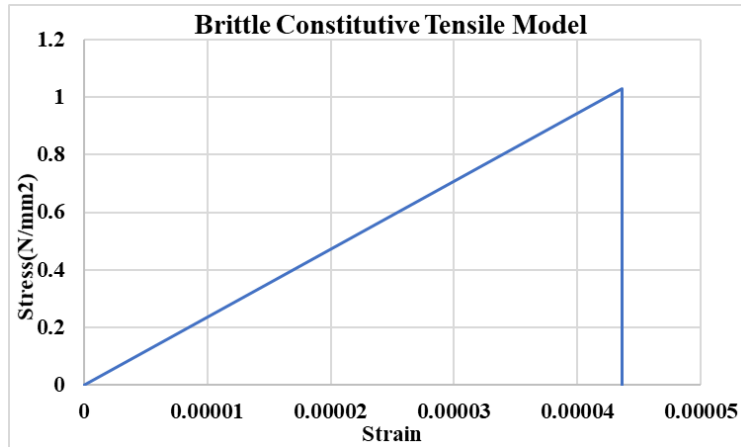
Figure 56 Tensile constitutive model for concrete
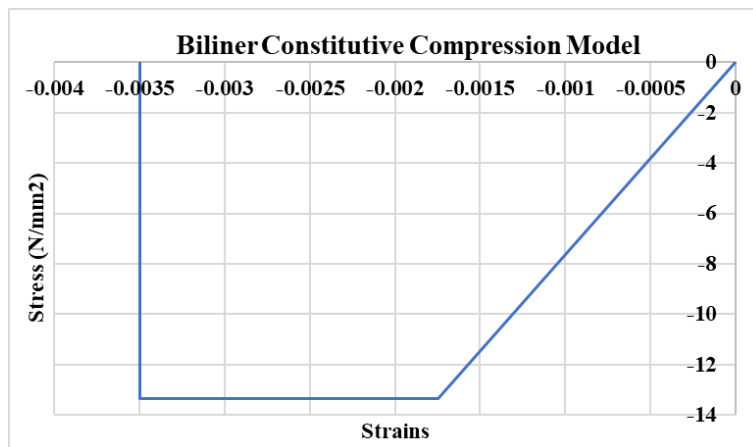
Figure 57 Compressive constitutive model for concrete

The reason behind the use of the brittle tensile constitutive model and the bilinear constitutive model was to compare the analytical results. The effect of Poison's ratio is neglected in all the analysis. Displacement controlled analysis was performed in all the models. Interface was used at the connection between the steel plate and the beam. No hardening was allowed in the steel reinforcement. Linear elastic properties were assigned to the steel plates. The load steps used are 0.5(20), 0.2(350). Detailed convergence criteria is mentioned in Table 16.

Table 16 Convergence criteria

Norms	Criteria
Energy norm	0.001
Force norm	0.01
Satisfaction of all norms was not included in the analysis	

For each angle of inclination a new model was constructed in DIANA, with the desired line imprinted on the beam, and the model was then analyzed as shown in Figure 58. The local axis of the elements were aligned such that the local x-axis of all the element is perpendicular to the inclined cut and the local y-axis of all the element is parallel to the inclined cross-section cut.
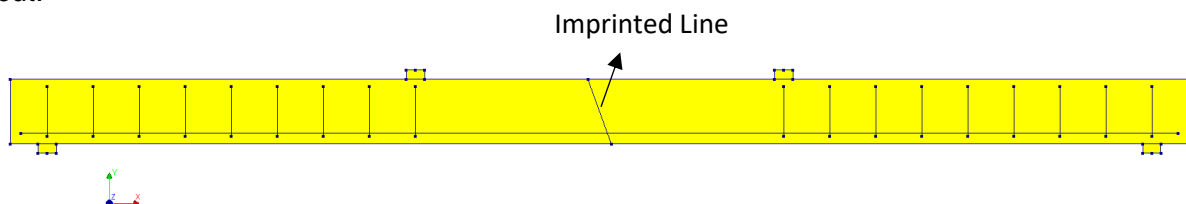
Figure 58 An example of the line imprinted on the beam (20 degree of angle of inclination)

To check the analytical calculations, a simple model with a vertical line imprinted in the center of the beam was first analyzed. The Load-Deflection curve is shown in Figure 59. The maximum deflection, obtained at the center of the beam, is considered in the graph. The little hiccup in the graph can be attributed to the beginning of the non-linearity i.e. cracking begins after point A. The maximum load that the beam can sustain is 23.58 kN, which is almost equal to the one obtained with the analytical calculation. The structure has a lot of ductility as the concrete crushes after reaching a deflection of about 75 mm (point D). At the deflection of about 55 mm, the steel is yielded (point C). After this point the load in the graph is almost constant. At this point the stresses in the top part of the structure have reached design compressive strength, but the strain at that very location have not reached 3.5×10^{-3}. This indicates that the strain in concrete is in the constant part of Figure 57, where the strain increases but the concrete strength remains constant. Point B depicts the load case where the concrete has reached a strain of 1.75×10^{-3}. Almost all the load steps in the analysis are converged. The inclined angled cut, which is to be imprinted on the model, is made with respect to the neutral axis at the center of the beam similar to the one shown in Figure 49.
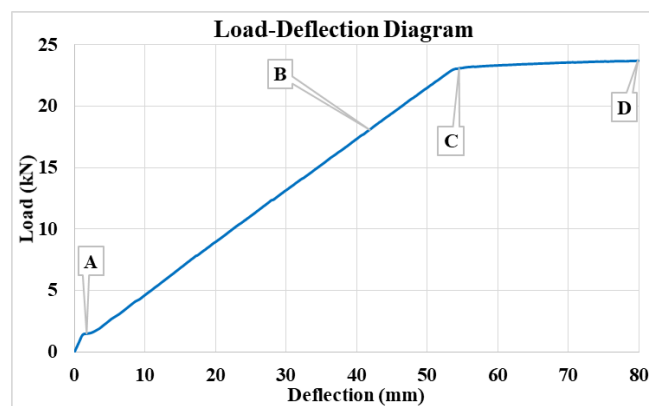
Figure 59 Load-Deflection curve

The bending moment resistance is calculated when the bottom steel reinforcement has yielded and the concrete above has reached f_{cd} i.e. at point C. To determine the compressive force, in the horizontal as well as in the perpendicular direction, the values of Local (σ_{xx}) and Global (σ_{XX}) Stresses in the X-direction along the desired line are plotted. An example of this is shown in Figure 60 for an angle of inclination of 20 degrees. As mentioned earlier, the concrete compressive force (N_{cu}) is obtained by multiplying the area of the cross-section cut, under which the compressive stress act, to the concrete compressive strength. Therefore, in general, the compressive force is obtained by numerically integrating the plot of σ_{XX} along the desired height of the cross-section cut and further multiplying with the width of the beam. The force obtained by numerically integrating the plot of σ_{xx} (Local stress) will act in the direction perpendicular to the cut (Local X-Direction) whereas the force obtained by numerically integrating the plot of σ_{XX} (Global Direction) will act in the horizontal direction. To calculate the bending moment resistance, it is important to check the horizontal equilibrium (or equilibrium in the perpendicular direction) in the cross-section cut. As the amount of bottom steel reinforcement (A_{sb}=452.39 mm^2) and the yield strength of steel reinforcement (f_{yd}=411 MPa) is known, the steel force (F_{sb}) can be calculated and the equilibrium is checked. Note that, to obtain the equilibrium in the perpendicular direction of the cut, the steel force is multiplied with the cosine of the angle of inclination so that it is aligned in the Local – x direction. All these results are tabulated in Table 17.

Stress in the Global and Local X-Direction
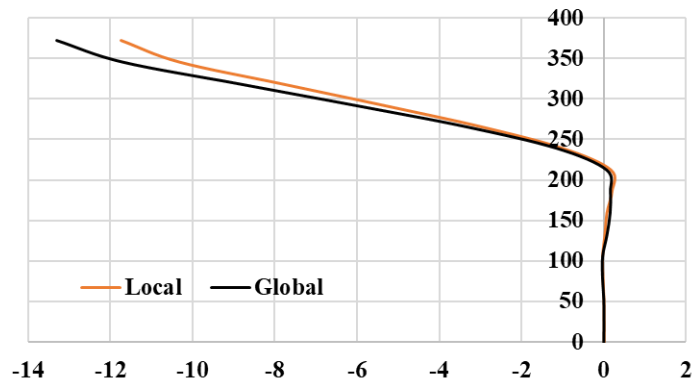
Figure 60 σ$_{xx}$ and σ$_{xx}$ for an angle of inclination of 20 degrees

Table 17 Global and local cross-section forces for different angle of inclination for DIANA model – 1

Angle (degrees)	F$_{sb}$ global (kN)	N$_{cu}$ global (kN)	F$_{sb}$ local (kN)	N$_{cu}$ local (kN)
0	185.94	-185.95	185.95	-185.68
5	186.13	-185.84	185.43	-185.06
10	186.5	-189.05	183.66	-183.37
15	186.19	-191.67	179.85	-178.90
20	186.39	-198.1	175.15	-175.28
25	186.51	-205.76	169.04	-168.41
30	186.04	-215.02	161.12	-161.48
35	186.32	-228.83	152.62	-153.20
40	186.37	-244.10	142.76	-142.87
45	186.40	-255.04	131.81	-131.85
50	186.45	-282.78	119.85	-117.81

From the data, it can be seen that as the angle of inclination increases, the difference between the steel force and the concrete compressive force in the global direction / horizontal direction keeps on increasing, and hence no horizontal equilibrium is obtained. On the other hand, the forces in the perpendicular direction of the cross-section cut are in equilibrium i.e. in the Local-x Direction. The cross-section forces on an angled cut, in the local direction, is similar to that mentioned in Figure 54 of Approach 3 (Section 3.2.3). The inclined concrete compressive zone for every cut is known, from the plot of σ$_{xx}$, and the Bending Moment resistance can be calculated which is given in Table 18. The error in the Bending Moment Resistance, due to the forces in the local direction, is plotted in Figure 61. From the figure and the numbers, it can be concluded that the Bending Moment Resistance (M$_{Rd}$) does not change when the cross-section cut is performed at different angle of inclination as was seen from the 3rd Approach (Section 3.2.3).
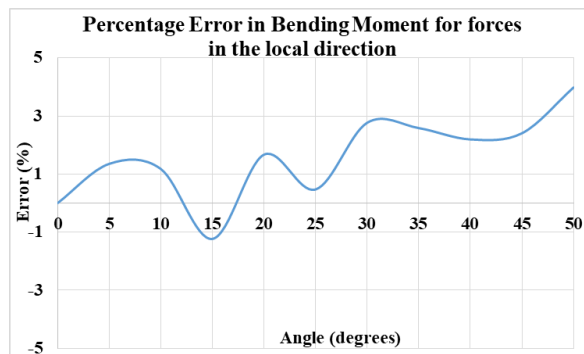
Figure 61 Percentage error in the bending moment resistance due to the forces in the local direction for DIANA model – 1

Table 18 Data in the local direction for different angle of inclination for DIANA model – 1

Angle (degrees)	F_{sb} local (kN)	N_{cu} local (kN)	$X_{u, inclined}$ (mm)	Error in Horizontal Equilibrium (%)	Moment (kN-m)
0	185.95	-185.68	154.18	0.14	44.92
5	185.43	-185.06	145.69	0.19	45.53
10	183.66	-183.37	150.12	0.16	45.45
15	179.85	-178.90	169.87	0.52	44.37
20	175.15	-175.28	153.06	-0.09	45.67
25	169.04	-168.41	168.82	0.37	45.13
30	161.12	-161.48	155.32	-0.26	46.17
35	152.62	-153.20	167.18	-0.30	46.08
40	142.76	-142.87	182.71	-0.07	45.91
45	131.81	-131.85	195.98	-0.04	46.00
50	119.85	-117.81	198.16	1.7	46.71

Interestingly, there is no equilibrium of forces in the Global-X direction. From Table 17, it can be observed that as the angle of inclination increases, the difference between the concrete compressive force and the steel force in the global direction keeps on increasing. This is similar to the case shown in Figure 51. As the angle of inclination increases, the length of the inclined compression zone also increases and according to the definition, the magnitude of the concrete compressive force keeps on rising, breaching the equilibrium with the steel force. However it was seen that horizontal equilibrium in the inclined cross-section cut was maintained when the compressive force is multiplied with the cosine of the angle of inclination as shown in Table 19. As the inclined concrete compressive zone for every angle of inclination is known, from the plot of σ_{XX} (Global Stress), the Bending Moment Resistance can be calculated and is tabulated in Table 19. Approach 2 (Section 3.2.2) is similar to this situation as the stresses are in the global direction and the compressive zone is inclined as shown in Figure 53. Figure 62 shows the percentage error in the bending moment resistance. It can be observed that as the angle of inclination increases, there is a slight increase in the percentage error. This is due to the mesh in the modelling, as it gets difficult to minimize the number of distorted and triangular elements.

Table 19 Data in the global direction for different angle of inclination for DIANA model - 1

Angle (degrees)	F_{sb} (kN)	N_{cu} (kN)	$N_{cu}.cos(angle)$ (kN)	x_u (mm)	Error in Horizontal Equilibrium (%)	Moment (kN-m)
0	185.94	-185.95	-185.95	154.18	0.00	44.93
5	186.13	-185.84	-185.14	143.57	0.53	45.66
10	186.50	-189.05	-186.18	148.32	0.16	45.56
15	186.19	-191.66	-185.13	159.15	0.56	45.01
20	186.39	-198.10	-186.15	155.48	0.12	45.53
25	186.51	-205.75	-186.48	164.08	0.01	45.4
30	186.04	-215.02	-186.21	161.65	-0.09	45.83
35	186.32	-228.83	-187.45	169.50	-0.6	45.97
40	186.37	-244.10	-186.99	186.79	-0.33	45.71
45	186.40	-255.04	-180.34	190.28	3.25	46.25
50	186.45	-282.78	-181.77	199.86	2.51	46.64
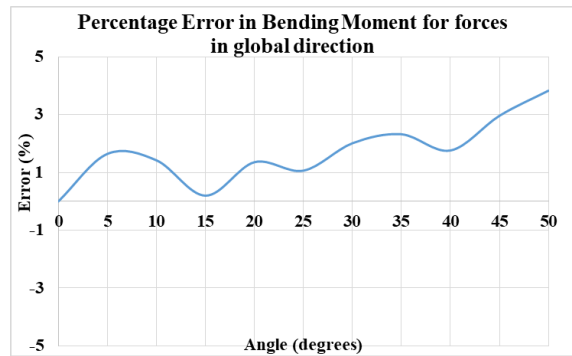
Figure 62 Percentage error in bending moment resistance due to forces in the global direction for DIANA model - 1

The reason for the multiplication of cosine of the angle of inclination to the concrete compressive force, in the Global Direction, is due to the increase in the length of the cross-section cut. When the angle of inclination increases, the length of the cross-section cut and therefore the length of the inclined compressive zone also increases. Integrating the stress block, shown in Figure 50, over an increased length of concrete compressive zone would obviously lead to a higher compressive force, breaking the equilibrium with the steel force. Hence this force should be reduced and further analyzed.

3.3.2 Model – 2

In the previous example the amount of reinforcement used was low (ρ = 0.7%) and hence the load bearing capacity was also less. Therefore another beam was analysed which was also subjected to four point bending test but with a comparatively higher reinforcement ratio (ρ = 1.2%) and higher load bearing capacity. Beam description and the material description are given in Table 20 and Table 21 respectively.

Table 20 Beam description for DIANA model - 2

Description	Value	Unit
Length	6400	mm
Span (L)	6000	mm
Height (d)	500	mm
Width (b)	300	mm
Concrete cover (c)	35	mm
Diameter of two legged stirrup($\phi_{stirrup}$)	12	mm
Diameter of bottom reinforcement (ϕ_{bot})	16	mm
Area of reinforcement (A$_{sb}$)	1608.5	mm^2
Shear span (a)	2000	mm
Effective depth (d$_{eff}$)	55	mm

Table 21 Material description for DIANA model - 2

Description	Value	Unit
Characteristic Concrete Compressive Strength (f$_{ck}$)	40	MPa
Design Concrete Compressive Strength (f$_{cd}$)	26.67	MPa
Design Concrete Tensile Strength (f$_{ctd}$)	1.64	MPa
Design Yield Strength (f$_{yd}$)	411	MPa
Young's Modulus of concrete	29814.5	MPa

All the symbols are as discussed previously. The same procedure to calculate the load bearing capacity of the beam, by equilibrating the bending moment resistance and the applied moment, is used. The bending moment resistance for different angle of inclination is then calculated and compared.

$$\text{Steel Force} = F_{sb} = f_{yd}.A_{sb} = 661\,\text{kN}$$

$$x_u = \frac{4.F_{sb}}{3.f_{cd}.b} = 110.18\ \text{mm}$$

$$\text{Lever arm} = z = d_{eff} - \frac{7.x_u}{18} = 402.15\ \text{mm}$$

$$\text{Moment Resistance} = M_{Rd} = F_{sb}.z = 265.85\ \text{kNm}$$

$$\text{Load} = \frac{M_{Rd}}{a} = 132.92\ \text{kN}$$

The beam is modelled and analysed in DIANA, with the concrete constitutive model given in Figure 63 and Figure 64. The convergence norm and criteria is similar to the one mentioned in Table 16. Figure 66 gives the Load-Deflection curve for the beam shown in Figure 65. The point A denotes the beginning of non-linearity, point B denotes the load case where the strain in the concrete has reached 1.75‰, point C depicts the yielding of steel and point D is where the concrete is crushed i.e the strain in the concrete has reached 3.5‰. The maximum load that the beam can carry is equal to 132.32 kN, which is equal to the analytical calculation. In this case also, for every angle of inclination a new model was analysed with the desired line imprinted on the beam.
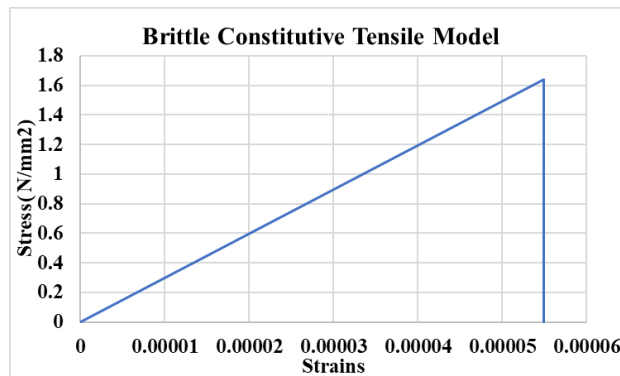
Figure 63 Tensile constitutive model for concrete
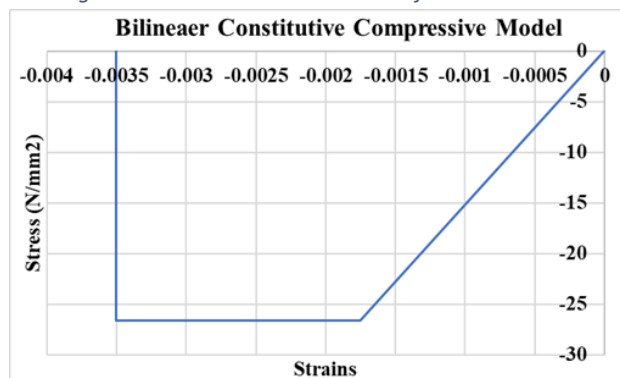
Figure 64 Compressive constitutive model for concrete
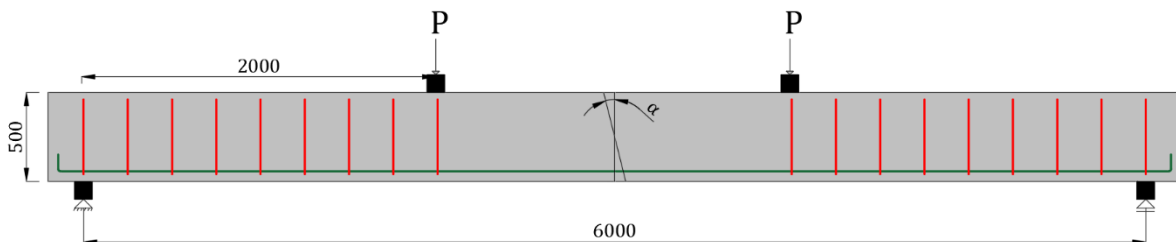
Figure 65 Beam dimensions for model - 2

49
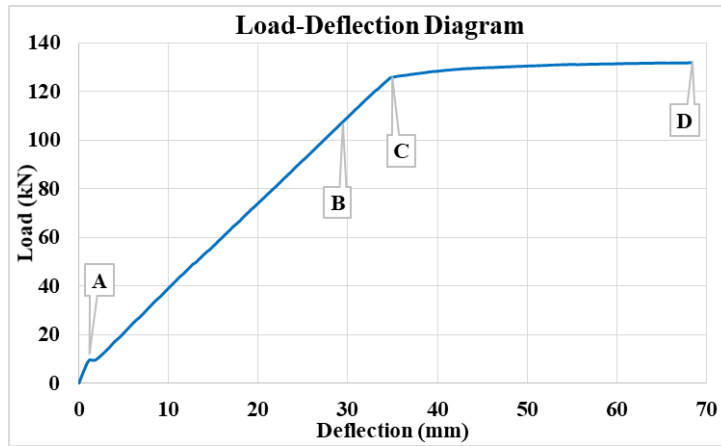
Figure 66 Force-Deflection diagram

Table 22 Global and local cross-section forces for different angle of inclination for DIANA model - 2

Angle (degrees)	F_{sb} (kN)	N_{cu} (kN)	F_{sb} local (kN)	N_{cu} local (kN)
0	665.54	-665.25	665.54	-665.25
5	664.81	-674.38	662.28	-661.45
10	663.21	-675.41	653.13	-655.09
15	664.30	-686.12	641.67	-641.50
20	665.12	-707.62	625.01	-625.38
25	665.15	-734.51	602.83	-603.20
30	664.50	-765.10	575.47	-578.41
35	664.58	-807.23	544.4	-544.00
40	663.99	-860.33	508.65	-510.66
45	664.03	-933.41	469.54	-467.36

Table 22 gives the cross-section forces in the local and the global direction that are calculated after the steel has yielded i.e. after point C. The same trend is followed in this case as well. As the angle of inclination increases, the concrete compressive force in the global direction keeps on increasing, breaching the horizontal equilibrium with the steel force. On the other hand, good coherence was observed when the cross-section forces are aligned in the local direction i.e. the perpendicular and parallel direction of the cross-section cut. From the stress block in the local direction, the height of the inclined compressive zone is known and the bending moment resistance for different angle of inclination is calculated. Table 23 shows the error for the local horizontal equilibrium, which is minimal, and also the bending moment resistance for different angle of inclination. It can be seen that the bending moment resistance has hardly changed. Moreover Figure 67 gives the percentage error in the bending moment resistance, for the forces directed in the local direction. In this case as well, the percentage error is negligible (less than -0.8%).

Table 24 shows the detailing of forces in the global direction. Also in this case it was observed, that when the concrete compressive force is multiplied with the cosine of the angle of inclination, horizontal equilibrium is maintained with the steel force. As the concrete compressive zone is known, the bending moment resistance for different angle of inclination is calculated and tabulated in Table 24. From Figure 68, it can be observed that the error in the bending moment resistance, when the forces are in the global direction, is also minimal (less than 1%).

Table 23 Data in the local direction for differnt angle of inclination for DIANA model - 2

Angle (degrees)	F_{sb} local (kN)	N_{cu} local (kN)	x_u (mm)	Error in Local Horizontal Equilibrium (%)	Moment (kN-m)
0	665.54	-665.25	148.41	0.04	263.24
5	662.28	-661.45	157.06	0.12	261.16
10	653.13	-655.09	146.62	-0.3	263.20
15	641.67	-641.50	156.70	0.02	262.10
20	625.01	-625.38	164.96	-0.06	261.61
25	602.83	-603.20	164.51	-0.06	262.93
30	575.47	-578.41	170.27	-0.51	263.04
35	544.39	-544.00	176.99	0.07	263.62
40	508.65	-510.66	199.66	-0.39	261.62
45	469.54	-467.36	204.32	0.46	263.51
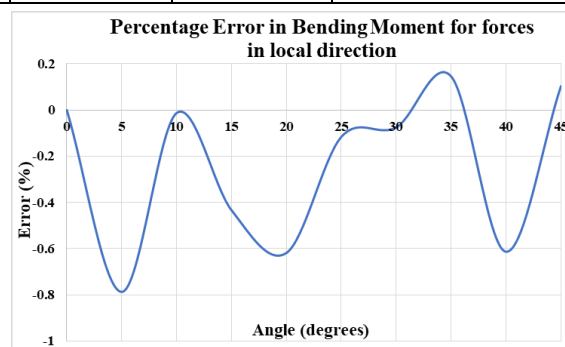
Figure 67 Percentage error in bending moment resistance due to the local cross-section forces for DIANA model - 2

Table 24 Data in the global direction for different angle of inclination in DIANA model - 2

Angle (degrees)	F_{sb} (kN)	N_{cu} (kN)	$N_{cu}.\cos(angle)$ (kN)	x_u (mm)	Error in Horizontal Equilibrium (%)	Moment (kN-m)
0	665.54	-665.25	-665.25	148.41	-0.04	263.24
5	664.81	-674.38	-671.82	149.75	-1.05	262.78
10	663.21	-675.41	-665.15	146.57	-0.29	263.21
15	664.30	-686.12	-662.74	153.11	0.23	262.86
20	665.12	-707.62	-664.95	155.88	0.02	263.50
25	665.15	-734.51	-665.69	159.98	-0.08	263.84
30	664.50	-765.10	-662.59	156.94	0.28	265.59
35	664.58	-807.23	-661.24	187.68	0.50	261.68
40	663.99	-860.33	-659.05	190.92	0.74	263.10
45	664.03	-933.41	-660.02	204.13	0.60	263.54
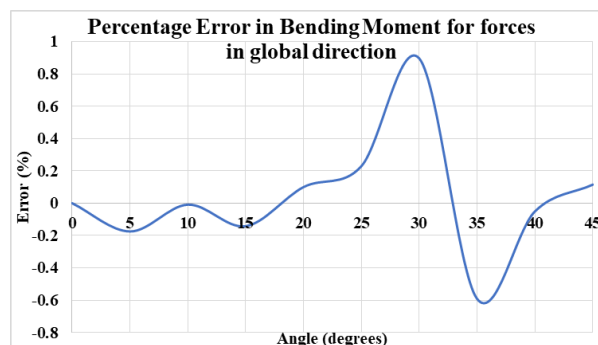
Figure 68 Percentage error in bending moment resistance due to the global cross-section forces in DIANA model - 2

4 Cross-Sectional Analysis on Reinforced Non-Prismatic Beams

This chapter describes, in detail, the procedure to calculate the shear capacity of reinforced non-prismatic beams, by comparing the experimental data discussed in Chapter 2 with the analytical results. Approaches to calculate the cross-section results, in reinforced non-prismatic beams, on an inclined cut is proposed and discussed further.

4.1 General Procedure for cross-sectional analysis on reinforced non-prismatic beam
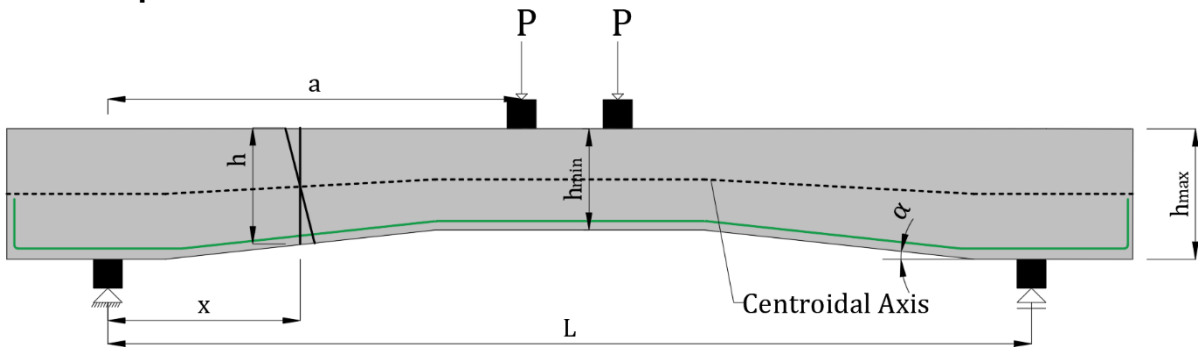
Figure 69 Negatively haunched beam with cross-section cut in the tapered zone

Consider the negatively haunched beam shown in Figure 69, with span L and the maximum height (h_{max}) at the support. The angle of taper is 'α' and the beam is subjected to four point bending test, with point loads applied at a distance of 'a' from the support. The bottom reinforcement is placed such that it is parallel to the bottom side of the beam. Cross-sectional analysis is performed in the tapered zone, at a distance of 'x' from the support of the beam shown in Figure 69.
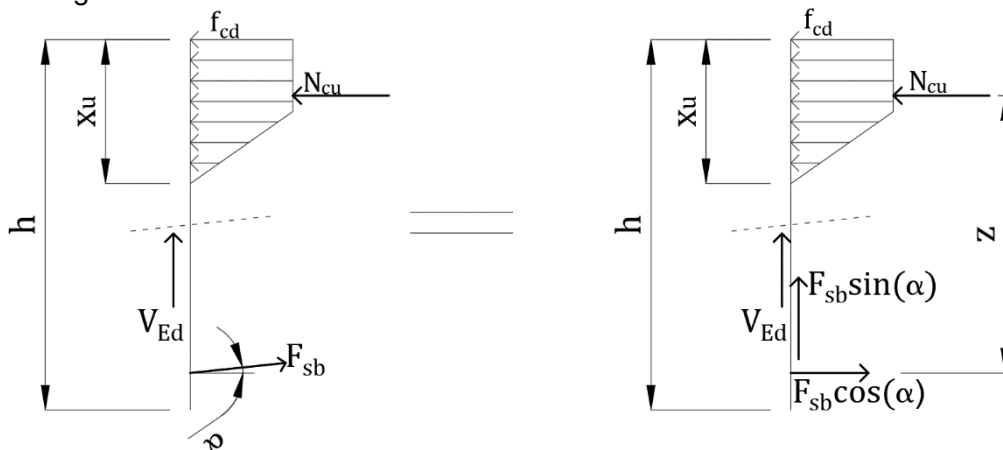
Figure 70 Cross-Sectional analysis performed on a vertical cut in the tapered zone of Figure 69

Figure 70 shows the cross-section forces for an analysis performed in the tapered zone. All the symbols are mentioned previously in Chapter 3. As the steel reinforcement is placed at the angle of taper, the steel force F_{sb} also acts at the given angle. This force is decomposed in two direction:

I.   Horizontal component, which is considered in the bending moment resistance formula
II. Vertical component, which according to the codes mentioned in Chapter 2, should be considered in the shear capacity of the beam.

The bending moment resistance calculation is given as follows,

$$N_{cu} = F_{sb}.\cos(\alpha)............(4.01)$$

$$N_{cu} = \frac{3.f_{cd}.b.x_u}{4}............(4.02)$$

$$x_u = \frac{4.F_{sb}.\cos(\alpha)}{3.f_{cd}.b}............(4.03)$$

$$M_{Rd} = F_{sb}.\cos(\alpha).z$$

54

$$z = d_{eff} - \frac{7.x_u}{18} = d_{eff} - \frac{14.F_{sb}.\cos(\alpha)}{27.b.f_{cd}}$$

$$M_{Rd} = F_{sb}.\cos(\alpha).\left(d_{eff} - \frac{14.F_{sb}.\cos(\alpha)}{27.b.f_{cd}}\right)............(4.04)$$

All the symbols are mentioned in the nomenclature. The cross-sectional analysis is performed at the Ultimate limit state, where the steel force (F_{sb}) is assumed to be yielded. This would indicate that the shear capacity has increased or decreased by the yielded steel force (F_{sb}) multiplied by the sine of the angle of taper (α). John J Orr et al. [11] designed positively haunched beams based on the theory that the vertical component of the 'yielded' longitudinal reinforcement contributes to the shear capacity of the beam. From the results, it was concluded that these beams failed at a much lower load than the design load and the concept of contribution of 'yielded' longitudinal reinforcement to the shear capacity was proven to be wrong.

Assuming that the vertical component is considered in the shear capacity of the beam, the formula for the effective shear resistance is given as

$$V_{Rd} = V_{Rd,c} + V_{Rd,s} \pm F_{sb}\big|_{\text{At given load case}} .\sin(\alpha)............(4.05)$$

where,

$V_{Rd,c} = $ Shear Resistance contributed by concrete $= 0.12.k.\left(100.\rho_l.f_{ck}\right)^{\frac{1}{3}}.b.d$

$V_{Rd,s} = $ Shear Resistance contributed by stirrups $= \dfrac{A_{sv}.f_{yvd}.z.\cot(\gamma)}{s}$

$k = 1 + \sqrt{\dfrac{200}{d}} > 2$

$\rho_l = \dfrac{A_{sb}}{b.d}$

$f_{ck} = $ Characteristic Compressive Strength

$A_{sb} = $ Area of bottom reinforcement

$d = $ Effective depth at the critical section

$A_{sv} = $ Area of shear reinforcement

$s = $ spacing of shear reinforcement

$\gamma = $ Angle of shear crack

$z = $ Lever arm

$f_{yvd} = $ Yield Strength of shear reinforcement

$\alpha = $ Angle of taper

$F_{sb}\big|_{\text{At given load case}} = $ Steel force for a given load case $= \dfrac{M_e}{z.\cos(\alpha)}$

$M_e = $ Applied Moment $= P.x$

$P = $ Load increment

$x = $ Distance of the critical section from the support

The formula for the effective shear resistance can also be written as,

$$V_{Rd} = V_{Rd,c} + V_{Rd,s} \pm \frac{M_e}{z}.\tan(\alpha)............(4.06)$$

Using this formula, the experimental data is validated to check whether the vertical component should be considered in the shear capacity equation or not. As the height of the non-prismatic beam varies along the length of the beam, the definition of critical section is important where the effective shear resistance is calculated. Also, the equation of shear resistance contributed by concrete and stirrups is based on design material properties. However, mean properties are used in experiments and the formula to calculate the shear capacity contributed by concrete and stirrups has been modified as shown below.

$$V_{Rm,c} = 0.15.k.\left(100.\rho_l.f_{cm}\right)^{\frac{1}{3}}.b.d \dots\dots\dots\dots(4.07)$$

$$V_{Rm,s} = \frac{A_{sw}.f_{ym}.z.\cot(\gamma)}{s} \dots\dots\dots\dots(4.08)$$

where

$f_{cm} = $ Mean compressive strength of concrete

$f_{ym} = $ Mean yield strength of stirrups

$$V_{Rm} = V_{Rm,c} + V_{Rm,s} \pm \frac{M_e}{z}.\tan(\alpha) \dots\dots\dots\dots(4.09)$$

4.2 Validation of Literature Study

This section comprises of the validation of the experimental data mentioned in Chapter 2. All experimental non-prismatic beams are briefly discussed and further comparison with the analytical results has been performed.

4.2.1 Arturo Tena-Colunga et al. [10]

The authors performed tests on 10 beams, 2 prismatic and 8 non-prismatic beams. The beams were subjected to four point bending test as shown in Figure 33. The first 5 beams were not reinforced with stirrups whereas the other 5 had minimum amount of shear reinforcement. Width of the beam was constant and was equal to 220 mm. The bottom reinforcement consists of 4 bars of 25.4 mm diameter.

Table 11 depicts the experimental value of shear forces with the given shear crack angle. The critical shear force denotes the force at which the first diagonal crack occurs. The ultimate shear force is the force where major shear cracking occurs and the collapse load is the capacity of the beam to carry the load. An example of reinforcement detailing present in the non-prismatic beam is shown in Figure 34. All these beams are validated using the effective shear resistance formula (equation 4.09).

The shear resistance is calculated at the critical section, which in this case is at the vertex of the haunch near the loading point. The reasons to consider the vertex as a critical section are as follows:

a. The height of the beam is minimum at this point.
b. The applied moment at this point is higher as compared to the other points of the tapered section and therefore the steel force would also be maximum at this section. The vertical component of the inclined steel force, which has a negative contribution with respect to the shear capacity of the beam, will have maximum effect on the resistance at this section.

The calculation of shear resistance for the beam TASCα2-R0 is shown below. Beam description is given in Table 25. The geometry of the specimen TASCα2-R0 with the given critical section is shown in Figure 71.

Table 25 Description of the specimen TASCα2-R0

Description	Value	Unit
Angle of taper (α)	6.12	degrees
Mean compressive strength (f_{cm})	29.5	MPa
Area of reinforcement (A_{sb})	2026.83	mm²
Minimum height (h_{min})	350	mm
Minimum effective depth (d)	310	mm

Figure 71 Geometry of the specimen TASCα2-R0

The shear resistance contributed by concrete is calculated as shown below. The reinforcement ratio (ρ_l) has also been calculated with the effective depth at the critical section.

$$k = 1 + \sqrt{\frac{200}{d}} = 1.8 < 2$$

$$\rho_l = \frac{A_{sb}}{b.d} = 0.029$$

$$V_{Rm,c} = 0.15.k.\left(100.\rho_l.f_{cm}\right)^{\frac{1}{3}}.b.d = 81.94 \text{ kN}$$

Figure 72 Moment-Kappa diagram for a beam subjected to bending

Figure 72 shows the moment-kappa diagram for a beam loaded under bending. In the linear elastic stage (Stage-I), till M_{cr}, the load is taken up by concrete and the steel force is zero. Once concrete has reached the flexural tensile strength, cracking occurs and the increased load is carried by the bottom reinforcement in the second and third stage. To calculate the

critical moment (M_{cr}) and the critical force (P_{cr}), above which cracking occurs and the steel force increases, the following formulas are used.

$$M_{cr} = f_{ctm,fl}.W \ldots\ldots\ldots(4.10)$$

$$f_{ctm,fl} = \text{Flexural Tensile Strength} = f_{ctm}.\left(1.6 - \frac{h}{1000}\right)\ldots\ldots\ldots(4.11)$$

$$W = \text{Section Modulus} = \frac{b.h^2}{6}\ldots\ldots\ldots(4.12)$$

h = Height of the beam at the critical section (in mm)

b = Width of the beam

$$P_{cr} = \frac{M_{cr}}{x}\ldots\ldots\ldots(4.13)$$

x = distance of critical section from the support

The concrete tensile strength and the young's modulus is calculated according to the formulas mentioned in Eurocode 1992-1-1 [1].

$$f_{ctm} = 0.3.\left(f_{ck}\right)^{\frac{2}{3}}$$
$$f_{ck} = f_{cm} - 8$$
$$E_{cm} = 22000.\left(\frac{f_{cm}}{10}\right)^{0.3}$$

Table 26 Critical Moment and Force Description of the specimen TASCα2-R0

Description	Value	Unit
Section Modulus (W)	4490682.5	mm^2
Flexural Tensile Strength (f$_{ctm,fl}$)	2.9	MPa
Critical Moment (M$_{cr}$)	13.02	kN-m
Distance of critical section from the support (x)	933	mm
Critical Force (P$_{cr}$)	13.96	kN

When the load reaches a value of 13.96 kN, cracking occurs and the steel reinforcement is responsible to carry the applied load. To calculate the horizontal component of the inclined steel force, the following formula is used

$$F_{sb}.\cos(\alpha) = \frac{M_e}{z}\ldots\ldots\ldots(4.14)$$

$$M_e = P.x\ldots\ldots\ldots(4.15)$$

$$z = \text{Lever arm} = d - \frac{x_s}{3}\ldots\ldots\ldots(4.16)$$

x_s = Height of the concrete compressive zone

The height of the concrete compressive zone can be calculated as follows,

$$\frac{x_s}{d} = -\alpha_e.\rho_l + \sqrt{\left(\left(\alpha_e.\rho_l\right)^2 + 2.\alpha_e.\rho_l\right)}\ldots\ldots\ldots(4.17)$$

$$\alpha_e = \frac{E_s}{E_c}$$

E_s = Young's Modulus of Steel

E_c = Young's Modulus of Concrete

Table 27 Lever arm calculation for the specimen TASCα2-R0

Description	Value	Unit
Young's Modulus of Steel	200000	MPa
Young's Modulus of Concrete	30434.72	MPa
Ratio between Young's Modulus (α_e)	6.57	-
Reinforcement Ratio (ρ_l)	2.9	%
Compressive zone (x_s)	142.43	mm
Lever arm (z)	262.49	mm

The critical force (P_{cr}), after which cracking occurs, is known which is equal to 13.94 kN. To calculate the horizontal component of the inclined tensile tie, lever arm is required which is equal to 262.49 mm (0.85*d). The shear resistance of the negatively haunched beam TASCα2-R0 can now be calculated as shown in Table 28.

Table 28 Analytical Calculation of the shear capacity for the specimen TASCα2-R0

Load (kN)	$F_{sb}.\cos(\alpha)$ (kN)	$F_{sb}.\sin(\alpha)$ (kN)	Effective Shear Resistance (kN)	Failure
1	0	0	81.94	NO FAILURE
13	0	0	81.94	NO FAILURE
14	49.76	5.34	76.61	NO FAILURE
15	53.32	5.72	76.23	NO FAILURE
25	88.86	9.53	72.42	NO FAILURE
35	124.41	13.34	68.61	NO FAILURE
45	159.95	17.15	64.79	NO FAILURE
55	195.50	20.96	60.98	NO FAILURE
56	199.05	21.34	60.60	NO FAILURE
57	202.61	21.72	60.22	NO FAILURE
58	206.16	22.10	59.84	NO FAILURE
59	**209.71**	**22.49**	**59.46**	**NO FAILURE**
60	213.27	22.87	59.08	FAILURE

Till the applied load is less than the critical force (13.96 kN), cracking does not occur and both the components of steel force are equal to zero. The moment the applied load is greater than the critical force, both the components of the inclined steel force are determined. To calculate the effective shear resistance of the beam, the vertical component of the inclined steel force ($F_{sb}.\sin(\alpha)$) is subtracted from the shear resistance contributed by concrete ($V_{Rm,c}$). Failure in the beam occurs when the effective shear resistance is less than the applied load and the shear capacity of the non-prismatic beam is determined. Using this procedure, analytically calculated shear capacity of the non-prismatic beam TASCα2-R0 is equal to 59.46kN which is almost equal to the experimental value of 60kN. If the vertical component of the inclined steel force is ignored, one would overestimate the shear capacity of the beam by 36.5%. This also shows that the capacity of non-prismatic beam depends on the applied loading.

Now consider the non-prismatic beam TASCα3-R1, which is reinforced with stirrups as shown in Figure 73. Beam description is given in Table 29.
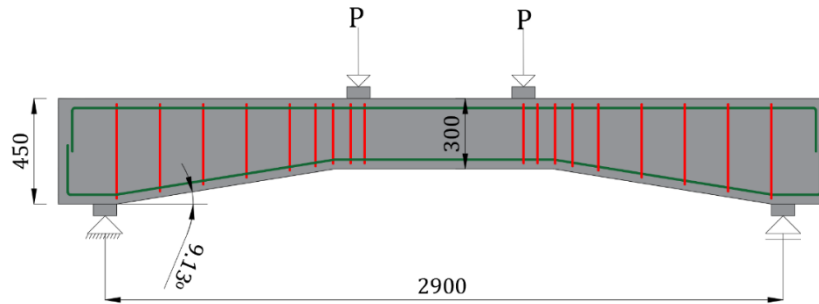
Figure 73 Geometry and Reinforcement detailing of the specimen TASCα3-R1

Table 29 Descripiton of the specimen TASCα3-R1

Description	Value	Unit
Angle of taper (α)	9.13	Degrees
Mean compressive strength (f_{cm})	28.8	MPa
Area of reinforcement (A_{sb})	2026.83	mm^2
Minimum height (h_{min})	300	mm
Minimum effective depth (d)	260	mm
Area of shear reinforcement (A_{sv})	100.53	mm^2
Spacing of shear reinforcement (s)	185	mm
Mean Yield Strength (f_{ym})	420	MPa
Shear Crack Angle (γ)	36	degrees

In this case also, the critical section is considered at the vertex of the haunch near the loading point. Table 30 gives the critical moment and the critical force, above which cracking occurs and steel reinforcement carries the additional load. All these are calculated based on the formula mentioned in equation 4.10, 4.11, 4.12 and 4.13.

Table 30 Critical Moment and Force description of the specimen TASCα3-R1

Description	Value	Unit
Flexural Tensile Strength ($f_{ctm,fl}$)	2.95	MPa
Section Modulus (W)	3301243.5	mm^2
Critical moment (M_{cr})	9.73	kN-m
Distance of critical section from the support (x)	933	mm
Critical force (P_{cr})	10.44	kN

The procedure to calculate the lever arm is also mentioned in equation 4.16 and 4.17 with the important details given in the following table.

Table 31 Lever arm calculation of the specimen TASCα3-R1

Description	Value	Unit
Young's Modulus of Steel	200000	MPa
Young's Modulus of Concrete	30216.24	MPa
Ratio between Young's Modulus ($α_e$)	6.62	-
Reinforcement Ratio ($ρ_l$)	0.034	-
Compressive zone (x_s)	127.26	mm
Lever arm (z)	217.64	mm

$$k = 1 + \sqrt{\frac{200}{d}} = 1.88 < 2$$

$$V_{Rm,c} = 0.15.k.\left(100.\rho_l.f_{cm}\right)^{\frac{1}{3}}.b.d = 75.27 \text{ kN}$$

The shear resistance contributed by stirrups is given by the following formula,

$$V_{Rm,s} = \frac{A_{sv}.f_{yvm}.z.\cot(\gamma)}{s} = 68.36 \text{ kN}$$

All the parameters are mentioned in Table 29. The lever arm calculated at the critical section is used in the above equation to calculate the shear resistance contributed by stirrups. Same procedure is applied to calculate the shear capacity of these beams as shown in Table 32.

Table 32 Analytical shear capacity calculation of the specimen TASCα3-R1

Load (kN)	$F_{sb}.\cos(\alpha)$ (kN)	$F_{sb}.\sin(\alpha)$ (kN)	Effective Shear Resistance (kN)	Failure
1	0.00	0.00	143.64	NO FAILURE
13	55.73	8.96	134.68	NO FAILURE
14	60.02	9.65	133.99	NO FAILURE
15	64.30	10.33	133.30	NO FAILURE
25	107.17	17.22	126.41	NO FAILURE
35	150.04	24.11	119.52	NO FAILURE
45	192.91	31.00	112.63	NO FAILURE
55	235.78	37.89	105.74	NO FAILURE
65	278.65	44.78	98.85	NO FAILURE
75	321.52	51.67	91.96	NO FAILURE
80	342.96	55.12	88.52	NO FAILURE
84	360.11	57.87	85.76	NO FAILURE
85	**364.39**	**58.56**	**85.07**	**NO FAILURE**
86	368.68	59.25	84.38	FAILURE

Shear failure occurs when the effective shear resistance is less than the applied load, as was the case previously. The experimental shear resistance was equal to 120 kN which is higher than the analytically obtained shear capacity where the vertical component is taken into account by the shear resistance. If this component is ignored, the shear capacity of the beam would be equal to 143.64 kN, overestimating the capacity by 19%.

Following the above procedure, all the beams are analysed and the shear capacities, including and excluding the vertical component of the inclined tensile tie, are compared with the experimental result.

Table 33 Experimental and Analytical shear capacity for all the specimen tested by Arturo et al. [10]

	Specimen	Angle of taper (degrees)	Experimental (kN)	Analytical including the vertical component (kN)	Analytical excluding the vertical component (kN)
1	TASC α0-R0	0	75	96.93	96.93
2	TASC α1-R0	3.06	67.5	77.64	90.13
3	TASC α2-R0	6.12	60	59.58	81.94
4	TASC α3-R0	9.13	37.5	42.43	70.43
5	TASC α4-R0	12.1	30	33.12	68.15
6	TASC α0-R1	0	250	198.36	198.36
7	TASC α1-R1	3.06	200	155.24	168.52
8	TASC α2-R1	6.12	170	135.9	173.9
9	TASC α3-R1	9.13	120	85.13	143.64
10	TASC α4-R1	12.1	80	68.04	132.91
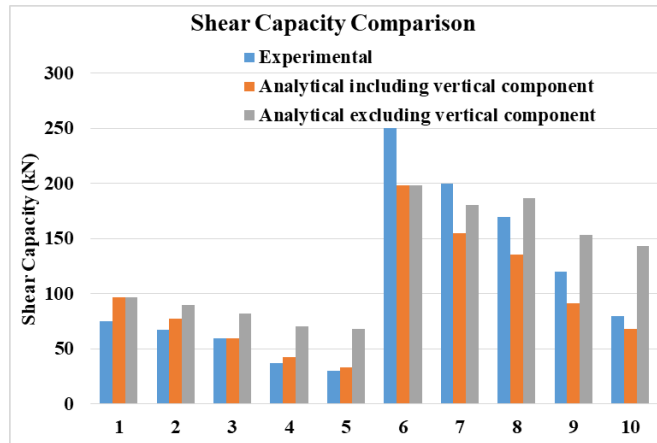
Figure 74 Shear Capacity Comparison for all the specimens tested by Arturo et al. [10]

Note that the shear resistance of all the non-prismatic beams is calculated at the critical section i.e. at the vertex of the haunch. From the experiments, it was seen that shear crack was initiated at the centre of the haunch and not at the vertex. Nevertheless, it can be seen from Table 33 and Figure 74 that the analytical results where the vertical component is taken into account by the shear capacity of the beam conforms well to the experimental results. On the other hand, the shear capacity of the beam is overestimated when the vertical component is ignored.

4.2.2 Vu Hong Nghiep [9]

The author performed three point bending test on non-prismatic beams such that the haunch is present at the top side of the beam as shown in Figure 27 and Figure 28. The author performed tests on 18 different beams – 2 prismatic beams, 12 positively haunched beams failed in shear and 4 positively haunched beams failed in flexure. The focus in this study will be on the 12 non-prismatic and 2 prismatic beams. The beams were designed such that the maximum height of the beam at the centre remains constant and equal to 340 mm. The width of the beam is equal to 200 mm. The bottom reinforcement consists of 3 bars of 20 mm diameter. The section 7.3.3.1 of the Model Code [3] states that in a cross-section design, the design shear force must in general be determined at a distance of 'd' i.e. effective depth from the support. It also state that this definition of the controlled section might change for different types of beams such as non-prismatic beams. To analytically calculate the shear capacity of the positively haunched beams tested by Nghiep, the critical section is considered at a distance of 'h_{min}' from the support. Figure 75 shows the beam specification for the beams 3L1-3L2. At the ULS, the cross-section forces acting on the cross-section cut is shown in Figure 76.
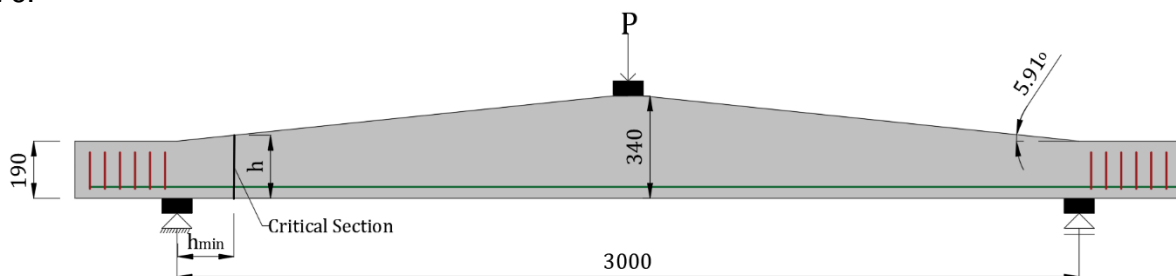
Figure 75 Geometry of the specimen 3L1-3L2

The inclined concrete compressive force (N_{cu}) is given as,

$$N_{cu} = \frac{3.f_{cd}.b.x_u}{4}$$

Due to the geometry of the beam, the compressive force acts at an angle at the top part of the cut. The force is assumed to act at the same angle as that of the angle of taper. This force is decomposed in the horizontal and the vertical direction as shown in Figure 76. The vertical component of the inclined compression chord decreases the applied shear force or increases the shear capacity of the beam. The procedure mentioned in the previous section is applied in these positively haunched beams and the vertical component of the inclined compression chord is calculated. The effective shear resistance is determined by adding this component to the shear capacity contributed by concrete, which is further compared with the applied loading. All the results are determined at the critical section i.e. at a distance of h_{min} from the support and tabulated below.
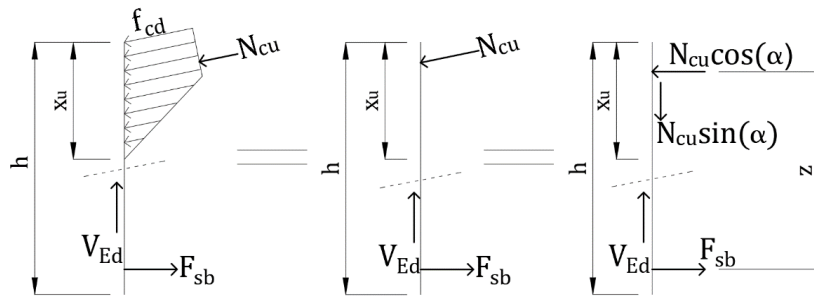
Figure 76 Cross-Sectional analysis performed at the critical section in Figure 75 (at ULS)

Table 34 Experimental and Analytical shear capacity of all the specimen tested by Vu Hong Nghiep [9]

	Specimen	Angle of taper (degrees)	Experimental (kN)	Analytical including the vertical component (kN)	Analytical excluding the vertical component(kN)
1	1L1	0	75.44	69.12	69.12
2	1L2	0	79.21	69.66	69.66
3	2L1	3.95	75.18	67.11	61.24
4	2L2	3.95	74.6	67.59	61.71
5	3L1	5.91	66.47	60.84	52.79
6	3L2	5.91	69.3	61.24	52.07
7	1K1	0	75.63	71.77	71.77
8	1K2	0	69.31	71.81	71.81
9	2K1	3.95	83.53	73.63	67.47
10	2K2	3.95	85	73.65	67.48
11	3K1	6.71	79.34	74.3	63.9
12	3K2	6.71	79.93	74.32	63.92
13	4K1	10.01	84.74	72.26	57.27
14	4K2	10.01	83.88	72.27	57.28
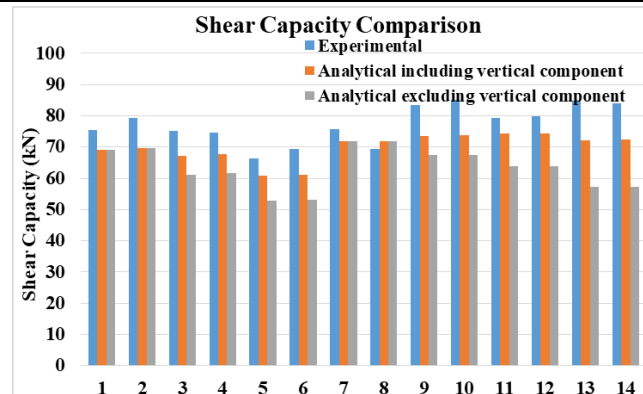
Figure 77 Shear Capacity Comparison for all the specimen tested by Vu Hong Nghiep [9]

Figure 77 shows the comparison of shear capacities of all the beams with the experimental data. The shear crack in the beam initiated near the support and propagated to the loading point and from the figure and the numbers, the assumption of the critical section near the support is quite reasonable. Figure 77 also shows that including the vertical component of the inclined compressive force to the analytical formula would significantly increase the shear capacity of the beam and is also close to the experimentally results.

4.2.3 Debaiky et al. [5]

The authors performed tests on 33 concrete beams which were subjected to four point bending test. The authors divided the beams under 6 different series. The differences between these series are the shear span, concrete strength, percentage of transverse reinforcement, percentage of longitudinal reinforcement, angle of inclination and different arrangement of longitudinal reinforcement detailing as given in Table 1. The shear crack angle of some non-prismatic beam was less than 21.5°, as shown in Table 3, which is the minimum angle allowed by Eurocode [1] and therefore these beams are not analysed. Detailing of the beams is given in Table 2. Figure 78 shows the beam specification of the negatively haunched beam C5.
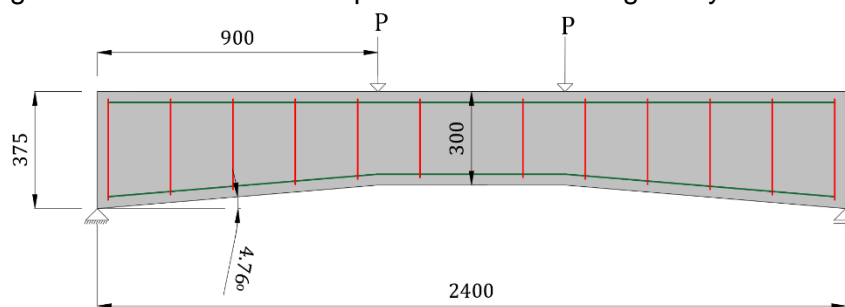
Figure 78 Geomtry and Reinforcement detailing of the specimen C5

Table 35 Experimental and Analytical shear capacity of the specimens tested by Debaiky et al. [5]

	Specimen	Angle of taper (degrees)	Experimental (kN)	Analytical including vertical component (kN)	Analytical excluding the vertical component (kN)
1	A1	0	73.5	54.48	54.48
2	A2	9.46	37.5	42.08	28.15
3	A3	4.76	35	51.19	44.02
4	A4	-4.76	30	40.05	53.41
5	A5	-9.46	35	31.82	53.07
6	B5	-12.1	40	36.06	60.11
7	B6	-16.7	40	31.27	51.88
8	C1	0	72.5	67.21	67.21
9	C3	4.76	37.5	68.56	59.09
10	C4	-9.46	35	37.67	62.87
11	C5	-4.76	35	44.35	59.32
12	D1	0	83.5	85.48	85.48
13	D2	0	75	118.8	118.8
14	D3	9.46	37.5	82.39	55.43
15	D4	9.46	27.5	79.51	53.49
16	D5	-9.46	25	52.65	88.12
17	D6	-9.46	37.5	55.06	92.5
18	F5	0	67	67.48	67.48
19	F6	0	62.5	54.3	54.3

The beams were designed in such a way that the height at the centre remains constant (300 mm) and varies at the support. The critical section in a negatively haunched beam is considered at the vertex of the haunch whereas for a positively haunched beam it was assumed to be at a distance of 'h$_{min}$' from the support. The same procedure to calculate the shear capacity of the non-prismatic beam is applied in this case as well and the results are compared with the failure load as shown in Table 35. In case of the negatively haunched beams (except specimen D5 and D6) the analytical results, where the vertical component is included, conforms quite well to the experimental data. Whereas in positively haunched beams, the analytical result shows quite some scatter when compared to experimental data as can be seen from Figure 79.
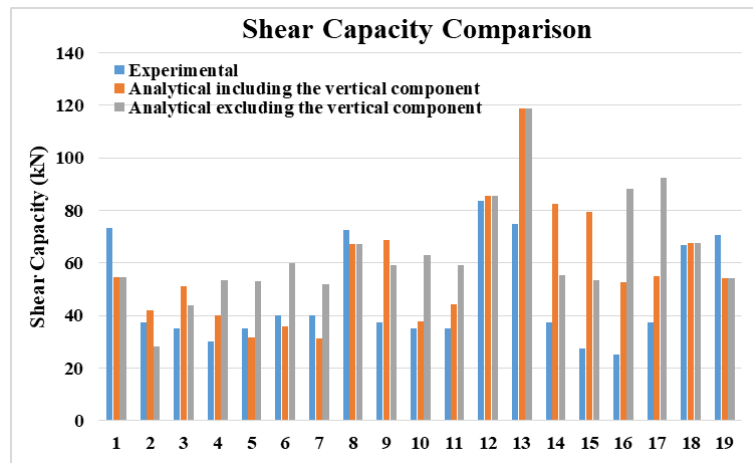
Figure 79 Shear Capacity comparison of the specimens tested by Debaiky et al. [5]

4.2.4   I.A. Macleod et al. [6]

The author performed tests on non-prismatic double cantilevered beams shown in Figure 13 and Figure 15. The reinforcement detailing present in these beams are different than the normal ones mentioned previously as shown in Figure 14. The tensile reinforcement placed on the top side of the beam consists of 2 bars of 20 mm diameter and 1 bar of 10 mm diameter.
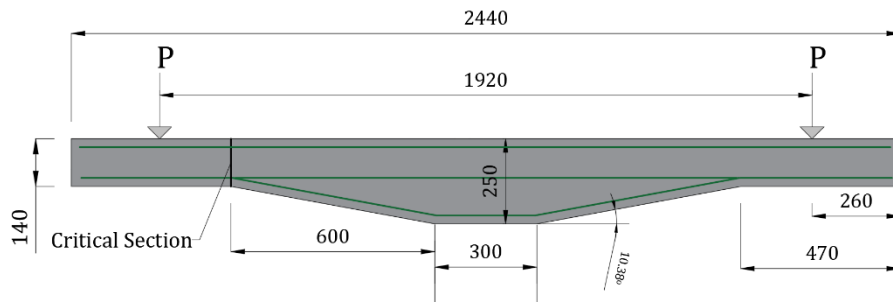
Figure 80 Geometry and Reinforcement detailing of the specimen 'Beam 6'

Except for the specimen 'Beam 4', the critical section in all the other positively haunched beams is at the vertex of the haunch away from the support and near the loading point as shown in Figure 80. The reasons to consider this as the controlled section are as follows:

1. The height of the beam is minimum at this point when compared to the other position of the haunch.
2. When a cross-sectional analysis is performed at this point, the vertical component of the inclined compression chord increases the shear resistance of the beam. At this point the magnitude of the compression chord would be minimum as the bending moment is small compared to the other parts of the haunch. Therefore the vertical component would have minimum assistance to the capacity.

65
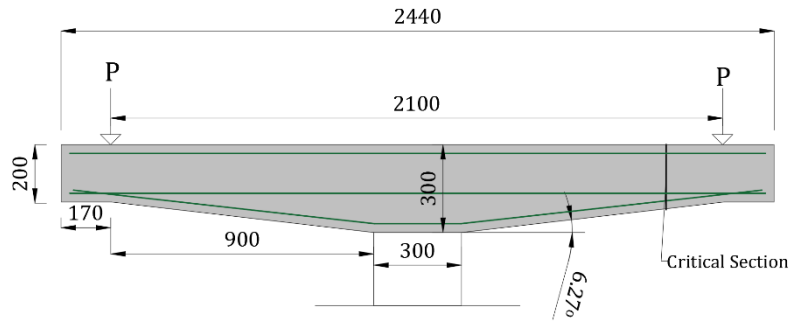
Figure 81 Geometry and Reinforcement detailing of the specimen 'Beam 4'

In the specimen 'Beam 4', the critical section is considered at a distance of 'h$_{min}$' from the vertex of the haunch near the support. At the vertex of the haunch, bending moment is zero and hence, theoretically, there will be no force in the compression chord and no increase in the shear resistance. Also, the flexural-shear crack is originated from one of the point loads and extended towards the support. Hence the assumption of the critical section in the beams might be correct. The critical load and the lever arm for each specimen is calculated and the shear capacity is further processed, as tabulated in Table 36.

Table 36 Experimental and Analytical shear capacity of all the specimen tested by Macloed et al. [6]

Specimen	Angle of taper (degrees)	Experimental (kN)	Analytical including vertical component (kN)	Analytical excluding vertical component (kN)
B2	4.74	36.4	38.52	33.63
B3	0	30.9	40.62	40.62
B4	6.277	38	40.65	34.92
B5	7.57	41	37.27	27.72
B6	10.38	42	44	23.33

Table 36 shows the experimental and analytical results for all the specimens. The table clarifies that including the vertical component of the inclined compression chord will give better prediction about the shear capacity of these double cantilevered positively haunched beams.

4.2.5 John J. Orr et al. [11]

The authors performed tests on positively haunched beam which were designed based on three different models – the Eurocode Model (EC2), the Compressive Force Path method (CFP) and the strut and tie model (STM). Beams designed using STM model and the CFP method failed in flexure and are not considered in this study whereas the beams modelled using EC2 model failed in shear. The beams were tested twice with two different support configurations. One of the support configuration leads to shear failure whereas the other leads to flexural failure as shown in Figure 82 and Figure 83 respectively. The bottom reinforcement consists of 2 bars of 10mm diameter whereas the stirrups are 3mm in diameter. Beam 4 EC2 is not included in this analysis as the shear span to depth ratio is less than 2.

Figure 82 Beam 2 EC2 shear failure configuration

Figure 83 Beam 2 EC2 flexural failure configuration

Table 37 Expeimental and Analytical shear capacity of all the specimen tested by John J Orr et al. [11]

Specimen	Angle of taper (degrees)	Experimental (kN)	Analytical load including vertical component (kN)	Analytical load excluding vertical component (kN)
Beam 1 EC2	9.09	19	20.81	15.74
Beam 2 EC2	15.43	28.2	18.03	12.64
Beam 3 EC2	12.95	17.1	14.66	11.14

The above table shows the experimental and the analytical load carrying capacity of the positively haunched beam. The critical section is considered at a distance of h_{min} from the support as shown in Figure 82. Once the critical load and the lever arm are calculated, the shear capacity of these haunched beam is determined and from this the load carrying capacity is further evaluated. The analytical results, including the vertical component, match quite well with the experimental results unlike the analytical results excluding the vertical component.

4.2.6 Chenwei HOU et al. [8]

Authors performed four point bending test on negatively haunched beam. The authors tested 10 negatively haunched beams which were divided in 4 different series based on 4 different parameters – position of the point load with respect to the end of the haunch, concrete cover, different arrangement of longitudinal reinforcement and amount of shear reinforcement as discussed in Chapter 2. The focus of this study is on the beams of Series-1. The bottom reinforcement consist of 2 bars of 25.4 mm diameter. Figure 84 shows the overall dimensions of the beam where 'b' denotes the distance between the point load and the vertex of the haunch and 'e' is equal to '650-b'. The number in the beam specimen also indicates the distance between the point load and the vertex of the haunch i.e. H-0 means the point load is applied at the vertex of the haunch on the top side and so on.

Arch mechanism, due to loss of bond between the steel reinforcement and the surrounding concrete [4], is very strong in the beam specimen H-0 and H-100, which drastically increases the shear capacity of the beam and are therefore not considered in this study. Also the length of the beam is very short, and the path which connects the point load to the support creates a strong strut action, as shown in Table 8, which also strengthens the capacity of the beam. Table 38 gives the comparison of shear capacities for the specimens H-200 and H-300.

Figure 84 Geometry and Reinforcement detailing of the specimens in Series I tested by Chenwei HOU et al. [8]

Specimen	Experimental (kN)	Analytical including vertical component (kN)	Analytical excluding vertical component (kN)
H-200	38.5	46.8	71.47
H-300	36	52.62	74.57

A decent coherence between the analytical results, where the vertical component is included in the shear resistance of the beam, and the experimental result is seen. In this case as well, the critical section is considered at the vertex of the haunch, as the cracking pattern from the experiments shows the formation of crack from the vertex towards the loading point and along the longitudinal reinforcement.

4.2.7   G. D. Stefanou [7]

Stefanou, from the University of Patras, Greece performed three point bending test on positively haunched beams. The data for these beams was limited and hence the 4 beams without shear reinforcement are analysed in this study. Two different type of beams were used – Type A and Type B as shown in Figure 19. Beam specification are given in Table 5. Figure 85 shows beam description of the specimen 'B1'. As the length of the beam is short and the vertex of the haunch is quite close to the support, the critical section is considered at a distance of h_{min} from the vertex as shown in Figure 85.
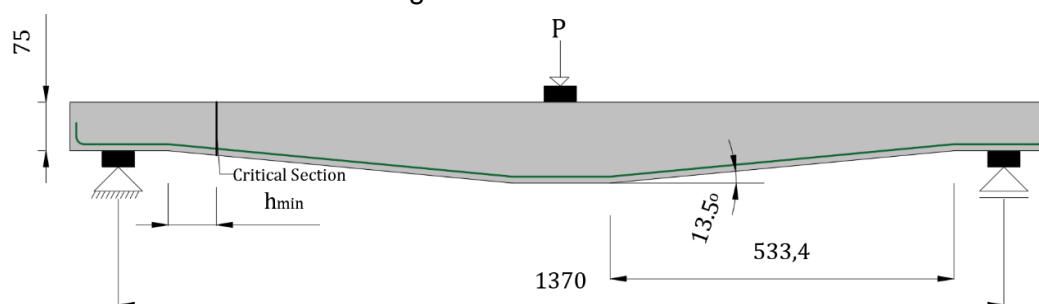
Figure 85 Geometry of the specimen 'B1'

Table 39 Experimental and Analytical shear capacity of the specimen tested by Stefanou [7]

Specimen	Type	Experimental (kN)	Analytical including vertical component (kN)	Analytical excluding vertical component (kN)
B1	Type A	15.8	16.39	9.05
B2	Type A	26.5	16.12	12.56
B3	Type B	27.5	15.23	8.35
B4	Type B	26.5	14.71	11.6

From Table 39, it can be said that the theory of effective shear resistance predicts a lower shear capacity than the experimentally calculated values and hence a conservative approach is seen. In this case, the assumption of the critical section does not comply with the shear cracks that occurs in the beam. The cracks are generally observed near the centre of the haunch and not so close to the support. As the length of the haunched beams is less, the likelihood of occurrence of the strut action might have significantly increased the shear capacity of the beams as shown by Chenwei HOU [8], but nothing was mentioned in the article.

4.3 Discussion

In this section all the beams that are mentioned above are accumulated and discussed further. The mean and standard deviation for the ratio between the experimental results and analytical

results are calculated to verify the inclusion of the vertical component to the shear capacity of the beam. The beams are divided into three different sections – Prismatic Beams, Negatively Haunched Beams and Positively Haunched Beams. The dead weight of the beam, obtained at the critical section, is added to the experimental value and then compared with the analytical results. All the forces are mentioned in 'kN' and angle of taper in 'degrees'

4.3.1 Prismatic Beams

Table 40 presents the data of shear capacity and height for all the prismatic beams. The ratio between the experimental value and the analytical value is tabulated. The mean for the ratio between the experimental (E) and the analytical value (A) is 1.04 with a standard deviation of 0.2. Figure 86 shows scatter plot of ratios for the shear capacity of prismatic beam, which is evenly distributed about the line. From the graph and the tables, the following equations are validated, which are used to calculate the shear capacity contributed by concrete and stirrups when mean material properties are provided.

$$V_{Rm,c} = 0.15.k.\left(100.\rho_l.f_{cm}\right)^{\frac{1}{3}}.b.d$$

$$V_{Rm,s} = \frac{A_{sv}.f_{yvm}.z.\cot(\gamma)}{s}$$

Table 40 Experimental and Analytical shear capacity of all the prismatic beams discussed above

Specimen	Height (mm)	Experimental (E)	Analytical (A)	E/A
TASC α0-R0	450	76.15	96.93	0.79
TASC α0-R1	450	251.15	198.36	1.27
A1	300	74.5	54.48	1.37
C1	300	73.5	67.21	1.09
D1	300	84.5	85.48	0.99
F5	300	68.5	67.48	1.02
F6	300	63.5	54.3	1.17
D2	300	76	118.8	0.64
1L1	340	77.41	69.12	1.12
1L2	340	81.18	69.66	1.17
1K1	340	76.58	71.77	1.07
1K2	340	70.26	71.81	0.98
Beam 2, Macleod	250	32.9	39.83	0.83
Mean				1.04
Standard Deviation				0.2
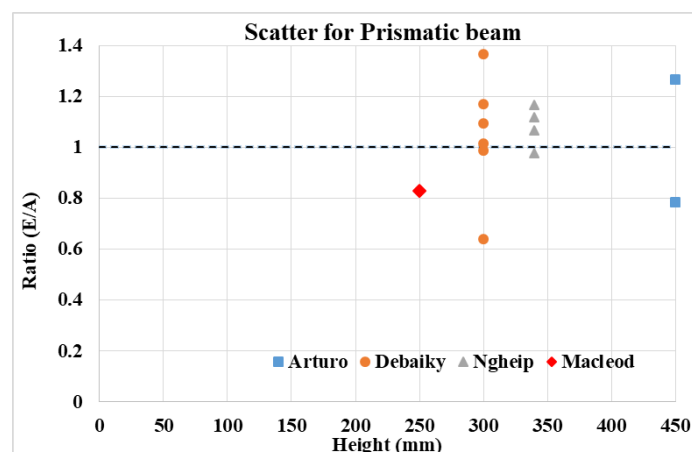
Figure 86 Scatter plot of the capacity ratio for prismatic beam discussed

69

4.3.2 Negatively Haunched Beams

Table 41 presents the data for the negatively haunched beams. The angle of taper for each specimen along with the respective experimental shear capacity (E), including the dead weight are mentioned. Analytical capacity, including and excluding the vertical components, are also tabulated. The mean and the standard deviation for the ratio between the experimental result (E) and the analytical results including the vertical component (AI) is 0.98 with a standard deviation of 0.24. On the other hand the mean and the standard deviation for the ratio between the experimental result (E) and the analytical result excluding the vertical component (AE) is 0.64 and 0.19 respectively.

Figure 87 shows scatter plot of the ratios for negatively haunched beams where the vertical component is included and Figure 88 for the negatively haunched beams where the vertical component is excluded. Overestimation of the shear capacity of the negatively haunched beam is observed if the analytical result is calculated without considering the vertical component of the inclined forces. Whereas accurate prediction of the shear capacity of the negatively haunched beam can be determined if the concept of effective shear resistance is applied as evident from the graphs and the tables.

Table 41 Experimental and Analytical shear capacity for the negatively haunched beams discussed above

Specimen	Angle	Experimental (E)	Analytical including vertical component (AI)	Analytical excluding vertical component (AE)	E/AI	E/AE
TASC α1-R0	3.07	69	77.48	90.13	0.89	0.77
TASC α2-R0	6.12	61.5	59.58	81.94	1.03	0.75
TASC α3-R0	9.13	39	42.43	70.43	0.92	0.55
TASC α4-R0	12.1	31.5	33.12	68.15	0.95	0.46
TASC α1-R1	3.07	201.5	155.24	180.26	1.30	1.12
TASC α2-R0	6.12	171.5	135.9	187.07	1.26	0.92
TASC α3-R0	9.13	121.5	91.5	153.4	1.33	0.79
TASC α4-R0	12.1	81.5	68.04	143.04	1.20	0.57
H-200	11.2	39.3	46.8	71.47	0.84	0.55
H-300	11.2	36.8	52.62	74.57	0.70	0.49
A4	4.76	30.4	40.05	53.41	0.76	0.57
A5	9.46	35.3	31.82	53.07	1.11	0.67
B5	12.1	40.2	36.06	60.11	1.11	0.67
B6	16.7	40.2	31.27	51.88	1.29	0.77
C4	9.46	35.3	37.67	62.87	0.94	0.56
C5	4.76	35.3	44.35	59.32	0.80	0.60
D5	9.46	25.5	52.65	88.12	0.48	0.29
D6	9.46	37.75	55.06	92.5	0.69	0.41
F1	9.46	42.65	40.71	67.48	1.05	0.63
Mean					0.98	0.64
Standard Deviation					0.24	0.19
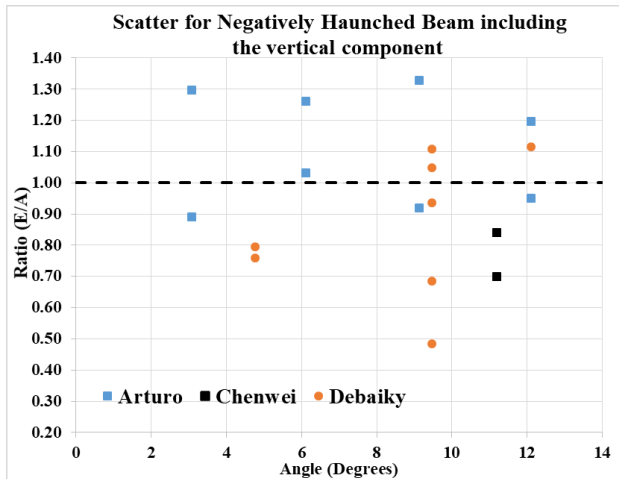
Figure 87 Scatter plot of the capacity ratio, including the vertical component, for negatively haunched beam
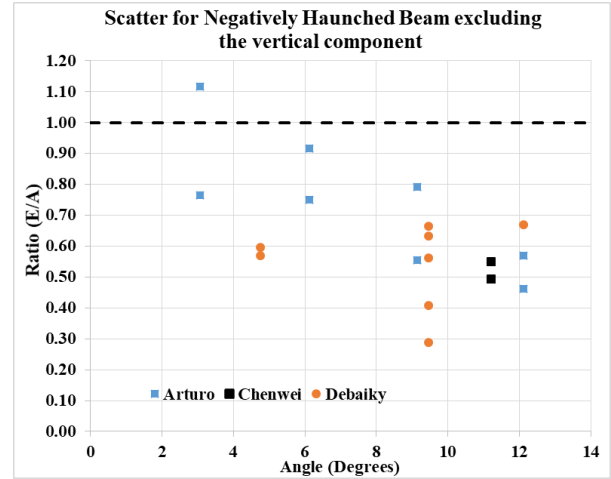
Figure 88 Scatter plot of the capacity ratio, excluding the vertical component, for negatively haunched beam

The specimens D5 and D6, tested by Debaiky [5], showed some irregularities in the results compared to the other specimens. Both these specimens have a higher amount of shear reinforcement than the other specimens tested by Debaiky et al. [5], as is evident from Table 2. Yet the shear capacity, at which major cracking occurs, is smaller than the other specimens, which is unexpected. If these two specimens are neglected, then the mean and standard deviation, for the ratio between experimental results to the analytical result including the vertical component, is 1.03 and 0.2 respectively. Nevertheless, from the data present it can be said that the vertical component of the inclined forces should be subtracted from the shear capacity of the negatively haunched beams.

4.3.3 Positively Haunched Beam

Table 42 presents the data for the positively haunched beams. The angle of taper and the experimental shear capacity, including the dead weight of the beam, for each specimen are mentioned. Ratios between the experimental and the analytical results are tabulated. The mean and the standard deviation for the ratio between the experimental values (E) to the analytical results (AI), where the vertical component of the inclined force is considered, is 1.09 and 0.36 respectively. Whereas for the ratio between the experimental results to the analytical results (AE), where the vertical component of the inclined forces is ignored is equal to 1.43 and 0.59 respectively.

Table 42 Experimental and Analytical shear capacity for the positively haunched beams discussed above

Specimen	Angle	Experimental (E)	Analytical including vertical component (AI)	Analytical excluding vertical component (AE)	E/AI	E/AE
2L1	3.95	76.86	67.11	61.24	1.15	1.25
2L2	3.95	76.28	67.59	61.71	1.13	1.24
3L1	5.91	68.2	60.84	52.79	1.12	1.29
3L2	5.91	71.03	61.24	53.06	1.16	1.34
2K1	3.95	84.47	73.63	67.47	1.15	1.25
2K2	3.95	85.94	73.65	67.48	1.17	1.27
3K1	6.71	80.28	74.30	63.90	1.08	1.26
3K2	6.71	80.87	74.32	63.92	1.09	1.27
4K1	10.01	85.68	72.26	57.27	1.19	1.50
4K2	10.01	84.82	72.27	57.28	1.17	1.48

B1,Stefanou	13.49	16	16.39	9.056	0.98	1.77
B2,Stefanou	7.96	26.8	16.122	12.56	1.66	2.13
B3,Stefanou	13.49	27.8	15.23	8.35	1.83	3.33
B4,Stefanou	7.96	26.7	14.71	11.6	1.82	2.30
Beam 1 EC2	9.53	19.4	20.81	15.74	0.93	1.23
Beam 2 EC2	15.43	28.6	18.03	12.64	1.59	2.26
Beam 3 EC2	12.95	17.5	14.66	11.14	1.19	1.57
A2	9.46	37.5	42.08	28.15	0.89	1.33
A3	4.76	35	51.19	44.02	0.68	0.80
C3	4.76	37.5	68.56	59.09	0.55	0.63
D3	9.46	37.5	82.39	55.43	0.46	0.68
D4	9.46	27.5	79.51	53.49	0.35	0.51
Beam 2,Macleod	4.74	36.65	38.52	33.63	0.95	1.09
Beam 4, Macleod	6.27	38	40.65	34.92	0.93	1.09
Beam 5, Macleod	7.57	41.25	37.27	27.72	1.11	1.49
Beam 6,Macleod	10.37	42.25	44	23.33	0.96	1.81
Mean					1.09	1.43
Standard Deviation					0.36	0.59
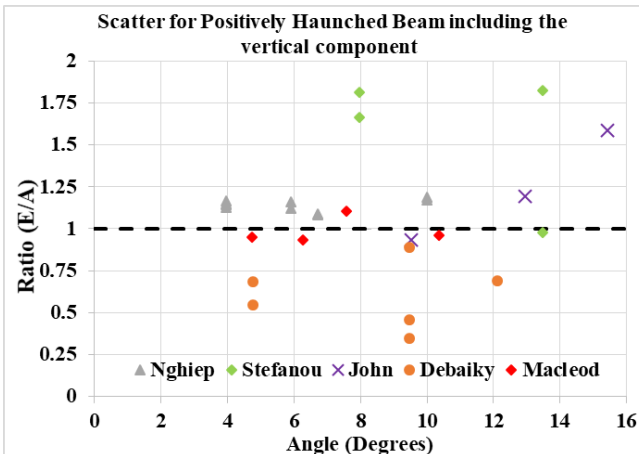
Figure 89 Scatter plot of capacity ratio, including vertical component, for positively haunched beams
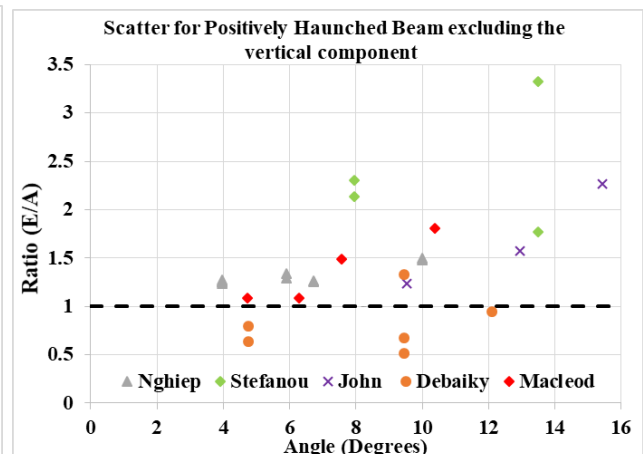
Figure 90 Scatter plot of capacity ratio, excluding vertical component, for positively haunched beams

Figure 89 and Figure 90 shows the scatter plot for positively haunched beam including the vertical component and the scatter for positively haunched beam excluding the vertical component respectively. One would underestimate the shear capacity of these haunched beams, if the vertical component is neglected whereas reasonable prediction of the shear capacity of the positively haunched beam can be obtained by applying the effective shear resistance formula. The scatter in this case is comparatively more than that of the negatively haunched beams as noticeable from the standard deviation. One of the reason is the assumption of critical section in positively haunched beams. In most cases, the critical section is considered near to the support and the cracking occurs mostly at the centre of the tapered section. Whereas in negatively haunched beam, cracking occurs near the critical section and therefore such a good coherence with the experimental result is observed in that case. To obtain better results, the positively haunched beams are analysed with different position of critical sections, from the support or the vertex (depending on the beam). The mean and

standard deviation for the ratio between experimental results and analytical results including the vertical component is also calculated for different positions of the critical sections and is tabulated in Table 43. From the table, it can be seen that as the critical section moves away from the support, the mean decreases and the standard deviation remains unaltered.

Table 43 Mean and Standard Deviaiton of positively haunched beam with different critical sections

Critical Section	Mean	Standard Deviation
Minimum height (h_{min})	1.09	0.36
Mean height (($h_{min} + h_{max}$)*0.5)	0.95	0.32
Maximum height (h_{max})	0.86	0.32

This constancy in the standard deviation might be due to the positively haunched beams tested by Debaiky [5] which failed in an instability type of shear failure. Due to this type of failure, it might be the case that analytical results does not correlate well with the experimental results. Table 44 shows the mean and standard deviation, for the ratio between experimental results and analytical results including the vertical component, for different position of critical sections excluding the Debaiky [5] series. From the table, it can be seen that the results are improved when the Debaiky [5] series is not considered. Moreover, when the critical section is chosen at a distance of h_{mean} from the support or the vertex (depending on the beam), the mean is close to unity with a reasonable standard deviation.

Table 44 Mean and Standard Deviaiton of positively haunched beam with different critical sections excluding Debaiky series

Critical Section	Mean	Standard Deviation
Minimum height (h_{min})	1.21	0.27
Mean height (($h_{min} + h_{max}$)*0.5)	1.06	0.23
Maximum height (h_{max})	0.96	0.25

Nonetheless, the above discussion proves the validity of the addition of the vertical component of the inclined cross-section forces to the shear resistance of the positively haunched beam

4.4 Approaches for Cross-Sectional Analysis in Non-Prismatic Beam

In Chapter 3, cross-section analysis on an inclined cut was performed on prismatic beams and it was proved that the cross-section results does not change. In this section, the same concept will be applied in haunched beams which has a non-linear layout of the centroidal axis as shown in Figure 69. Cross-section analysis on a vertical cut is already mentioned in the general approach section of this chapter. The following sub-section would indicate about the cross-sectional analysis on an angled cut, which is perpendicular to the centroidal axis.

4.4.1 Approach 1 – Vertical Compressive zone with forces in the global direction
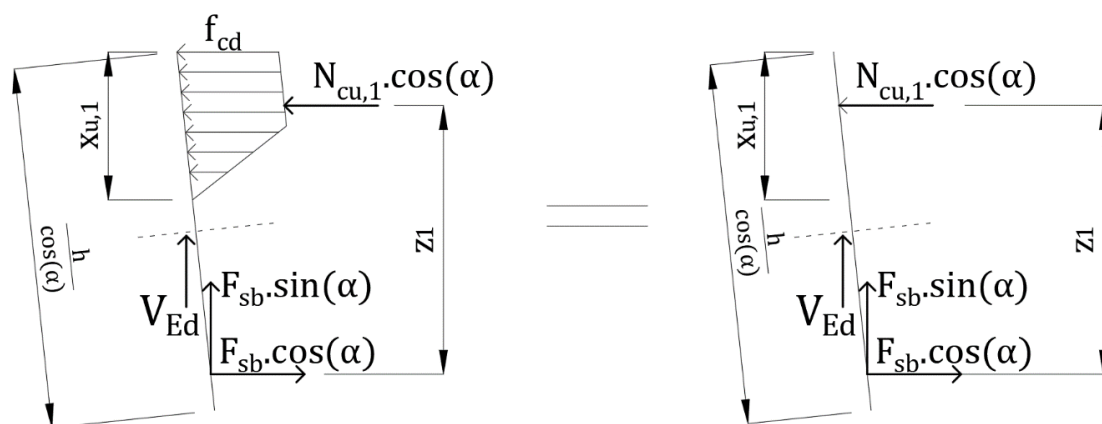
Figure 93 Stress distribution and forces in the global direction on an angled cut with vertical compression zone in non-prismatic beam

Figure 93 shows the stress distribution in an inclined angled cut in a non-prismatic beam. The figure is similar to Figure 52, except the vertical component of the inclined steel force. The definition of concrete compressive force is equal to the area under which stresses are applied and multiplied with the concrete compressive strength. If this definition is applied, the concrete compressive force is reduced by the cosine of angle of inclination to nullify the increased length of the inclined compression zone as mentioned in Chapter 3. By applying the horizontal equilibrium in the cross-section cut, the compressive zone can be determined as follows,

$$N_{cu,1}.\cos(\alpha) = F_{sb}.\cos(\alpha)..............(4.18)$$

$$N_{cu,1} = \frac{3.f_{cd}.b.x_{u,1}}{4.\cos(\alpha)}..............(4.19)$$

$$x_{u,1} = \frac{4.F_{sb}.\cos(\alpha)}{3.f_{cd}.b} = x_u..............(4.20)$$

Taking the moment about the point of application of the steel force, the following is obtained

$$M_{Rd,1} = N_{cu,1}.\cos(\alpha).z_1 = F_{sb}.\cos(\alpha).z_1$$

$$z_1 = d_{eff} - \frac{7.x_{u,1}}{18} = d_{eff} - \frac{14.F_{sb}.\cos(\alpha)}{27.f_{cd}.b} = z$$

$$M_{Rd,1} = F_{sb}.\cos(\alpha).\left(d_{eff} - \frac{14.F_{sb}.\cos(\alpha)}{27.f_{cd}.b} \right)..............(4.21)$$

In non-prismatic beam, the equation of bending moment resistance calculated on an inclined cut, which is perpendicular to the centroidal axis and with forces in the global direction, is similar to that obtained on a vertical cut i.e. equation 4.21 and equation 4.04 are same. Also the vertical component of the inclined steel force is added up in the applied shear force, which is similar to the one where the cross-sectional analysis is performed on a vertical cut. From the above formulation, the equation of the vertical compression zone is also same in both the cases – in an angled cut (equation 4.20) as well as on a vertical cross-section cut (equation 4.03).

4.4.2 Approach 2 – Inclined Compressive zone with forces in the global direction
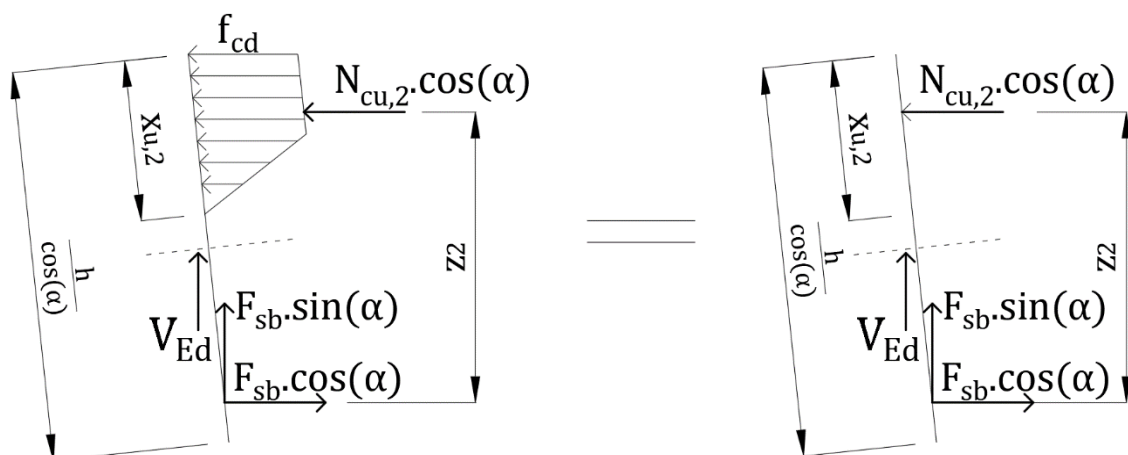
Figure 94 Stress distribution and forces in the global direction on an angled cut with inclined compression zone in non-prismatic beam

Figure 94 shows the stress distribution in an angled cut, with an inclined compressive zone ($x_{u,2}$) with the forces located in the global direction. The above figure is similar to the Figure

53, except the vertical component of the inclined steel force. The inclined compressive zone is calculated using the horizontal equilibrium as shown in equation 4.22.

$$N_{cu,2}.\cos(\alpha) = F_{sb}.\cos(\alpha)..............(4.22)$$

$$N_{cu,2} = \frac{3.f_{cd}.x_{u,2}.b}{4}..............(4.23)$$

$$x_{u,2} = \frac{4.F_{sb}}{3.f_{cd}.b} = \frac{x_u}{\cos(\alpha)}..............(4.24)$$

The bending moment resistance is calculated along the point of application of the steel force

$$M_{Rd,2} = N_{cu,2}.\cos(\alpha).z_2$$

$$M_{Rd,2} = F_{sb}.\cos(\alpha).z_2$$

As the lever arm is vertical, the inclined compression zone is first decomposed in the vertical direction by the multiplication of cosine of angle of inclination, and then further subtracted by the effective depth as shown below.

$$z_2 = d_{eff} - \frac{7.x_{u,2}.\cos(\alpha)}{18} = d_{eff} - \frac{14.F_{sb}.\cos(\alpha)}{27.f_{cd}.b} = z..............(4.25)$$

$$M_{Rd,2} = F_{sb}.\cos(\alpha).\left(d_{eff} - \frac{14.F_{sb}.\cos(\alpha)}{27.f_{cd}.b} \right) = F_{sb}.z_2.\cos(\alpha)..............(4.26)$$

The equation of lever arm remains the same as is the case when the analysis is performed on a vertical cut and hence the bending moment resistance is unaltered in this case as well. The vertical component of the inclined tensile tie is taken into account by the applied shear force, which was also seen in a Section 4.1. From the above formulation, the equation of the inclined compression zone for an angled cut (equation 4.24) is equal to $\frac{x_u}{\cos(\alpha)}$, which is as expected.

4.4.3 Approach 3 – Inclined Compression zone with forces in the local direction
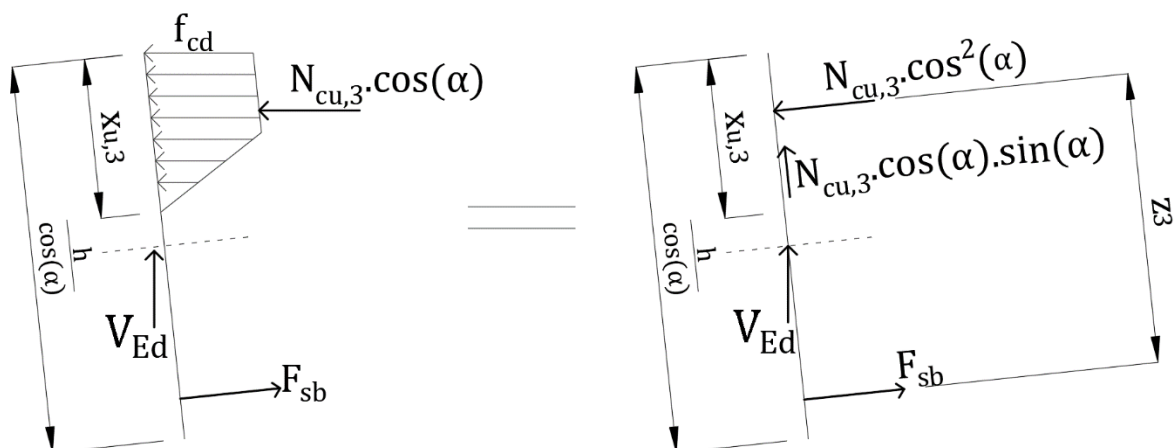
Figure 95 Stress distribution and forces in the local direction on an angled cut with inclined compression zone in non-prismatic beam

Figure 95 shows the cross-section forces directed in the local direction (Parallel and Perpendicular to the cross-section cut) with inclined compression zone. The lever arm is also

parallel to the cross-section cut. Equilibrium in the perpendicular direction of the cross-section cut is used to calculate the equation of inclined compression zone as shown below.

$$N_{cu,3}.\cos^2(\alpha) = F_{sb}..............(4.27)$$

$$N_{cu,3} = \frac{3.f_{cd}.b.x_{u,3}}{4}..............(4.28)$$

$$x_{u,3} = \frac{4.F_{sb}}{3.f_{cd}.b.\cos^2(\alpha)} \neq x_{u,2}..............(4.29)$$

In a beam, when a cross-section analysis is performed at the Ultimate Limit State, the equation of the vertical compression zone at a particular section, should be constant and the decomposition of that in the inclined direction should also be unchanged. However the equation of the compression zone (equation 4.29) obtained for the internal forces shown in Figure 95 is different than that obtained when the analysis is performed on an inclined cut with inclined compression zone with forces directed in the global direction i.e. Section 4.4.2 (equation 4.24). One cannot decompose the applied shear force / shear resistance in the local direction, as the perpendicular components would contribute to the bending moment resistance and that cannot be the case (shown in Appendix A). Also the parallel component of the compressive force does not contribute to the shear as the applied shear force is directed along the vertical direction.

To overcome this problem, the following iterative method is used.

a. Decomposition of the parallel concrete compressive force into the vertical and horizontal direction.
b. The horizontal component is further decomposed in the local direction (perpendicular and parallel direction) leading to an iterative process as shown in Figure 96.
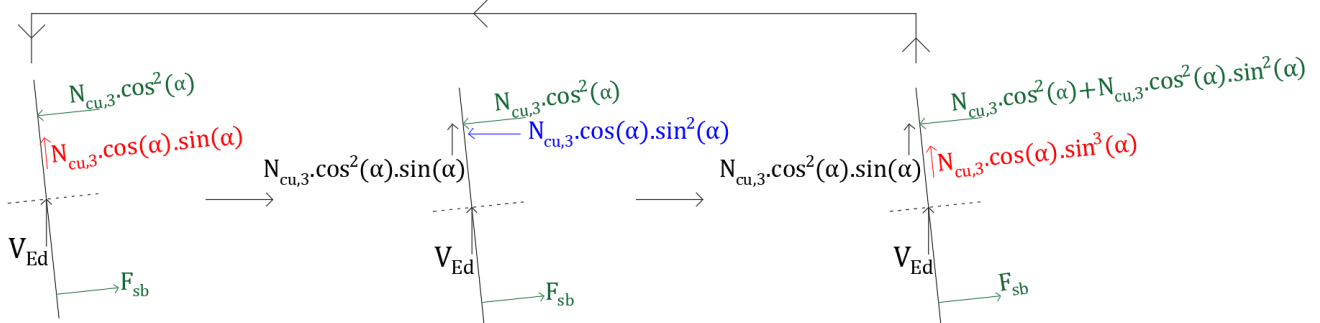
Figure 96 Decomposition of parallel compressive force - Iterative Procedure. Color Annotation, Black – Vertical direction, Blue – Horizonal Direction, Red – Parallel Direction, Green – Perpendicular Direction

As mentioned, the concrete compressive force in the parallel direction of the cross-section cut (red) is decomposed in the vertical component (black) and horizontal component (blue). The horizontal force (blue) is now again decomposed in the local direction i.e. in the perpendicular (green) and parallel (red) direction of the cross-section cut and the procedure continues. In conclusion, the forces are aligned in the perpendicular direction of the cross-section cut and in the vertical direction as shown in Figure 97. The reason for aligning the forces in the vertical direction is considering the fact that in Eurocode 2, the clause 6.2.1 states that the "vertical component" of the inclined force is considered in the shear resistance of the beam. The final forces are given as follows,

Perpendicular direction $\rightarrow N_{cu,3}.\cos^2(\alpha) + N_{cu,3}.\cos^2(\alpha).\sin^2(\alpha) + N_{cu,3}.\cos^2(\alpha).\sin^4(\alpha) +$

$N_{cu,3}.\cos^2(\alpha).\sin^6(\alpha) + N_{cu,3}.\cos^2(\alpha).\sin^8(\alpha) + ...$

Vertical direction $\rightarrow N_{cu,3}.\cos^2(\alpha).\sin(\alpha) + N_{cu,3}.\cos^2(\alpha).\sin^3(\alpha) + N_{cu,3}.\cos^2(\alpha).\sin^5(\alpha) +$

$N_{cu,3}.\cos^2(\alpha).\sin^7(\alpha) + N_{cu,3}.\cos^2(\alpha).\sin^9(\alpha) + ...$

$$\text{Perpendicular direction} \rightarrow N_{cu,3}.\cos^2(\alpha).\sum_{i=0}^{0,2,4} \sin^i(\alpha)$$

$$\text{Vertical direction} \rightarrow N_{cu,3}.\cos^2(\alpha).\sin(\alpha)\sum_{i=0}^{0,2,4} \sin^i(\alpha)$$

Taking the equilibrium in the perpendicular direction, the following equation is obtained

$$N_{cu,3}.\cos^2(\alpha).\sum_{i=0}^{0,2,4} \sin^i(\alpha) = F_{sb}\text{..............}(4.30)$$

From basic trigonometry,

$$\sum_{i=0}^{0,2,4} \sin^i(\alpha) = \frac{1}{\cos^2(\alpha)}\text{..............}(4.31)$$

Therefore,

$$N_{cu,3} = F_{sb}\text{..............}(4.32)$$

$$\frac{3.f_{cd}.b.x_{u,3}}{4} = F_{sb}\text{..............}(4.33)$$

$$x_{u,3} = \frac{4.F_{sb}}{3.f_{cd}.b} = x_{u,2} = \frac{x_u}{\cos(\alpha)}\text{..............}(4.34)$$

By this approach, the equation of the inclined concrete compression zone (equation 4.34) is equal to the one that was obtained when the analysis was performed on an angled cut with inclined compression zone and forces in the global direction (equation 4.24). From this equilibrium condition, the vertical component can be written as,

$$\text{Vertical direction} \rightarrow N_{cu,3}.\cos^2(\alpha).\sin(\alpha)\sum_{i=0}^{0,2,4} \sin^i(\alpha) \rightarrow N_{cu,3}.\sin(\alpha) \rightarrow F_{sb}.\sin(\alpha)\text{..............}(4.35)$$

The force in the vertical direction remains the same as the case in the previous approaches and hence the equation of effective shear force/resistance remains the same. Now the cross-section forces with the given lever arm is shown in Figure 97.
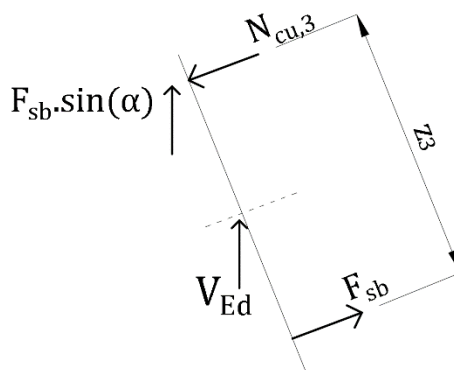
Figure 97 Cross-Section forces on an inclined cut with the lever arm

The bending moment resistance is calculated at the point of application of concrete compressive force and the formulation is shown below.

$$M_{Rd,3} = F_{sb}.z_3$$

$$z_3 = \frac{d_{eff}}{\cos(\alpha)} - \frac{7.x_{u,3}}{18} = \frac{d_{eff}}{\cos(\alpha)} - \frac{14.F_{sb}}{27.f_{cd}.b}$$

$$M_{Rd,3} = F_{sb}.\left(\frac{d_{eff}}{\cos(\alpha)} - \frac{14.F_{sb}}{27.f_{cd}.b}\right) \neq M_{Rd,i} \quad\text{................(4.36)}$$

From the above formulation, it can be seen that the equation of bending moment resistance calculated on an inclined cut (equation 4.36), with forces in the perpendicular and vertical direction of the cut is not equal to the one obtained from the previous approaches (equation 4.04, 4.21, 4.26). To be precise the above equation can be written in the following terms as,

$$M_{Rd,3} = F_{sb}.\left(\frac{d_{eff}}{\cos(\alpha)} - \frac{14.F_{sb}}{27.f_{cd}.b}\right)$$

$$M_{Rd,3} = F_{sb}.\left(\frac{d_{eff}}{\cos(\alpha)} - \frac{14.F_{sb}}{27.f_{cd}.b}\right).\frac{\cos(\alpha)}{\cos(\alpha)}$$

$$M_{Rd,3} = \frac{F_{sb}.\left(d_{eff} - \frac{14.F_{sb}.\cos(\alpha)}{27.f_{cd}.b}\right)}{\cos(\alpha)}$$

The equation of lever arm in the above formulation is similar to the one mentioned in equation 4.25. Therefore, the above equation of bending moment resistance can be written as,

$$M_{Rd,3} = \frac{F_{sb}.z_2}{\cos(\alpha)} = \frac{M_{Rd,2}}{\cos^2(\alpha)} = \frac{M_{Rd,i}}{\cos^2(\alpha)} \quad\text{..................(4.37)}$$

The equation of bending moment resistance calculated using this approach (equation 4.37) is different and greater than that obtained from the previous approaches, which was not as expected. To validate the above mentioned formulation the use of a simplified approach is made which is shown in the next section.

4.5 Simplified Approach

Engineers in practice do not follow the detailed procedure mentioned in the previous section, but apply a simple approach to calculate the area of reinforcement and/or bending moment resistance. In this approach, the concrete compressive zone is not determined. Instead, the bending moment resistance is calculated directly with the assumption of lever arm $z=0.9*d_{eff}$, which is then multiplied with the cross-sectional force. This approach is only used to check the bending moment resistance for different angled cross section cuts and therefore the vertical component or the parallel component of the inclined forces is ignored. This approach is applied to the prismatic beam, negatively haunched beam and positively haunched beam.

4.5.1 Prismatic Beam

The concept of simplified approach is first applied to the prismatic beam which is subjected to four point bending test as shown in Figure 49. The analysis is performed in the constant bending moment zone, between the point loads.

a. Vertical cut

Figure 98 shows the horizontal cross-section forces in a vertical cross-section cut with a vertical lever arm. The bending moment resistance is equal to the force multiplied with the lever arm, which is quite straightforward.

b. Angled cut

Figure 99 shows the cross-section forces directed in the local direction on an inclined cut with the lever arm parallel to the cut. The bending moment resistance is equal to the perpendicular component of the steel force/compressive force multiplied with the increased length of the lever arm. In this case the perpendicular component of the cross-section force is reduced by the cosine of angle of inclination and the lever arm is further increased by the same amount, leading to the same equation of the bending moment resistance.
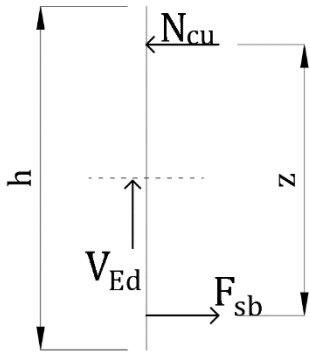
Figure 98 Cross-section forces on a vertical cross-section cut in prismatic beam (Simplified Approach)

Figure 99 Cross-section forces on an inclined cross-section cut in prismatic beam (Simplified Approach)

$$M_{Rd} = F_{sb}.z.............(4.38)$$

$$M_{Rd} = F_{sb}.\cos(\alpha).\frac{z}{\cos(\alpha)} = F_{sb}.z.....(4.39)$$

From the simplified approach method it can be noted in a prismatic beam subjected to four point bending test, the cross-section results does not change when the cross-sectional analysis is performed on a vertical cut and on an inclined cut. This further validates the approaches that were proposed in Chapter 3.

4.5.2 Negatively Haunched beam

The concept of simplified approach is now applied to the negatively haunched beam shown in Figure 69. The analysis is performed in the tapered zone of the beam.

a. Vertical cut

Figure 100 shows the vertical cross-section cut, where the steel force is applied at an angle and the concrete compressive force is horizontal. The steel force is decomposed in the horizontal and vertical component and the bending moment resistance is calculated using the vertical lever arm.
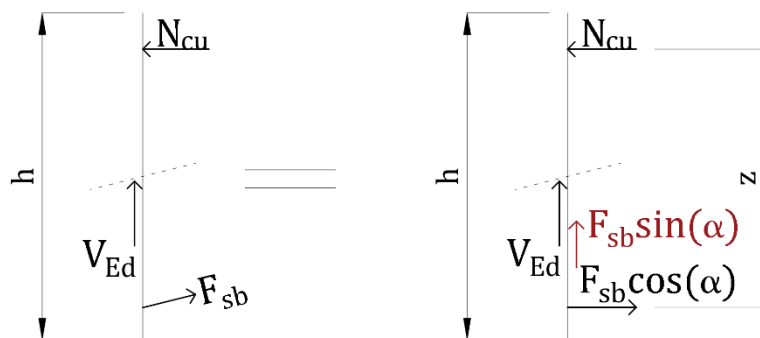
Figure 100 Cross-section forces on a vertical cross-section cut in negatively haunched beam (Simplified Approach)

$$M_{Rd,1} = F_{sb}.\cos(\alpha).z = N_{cu}.z.............(4.40)$$

The equation of the bending moment resistance is similar to that obtained from the general procedure (Section 4.1), Approach 1 (Section 4.4.1) and Approach 2 (Section 4.4.2). If the

applied bending moment (M_{ed}) is known, the area of bottom reinforcement ($A_{sb,m}$) can be calculated which is given as follows.

$$M_{Rd,1} = M_{ed}$$
$$M_{ed} = F_{sb}.\cos(\alpha).z$$

The general equation of lever arm is equal to $0.9*d_{eff}$ and the steel force (F_{sb}) can be written as $F_{sb} = A_{sb,m.}\,f_{yd}$. Hence,

$$M_{Rd,1} = A_{sb,m}.f_{yd}.\cos(\alpha)*0.9d_{eff}$$
$$A_{sb,m} = \frac{M_{ed}}{0.9*d_{eff}.f_{yd}.\cos(\alpha)}\dots\dots\dots(4.41)$$

where f_{yd} is the design yield strength of the steel reinforcement

b. Inclined cut

Figure 101 shows the cross-section forces for an angled cross-section cut, which is perpendicular to the centroidal axis. All the forces are directed in the local direction and the lever arm is considered parallel to the cross-section cut. The bending moment resistance is given as follows:
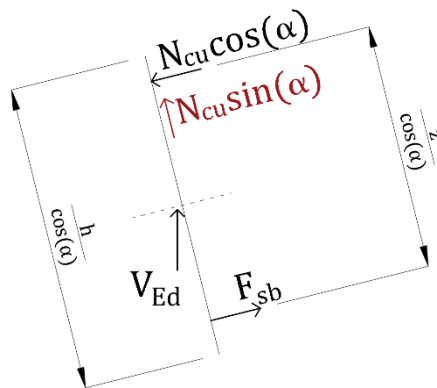
Figure 101 Cross-section forces on an inclined cross-section cut in negatively haunched beam (Simplified Approach)

$$M_{Rd,2} = N_{cu}.\cos(\alpha).\frac{z}{\cos(\alpha)} = N_{cu}.z = F_{sb}.\frac{z}{\cos(\alpha)} = \frac{M_{Rd,1}}{\cos^2(\alpha)}\dots\dots\dots(4.42)$$

The above simplified approach proves that in a negatively haunched beam, the bending moment resistance calculated on an inclined cross-section cut (equation 4.42), which is perpendicular to the centroidal axis with the forces aligned in the local direction, is greater than that calculated on a vertical cut (equation 4.40).The above formulation also confirms the outcome of Approach 3 (Section 4.4.3), where the bending moment resistance is greater than the previous obtained equation. The area of bottom reinforcement ($A_{sb,n}$) can be calculated by applying the moment equilibrium as shown below:

$$M_{Rd,2} = M_{ed}$$
$$M_{ed} = \frac{F_{sb}.z}{\cos(\alpha)}$$
$$M_{ed} = \frac{A_{sb,n}.f_{yd}*0.9.d_{eff}}{\cos(\alpha)}$$
$$A_{sb,n} = \frac{M_{ed}.\cos(\alpha)}{0.9*d_{eff}.f_{yd}} = A_{sb,m}.\cos^2(\alpha)\dots\dots\dots(4.43)$$

The above calculation further proves, that one would provide less amount of reinforcement in a negatively haunched beam if a simplified approach is performed on an inclined cut, with forces in the local direction. The maximum angle of taper allowed in construction industry, and also from the experimental data available, is 16.1°. If an analysis is performed with the cut perpendicular to the centroidal axis with the forces aligned in the local direction, then the amount of reinforcement provided would be less by 7.5% than that calculated on a vertical cut.

4.5.3 Positively Haunched Beam

The concept of simplified approach is now applied to the positively haunched beam shown in Figure 102. Vertical and Inclined cross-sectional analysis is performed at a distance 'x' from the left support.
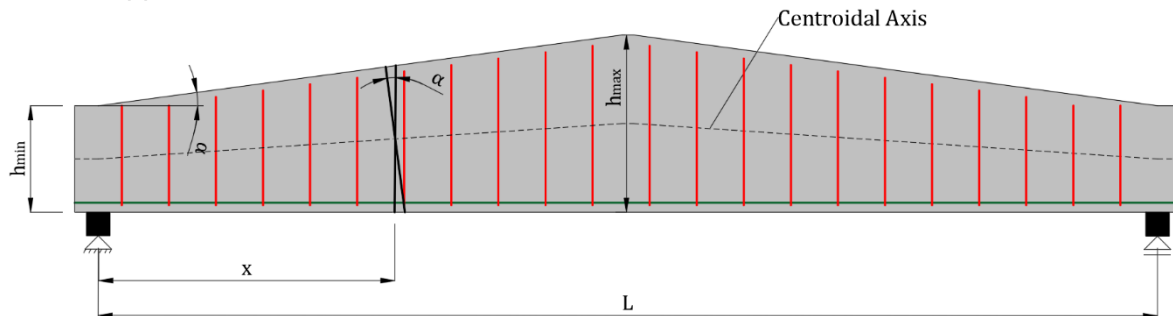
Figure 102 Positively haunched beam

a. Vertical cut

Figure 103 shows the analysis on a vertical cross-section cut, where the steel force is applied perpendicular to the cross-section cut and the compressive force is applied at an angle. The compressive force is decomposed in the horizontal and vertical direction and the bending moment resistance is equal to the steel force multiplied with the vertical lever arm.
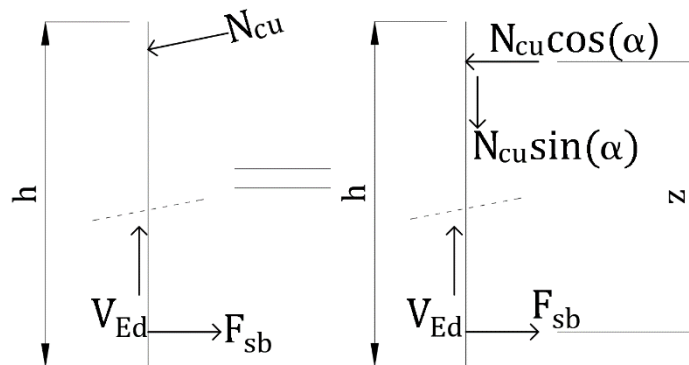
Figure 103 Cross-section forces on a vertical cross-section cut in positively haunched beam (Simplified Approach)

$$M_{Rd,1} = F_{sb}.z = N_{cu}.\cos(\alpha).z.............(4.44)$$

If the applied bending moment is known, the area of reinforcement to be provided can be calculated as follows:

$$M_{Rd,1} = M_{Ed} = F_{sb}.z$$

$$F_{sb} = \frac{M_{Ed}}{z} = A_{sb,m}.f_{yd}$$

$$A_{sb,m} = \frac{M_{Ed}}{0.9 * d_{eff}.f_{yd}}.............(4.45)$$

b. Inclined cut

Figure 104 shows the analysis performed on an inclined cut, where the compressive force acts perpendicular to the cut whereas the steel force is decomposed in the local direction. The bending moment resistance in this case is equal to the perpendicular component of the steel force multiplied with the increased length of the lever arm. This bending moment resistance is also equal to the compressive force multiplied with the increased length of the lever arm, leading to a different equation when compared to the vertical cut (equation 4.44).

$$M_{Rd,2} = F_{sb}.\cos(\alpha).\frac{z}{\cos(\alpha)} = F_{sb}.z = N_{cu}.\frac{z}{\cos(\alpha)} \neq M_{Rd,1} ....(4.46)$$
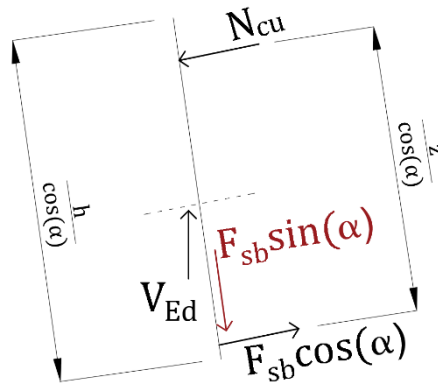
Figure 104 Cross-section forces on an inclined cross-section cut in positively haunched beam (Simplified Approach)

The amount of reinforcement to be provided, to resist the given loading can be calculated as follows:

$$M_{Ed} = M_{Rd,2} = F_{sb}.z$$

$$F_{sb} = \frac{M_{Ed}}{z} = A_{sb,n}.f_{yd}$$

$$A_{sb,n} = \frac{M_{Ed}}{0.9 * d_{eff}.f_{yd}} = A_{sb,m} ....(4.47)$$

From the above calculation, it can be seen that the bending moment resistance calculated on an inclined cut in a positively haunched beam is higher than that obtained on a vertical cut, similar to the case of the negatively haunched beam. However the area of reinforcement calculated on both the cross-section cut is exactly the same (equation 4.45 and 4.47), unlike negatively haunched beam. This difference is due to the fact that in negatively haunched beam the steel force is placed at an angle whereas in the positively haunched beam, shown in Figure 102, the steel force is aligned horizontally.

Let's assume that the scenario is reversed i.e. the area of reinforcement is known and the concrete class is to be calculated. When the analysis is performed in the tapered zone of the negatively haunched beam shown in Figure 69, then the equation of design compressive strength (f_{cd}) would remain constant, irrespective of whether the analysis is performed on a vertical or inclined cut. Conversely in case of positively haunched beam, the equation of design compressive strength obtained on an inclined cut is different than that obtained on a vertical cut. This is similar to the case of negatively haunched beam with respect to the area of reinforcement (equation 4.41 and equation 4.43). These inconsistency in the results are due to the geometry of the non-prismatic beam.

4.6 Comparison between Prismatic and Non-Prismatic beam

So far when the non-prismatic beams are analysed, the vertical component of the inclined force is taken into account in the shear resistance of the beam. But while designing the non-

prismatic beams, this component should be considered in the applied shear force and the shear reinforcement should be designed accordingly. Consider the prismatic and non-prismatic beam, both of which are subjected to four point bending test, shown in Figure 105 and Figure 106 respectively. The span of both the beam is 'L' and the point loads are applied at a distance of 'a' from the support. The height of the prismatic beam is h_{min} whereas the maximum height of the non-prismatic beam is at the support equal h_{max} and the minimum is at the centre of the beam which is h_{min}. Assuming that the percentage of longitudinal reinforcement in both the beams are same, the maximum load 'P' can be determined by performing a cross-sectional analysis in the zone of maximum bending moment i.e. at the centre of the beam. Hence the maximum load carried by both the beams will be the same, as long as sufficient amount of shear reinforcement is provided and all the other parameters such as the yield strength of the reinforcement, cover, concrete strength, width etc. remains constant.
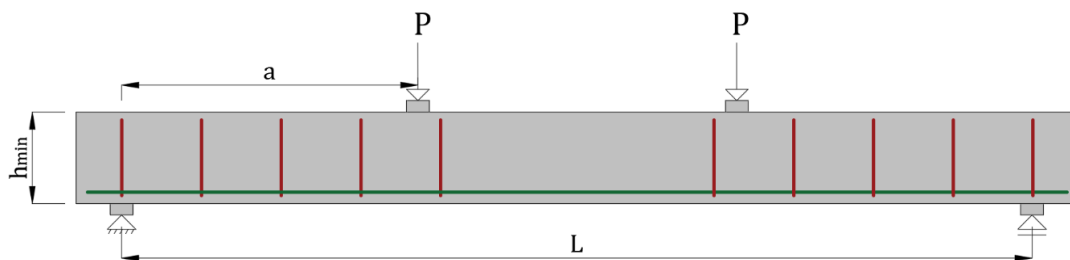
Figure 105 Prismatic beam subjected to four point bending test
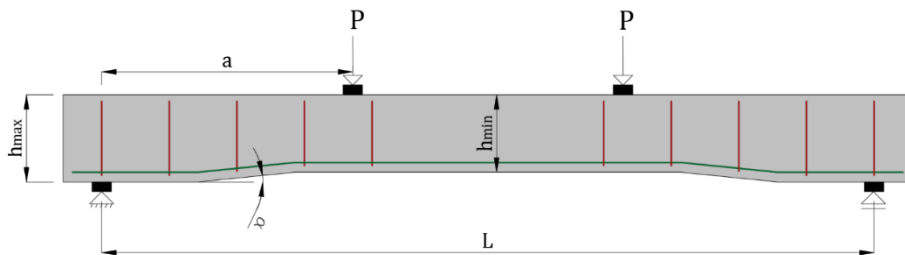
Figure 106 Negatively haunched beam subjected to four point bending test

Stirrups are designed based on the maximum applied shear force. As mentioned earlier, the vertical component of the inclined steel force should be considered in the applied shear force while designing non-prismatic beams. Hence the shear force diagram (SFD) of the negatively haunched beam would be different than that of the prismatic one as shown in Figure 108. Note that the SFD of the negatively haunched beam is not in equilibrium with the external loading, but to consider the vertical component and to analyse the beam a fictitious SFD is assumed.

Figure 107 Shear force diagram for prismatic beam shown in Figure 105
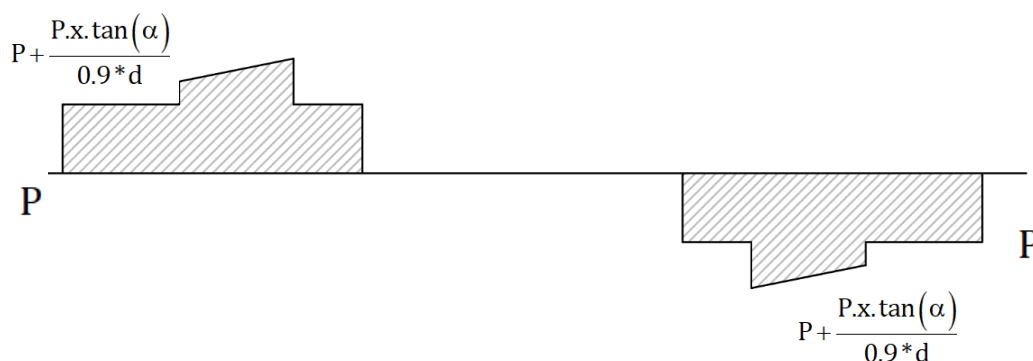
Figure 108 Fictitious shear force diagram for negatively haunched beam shown in Figure 106

In Figure 108, 'x' denotes the distance of the section from the support and 'd' denotes the effective depth at the given point. The formula for the effective shear force is given by,

$$V_{ed} = P + \frac{M_e.\tan(\alpha)}{z}$$

$$M_e = P.x$$

$$z \approx 0.9 * d_{eff}$$

As the applied shear force in a non-prismatic beam is greater than the prismatic beam (due to the vertical component), the amount of shear reinforcement required to produce a flexural failure in the haunched beam is more than that of the prismatic beam. Figure 106 can be visualized as adding concrete to some parts of the prismatic beam leading to a haunch shaped beam. This would suggest that the volume of concrete used to construct the negatively haunched beams is more when compared to the prismatic beam and yet the percentage of shear reinforcement provided to ensure flexural failure is high in case of negatively haunched beams. Even though there is no conclusive proof mentioned in this regard, it can be deduced from the literature review. Arturo et al. [10] showed that negatively haunched beam exhibits a ductile behaviour even if the beam fails in shear. The beams tested by the author were such that the height of the beam at the support is constant and varies at the centre as shown in Figure 33. When the beams with the same amount of shear reinforcement were tested, the collapse load for the negatively haunched beam decreased with the increase in the haunch angle. Nothing was mentioned about the ductility of the non-prismatic beams tested by Debaiky et al. [5]. The beams tested by the authors were such that the height of the beam at the support was varying and remain constant at the centre, just as the case discussed above. From the results, one can infer that when the same amount of shear reinforcement is provided in both the straight and the negatively haunched beams, the latter failed at a smaller load than the former one even though the amount of material used in the negatively haunched beam is more as shown in Figure 109. From Figure 109 it can be seen that as the volume of concrete increases, the capacity first decreases and increases slightly with further increase in the volume. This increase might be due to the strut mechanism in the negatively haunched beam. However this capacity is still smaller than the prismatic beam. In conclusion, to avoid shear failure, negatively haunched beams requires more amount of stirrup compared to the prismatic beam because of the vertical component of the inclined force which increases the applied shear force.
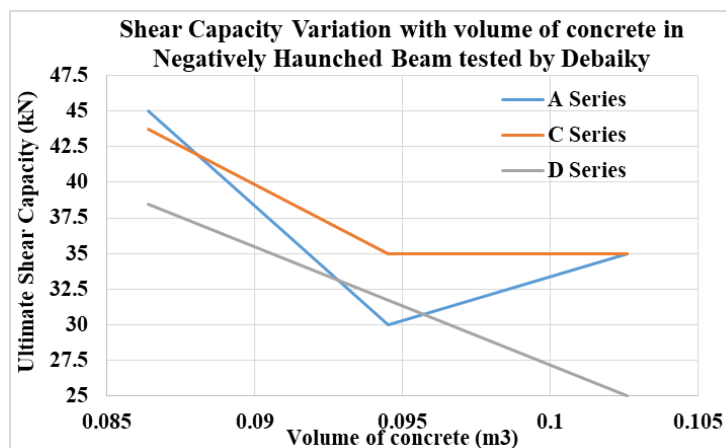
Figure 109 Shear capacity variation with the volume of concrete for the beams tested by Debaiky et al. [5]

As mentioned in Chapter 2, Macleod et al. [6] performed tests on positively haunched double cantilevered beam shown in Figure 13. The height of the beam at the support is constant and decreases at the free end. From the results, it was seen that the shear capacity of the positively haunched beam increases with increase in the angle of inclination. Also as the angle of inclination increases, the volume of concrete decreases and the shear capacity increases as

evident from Figure 110. This is related to the first and the fourth paradox proposed by Pagletti [12], shown in Figure 45, where the author states that if the theory of effective shear resistance is applied, then Figure 45(a) would fail at a larger load than Figure 45 (b). But the author objects that this should not be the case, as the amount of material used in the non-prismatic beam is less than that of the prismatic beam. However tests conducted by Macleod and Figure 110 shows that as the volume of concrete decreases, in a cantilevered haunched beam, the shear capacity increases, because of the vertical component of the inclined compression chord.
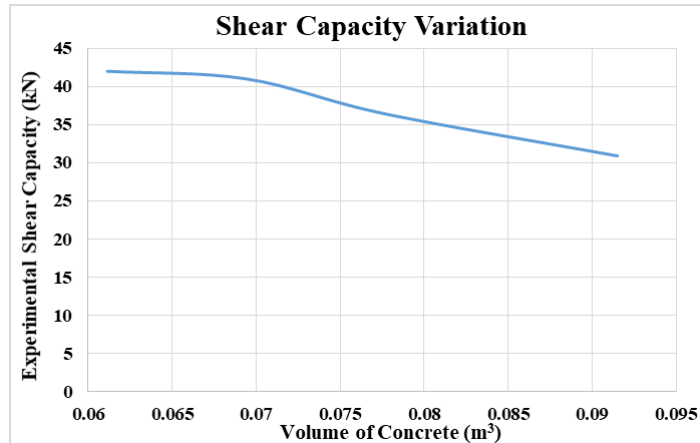
Figure 110 Shear capacity variation with the volume of concrete for the beams tested by Macleod [6]

The second paradox by Pagletti [12] states that if the concept of effective shear resistance is considered, the shear force diagram will change and hence no equilibrium will be maintained with the external load as seen from Figure 108. To avoid that, the vertical component of the inclined force should be added or subtracted from the shear resistance and not subtracted or added to the applied shear force. That's how all the beams in this study are analysed and equilibrium is maintained with the external loading.

The author also mentioned another paradox which describes the neutralization of the vertical force on one side of the section by that on the other side as shown in Figure 47. This would also suggest that there is no horizontal force present in the section and hence the bending moment resistance would be zero. But that's not how a cross-section analysis is performed. Forces from one direction are considered and the cross-section results are calculated based on these forces.

5 Cross-Sectional Analysis of Prestressed Non-Prismatic Beam

This chapter describes different issues one might come across while performing cross-sectional analysis in prestressed non-prismatic beam and provides solutions regarding the same. Non-prismatic prestressed beams are modelled in DIANA and further analysed to overcome the issues. Cross-sectional analysis is then performed on a continuous non-prismatic prestressed beam.

5.1 Prismatic Prestressed Beam

Consider the prestressed concrete beam shown in Figure 111. The prismatic beam is prestressed with parabolic tendons such that the radius of the 1st parabola, with a span of L_1, is R_1 whereas the radius of the second parabola is R_2 ($R_2>R_1$), with a span L_2. The equation of these parabolas were assumed to be $y = \dfrac{x^2}{2.R_i}$. Due to eccentricity, moments are generated at the ends. The origin of the parabola is at the intersection of the two parabolas, which is at a distance of L_1 from the left support. Figure 112 shows the cross-section analysis at the midpoint of the beam i.e. at a distance of $\dfrac{L}{2}$ from either supports or at a distance of x_1 from the origin of the parabola.
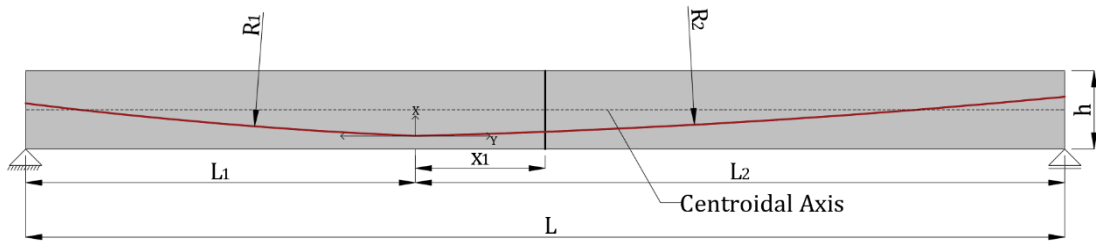
Figure 111 Prismatic prestressed concrete
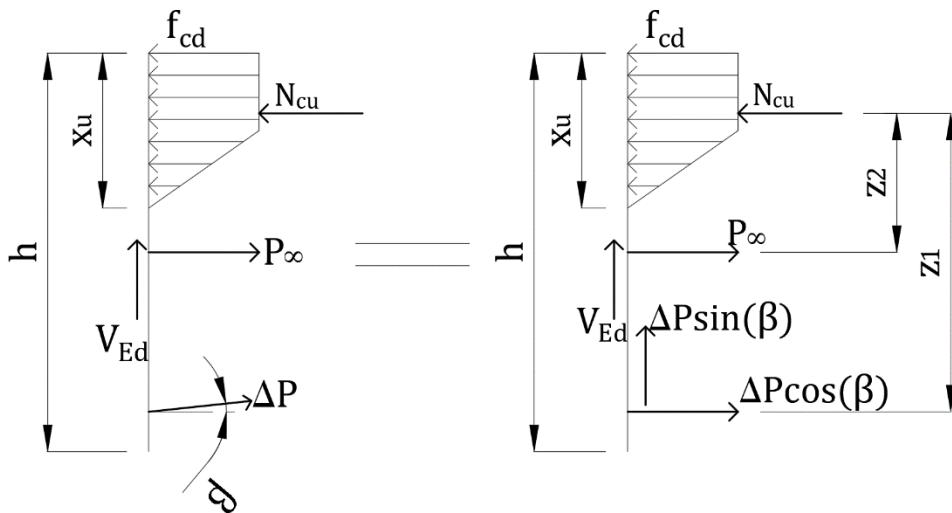
Figure 112 Cross-Section forces at the midpoint of the beam Figure 111

The concrete compressive force N_{cu} acts perpendicular to the cross-section cut at the top side. The prestressing force P_∞ also acts horizontally at the position of the centroidal axis i.e. at a distance of $\dfrac{h}{2}$ from the top or bottom. Due to the parabolic layout of the tendon, the increase in the prestressing force ΔP acts at an angle 'β' with respect to the horizontal axis. Decomposition of this force yields a horizontal component which is considered in the moment resistance of the beam and a vertical component which should be taken into account by the shear resistance, according to Eurocode 1992-1-1 [1].

The cross-section forces can be calculated using the following formula,

$$N_{cu} = \frac{3.b.f_{cd}.x_u}{4} \dots\dots\dots\dots(5.01)$$

$$P_\infty = A_p.\sigma_{p,\infty} \dots\dots\dots\dots(5.02)$$

$$\Delta P = A_p.\left(\sigma_{p,tot} - \sigma_{p,\infty}\right)\dots\dots\dots\dots(5.03)$$

Using horizontal equilibrium the following equations are obtained

$$N_{cu} = P_{\infty} + \Delta P.\cos(\beta)............(5.04)$$

$$x_u = \frac{4.(P_{\infty} + \Delta P.\cos(\beta))}{3.f_{cd}.b}$$

Calculating the moment resistance at the point of application of concrete compressive force (N_{cu}), the following formulation is achieved:

$$M_{Rd} = \Delta P.\cos(\beta).\left(d_{eff} - \frac{7.x_u}{18}\right) + P_{\infty}.\left(\frac{h}{2} - \frac{7.x_u}{18}\right)$$

$$M_{Rd} = \Delta P.\cos(\beta).\left(d_{eff} - \frac{14(\Delta P.\cos(\beta) + P_{\infty})}{27.f_{cd}.b}\right) + P_{\infty}.\left(\frac{h}{2} - \frac{14(\Delta P.\cos(\beta) + P_{\infty})}{27.f_{cd}.b}\right)............(5.05)$$

$$M_{Rd} = \Delta P.\cos(\beta).z_1 + P_{\infty}.z_2............(5.06)$$

The shear resistance of this prismatic prestressed concrete beam is given as,

$$V_{Rd} = \left(0.12k.(100.\rho_l.f_{ck}) + k_1.\sigma_{cp}\right).b.d_{eff} - \Delta P.\sin(\alpha)..........(5.06)$$

where,

A_p = Area of prestressing

f_{ck} = Charachteristic concrete compressive strength

$$k = 1 + \sqrt{\frac{200}{d_{eff}}}$$

$$d_{eff} = h - y_1 = h - \frac{x_1^2}{2.R_2}$$

b = width of the beam

ρ_l = Reinforcement ratio

$$\sigma_{cp} = \frac{P_{\infty}}{A_c} < 0.2f_{cd}$$

$$k_1 = 0.15$$

$$\sigma_{p,tot} = \frac{f_{p0.1,k}}{\gamma_s} = \text{Working prestress}$$

$\sigma_{p,\infty}$ = Stresses after considering the prestress losses

$$\beta = \frac{dy}{dx}_{\text{at the section}} = \frac{x_1}{R_2}$$

The shear resistance of the above mentioned prismatic prestressed beam is reduced by the vertical component of the inclined prestress force ΔP. It should be noted that the cross-sectional analysis performed in a prestressed beam is different when compared to a reinforced concrete beam. Moreover, it can be seen that even in a prismatic beam there can be a situation where the cross-section force acts at an angle, which changes the shear resistance of the beam.

5.2 Prestressed Haunched Beam

Haunched prestressed beams are generally used in bridges with taper near the mid-support as shown in Figure 113. Due to the shape of the beam, the centroidal axis has a non-linear layout along the length of the beam as seen by the dotted lines in Figure 113. The cross-sectional analysis is performed at a distance of 'x' from the vertex of the haunch.
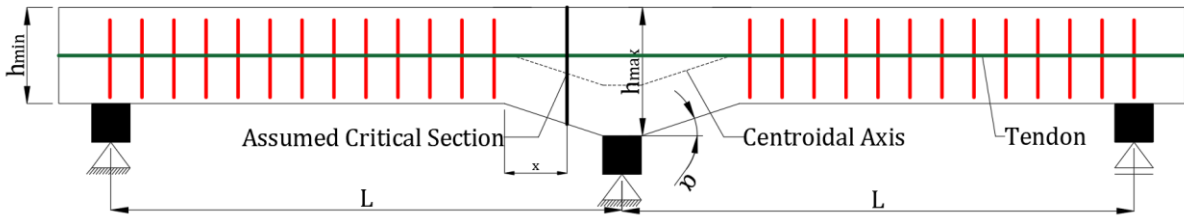
Figure 113 Continuous beam with haunch near the intermediate support

Assuming that at the ultimate limit state hogging moment is generated near the intermediate support, the cross-section force N_{cu} acts at an angle 'α' to the cross-section cut at the bottom side. The increase in the prestressing force ΔP acts perpendicular to the cut as the prestressing tendon is linear. The problem lies with the application of the prestressing force P_∞. The two issues are regarding the direction of the force P_∞ and the position of the force P_∞.

5.2.1 Direction of the force P_∞
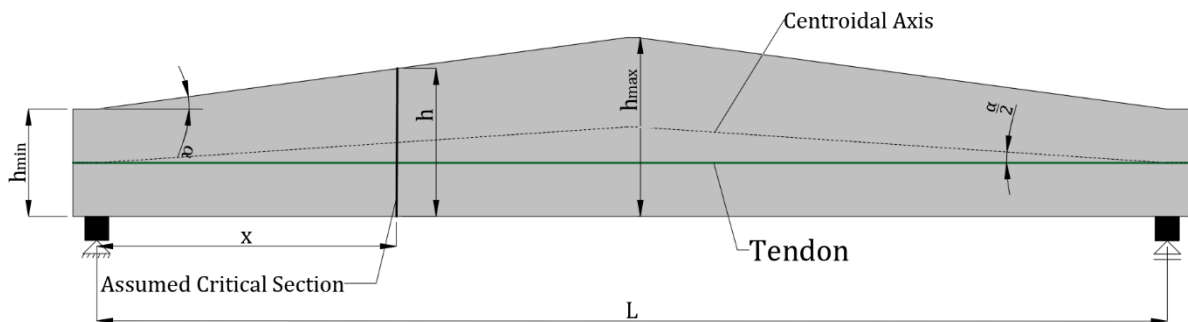
Figure 114 Positively Haunched beam with linear tendons

Consider the prestressed haunched beam shown in Figure 114, which is centrically prestressed. The angle of inclination of the haunch is 'α'. The height is minimum at the support and maximum at the centre. The angle of inclination of the centroidal axis with the horizontal tendon is $\dfrac{\alpha}{2}$. The cross-sectional analysis is performed at a distance 'x' from the left support as shown in Figure 115. The height of the beam at this point is 'h'.
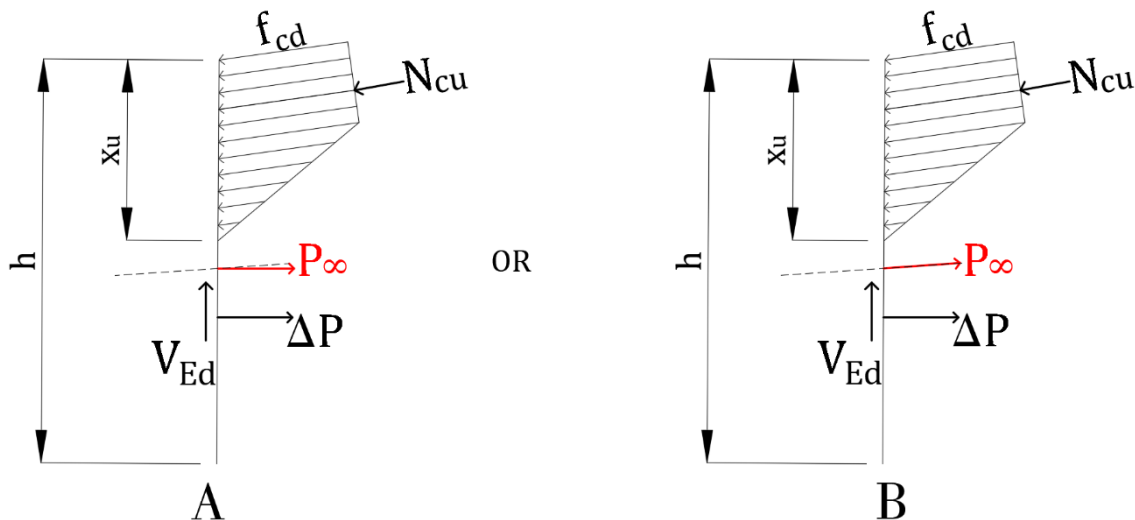
Figure 115 Direction of force P_∞ - horizontal or along the centroidal axis?

Due to the haunch, the concrete compressive force (N_{cu}) acts at an angle 'α'. The two scenarios regarding the direction of the force P_∞ is given in Figure 115, wherein the force either acts perpendicular to the cross-section cut or along the centroidal axis, which is at an angle with respect to the horizontal line. Horizontal equilibrium is used to check which one of

the above two scenarios is the correct one. For simplicity, the force P_∞ is applied at the centre of the cross-section height. The study of the position of the force P_∞ is done in the next section. In scenario A from Figure 115, the horizontal equilibrium is quite straightforward – the horizontal component of the inclined concrete compressive force should be equal to the total prestressing force i.e. the addition of P_∞ and ΔP. Horizontal equilibrium in the second situation is bit complicated – the horizontal component of the inclined concrete compressive force is equal to the horizontal component of P_∞ and the force ΔP.

$$N_{cu}.\cos(\alpha) = P_\infty + \Delta P ....(A)$$

$$N_{cu}.\cos(\alpha) = P_\infty.\cos\left(\frac{\alpha}{2}\right) + \Delta P ....(B)$$

The formulation of P_∞ and ΔP are given in equation 5.02 and 5.03 respectively. To find the solution for the above mentioned problem, models in DIANA are made and the horizontal force equilibrium is checked. The beam model is shown in Figure 116. Beam description is mentioned in Table 45. The concrete properties are mentioned in Table 46. Characteristic concrete properties are used. The constitutive model for the prestressing tendons is shown in Figure 117. The horizontal equilibrium check is applied at a distance of 2500 mm from the left support as shown in Figure 116. This equilibrium check is applied when the beam is fully prestressed i.e. when the stresses in the strands are equal to $\sigma_{p,\infty}$. To calculate the horizontal component of the inclined compressive force, σ_{xx} is plotted along the respective height of the beam as shown in Figure 118. All the stress plot follows the formula of $\sigma = -\dfrac{P}{A_c} \pm \dfrac{M}{W}$ and are around -1.8 MPa, which is the initial stress in concrete due to prestressing in a prismatic beam. The horizontal component of the inclined compressive force can be obtained by integrating these stress blocks along the height of the cross-section cut (h) and then multiplying it with the width of the beam (b). This force should either be equal to P_∞ or $P_\infty.\cos\left(\dfrac{\alpha}{2}\right)$ as $\sigma_{p,tot} = \sigma_{p,\infty}$ and therefore $\Delta P = 0$. Also the check is performed in the linear elastic stage. The dead weight of the beam is ignored.

Table 45 Beam description for positively haunched prestressed beam

Description	Value	Unit
Length	9400	mm
Span (L)	9000	mm
Height at the support (h_{min})	900	mm
Width (b)	500	mm
Area of Prestressing (A_p)	2000	mm^2
Stress in tendons (σ_∞)	400	MPa
Prestressing Force (P_∞)	800	KN
Angle of inclination (α)	0, 1.28, 2.57, 3.85, 5.17, 10.19, 16.28	degrees
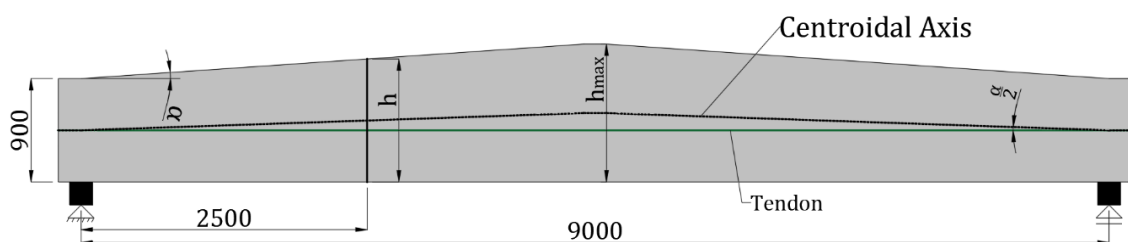
Figure 116 Beam dimensions of DIANA model

Table 46 Concrete Properties for positively haunched prestressed beam

Description	Value	Unit
Concrete Compressive Strength (f_{ck})	45	MPa
Concrete Tensile Strength (f_{ctk})	2.6	MPa
Young's Modulus (E_c)	35495	MPa
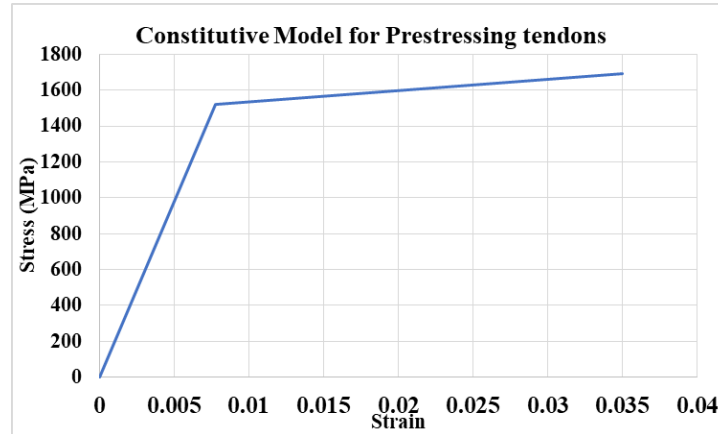
Figure 117 Constitutive model for prestressing tendons
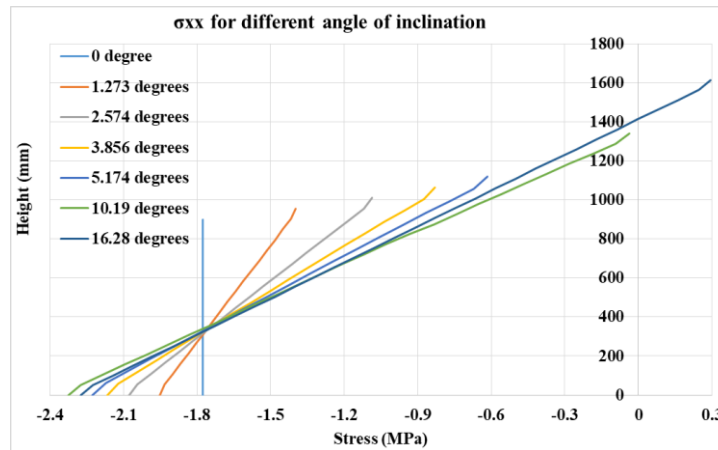
Figure 118 Stress block at a distance of 2500 mm from the left support for different angle of inclination

All the curves shown in Figure 118 are numerically integrated along their respective height to obtain the horizontal component of the inclined compression chord (N_{cu}). It was seen that for every angle of inclination, the magnitude of this component was more or less the same, and follows the trend of P_∞ and not $P_\infty . \cos\left(\dfrac{\alpha}{2}\right)$ as can be seen from Table 47. Figure 119 gives the graph for the percentage error in horizontal equilibrium of the section for the two scenarios.

Table 47 Horizontal force equilibrium check for different angle of inclination

Angle of inclination (α) (degrees)	$N_{cu}.\cos(\alpha)$ (kN)	P_∞ (kN)	$P_\infty.\cos(\alpha/2)$ (kN)
0.00	-799.99	801.64	801.64
1.27	-799.99	801.64	801.59
2.57	-799.99	801.64	801.44
3.86	-799.99	801.64	801.19
5.14	-800.00	801.64	800.83
10.19	-801.34	801.64	798.47
16.28	-800.00	801.64	793.56
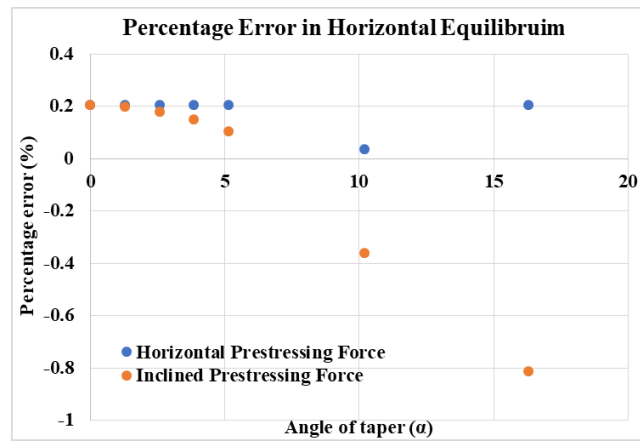
Figure 119 Percentage error in horizontal equilibrium for scenario A and B

The percentage error in horizontal equilibrium for scenario A, in which the prestressing force P_∞ acts perpendicular to the cross-section cut, is less than 0.2 for most of the models. On the contrary the percentage error in horizontal equilibrium for scenario B, where the prestressing force P_∞ acts along the centroidal axis, keeps on increasing with the increase in the angle of taper. For smaller angle of taper, the error in scenario B is less than 0.2% but as the angle of inclination increases the error keeps on increasing. From the curve, it can be seen that the maximum percentage error for situation B is less than 0.8, which is acceptable. But if it is assumed that the prestressing force P_∞ acts along the centroidal axis, at an angle, then the shear capacity of the beam would significantly alter due to the vertical component of this "assumed" inclined prestress force. Moreover, the normal force would act at its original linear path rather than acting at an angle. Hence option A from Figure 115, where the prestressing force P_∞ acts perpendicular to the cross-section cut, is the correct one.

5.2.2 Position of the force P_∞

The second query about the cross-sectional analysis of prestressed haunched beam is where does the horizontal prestressed force P_∞ acts – at the centre of the cross-section height (h) or at the centre of the height of the beam where the tendons are initially prestressed (h_{min}) as shown in Figure 120.
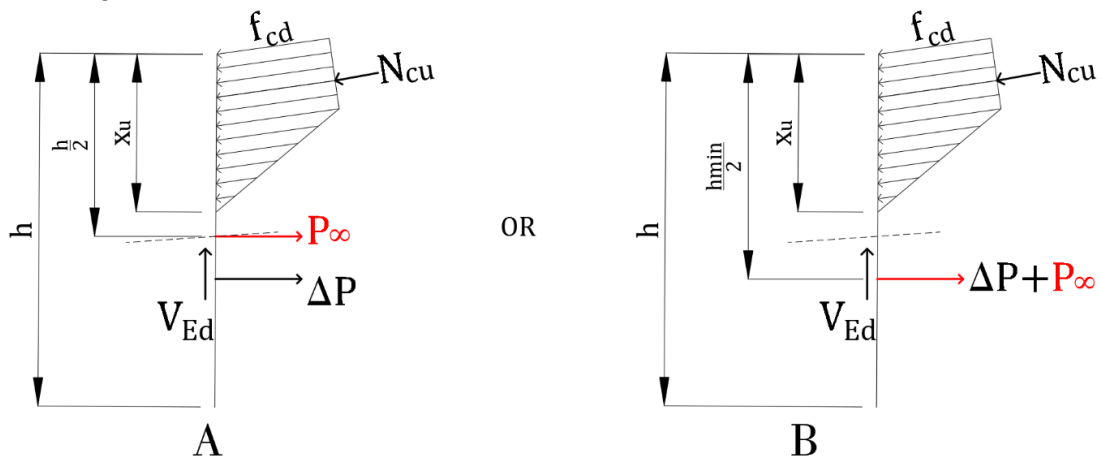
Figure 120 Point of application of force - at the center of cross-section cut or at the center of the minimum height ?

To check which of the above scenario is the correct one, DIANA models are made and further analysed. The beam shown in Figure 116 is centrically prestressed with straight tendons and according to the basic concepts, the displacement in the Y-direction should be zero. Note that the dead weight of the beam is ignored. However it was seen that as the angle of the haunch increases, the beam deflected in the positive Y-direction (upwards). Table 48 gives the maximum deflection of the haunched beam, when the beam is fully prestressed. This would suggest that a load is acting in the upward direction which results in the positive deflection. The reader of CIE 4160 – Prestressed Concrete [13] shows how to deal with prestressed beams which have a non-linear layout of centroidal axis. This concept introduces point loads

to the position where there is a kink in the centroidal axis. These point loads are then applied to the "adjusted centroidal axis" which is linear. This concept is applied on the positively haunched beams and further validated.

Table 48 Deflection at the center of the beam with varying angle of inclination calculated by DIANA

Angle (degrees)	Maximum Height (mm)	Deflection (mm)
0	900	0
1.27	1000	0.21
2.57	1100	0.33
3.85	1200	0.40
5.17	1300	0.45

The static scheme of these 2-D haunched beams can be given by Figure 121 and Figure 122.
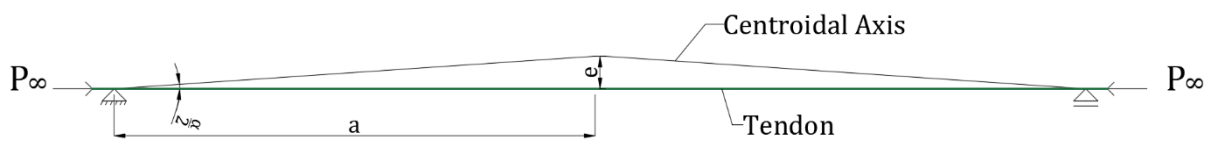
Figure 121 Static scheme - I
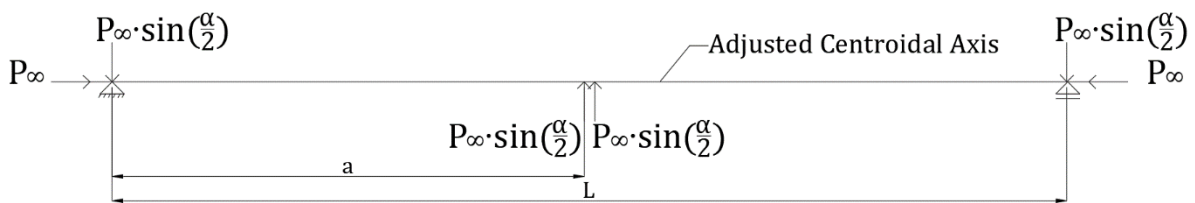
Figure 122 Static scheme - II

Figure 121 is the static scheme obtained from the 1-D model of the prestressed haunched beam, where the centroidal axis has a non-linear layout which is subjected to normal loading (P_∞). Figure 122 is the static scheme where the centroidal axis is adjusted, which is then subjected to point loads calculated according to the concept mentioned in the reader of CIE 4160 – Prestressed Concrete [13]. The deflection using both these static schemes are calculated and further discussed.

In static scheme-I, the bending moment along the length of the beam is equal to the prestressing force (P_∞) multiplied with the eccentricity 'y'. This eccentricity 'y' can be written in terms of the angle of inclination and the horizontal distance as:

$$y = x.\tan\left(\frac{\alpha}{2}\right)$$

The concrete parameters for the model is given in Table 46. The deflection at the centre of the beam can be calculated using the following formula:

$$M = EI.\frac{\partial^2 w}{\partial x^2}$$

where,

$M = $ Moment at position x=P_∞.x.$\tan\left(\dfrac{\alpha}{2}\right)$

$E = $ Elastic Modulus of concrete

$I =$ Moment of Inertia which is varying along the length of the beam $= \dfrac{b.\left(h + x.\tan(\alpha)\right)^3}{12}$

$w =$ Deflection in the y-direction

This differential equation is solved in MAPLE and the deflection at the centre of the beam is calculated. For the validation of the 2nd static scheme, the 4 point loads are applied on the 2-D haunched beam as shown in Figure 123 and the deflection at the centre of the beam is calculated in DIANA. The deflection, for different angle of inclination, due to both these static schemes are tabulated in Table 49. It can be seen that both these static scheme result into more or less the same deflection, which is also equal to the one obtained by the application of prestressing force to the 2-D haunched beam shown in Table 48. The small difference between the deflections from the two static schemes can be attributed to the inclusion of shear deformation in the Finite Element Model.
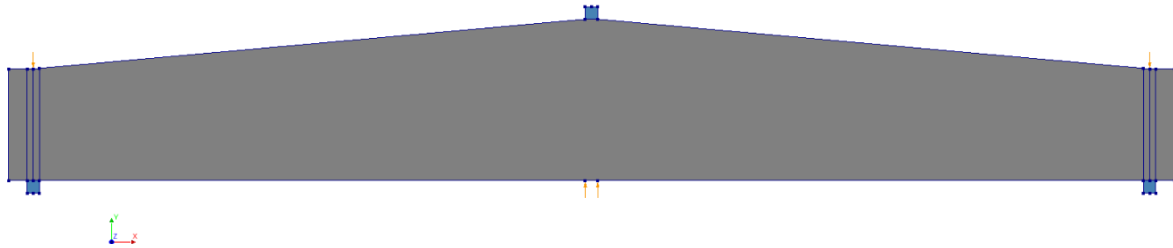
Figure 123 2-D haunched beam subjected to point loads

Table 49 Deflection comparison from both static schemes for different angle of inclination

Angle of inclination (degrees)	Deflection due to scheme-I (mm)	Deflection due to scheme-II (mm)
1.27	0.20	0.20
2.57	0.32	0.33
3.85	0.39	0.41
5.17	0.43	0.45

Moreover the bending moment diagram for both of these static scheme is approximately equal. The maximum bending moment, at the centre of the beam, for both the static schemes can be given as:

$$M_{\text{max},I} = P_\infty . e = P_\infty . a . \tan\left(\frac{\alpha}{2}\right) \approx P_\infty . a . \sin\left(\frac{\alpha}{2}\right)$$

$$M_{\text{max},II} = P_\infty . \sin\left(\frac{\alpha}{2}\right) . a$$

Both the mechanical schemes results in almost the same deflection and bending moment. Hence both these static schemes are similar. Nasreddin El-Mezaini et al. [14] analysed different frames which has non-prismatic sections. Author's statement regarding Figure 124 was that if one of the segment of the non-prismatic section is subjected to axial force, then due to the eccentricity in the centroidal axis, moment is generated in the other segment and the axial force is applied at the centre of the height of the other segment.
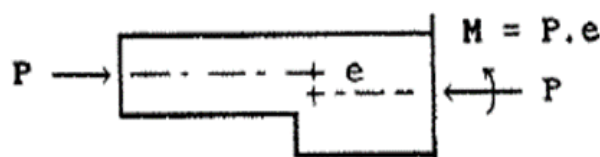
Figure 124 Normal force in a haunched beam [14]

95

Using this concept, if the cross-sectional analysis is performed at the centre of the haunched prestressed beam shown in Figure 116, then the prestressing force P_∞ should be applied at the centre of the cross-section height, at the centroidal axis level. This can be done provided the moment due to the shift in the centroidal axis is either subtracted from the applied bending moment equation or added to the bending moment resistance. Hence option A from Figure 120 is the correct one, provided the bending moment due to the variation in the centroidal axis is considered.

Once the beam is prestressed, the tendons act as a reinforcement and the procedure to calculate the shear capacity of the prestressed non-prismatic beam is similar to that of the reinforced non-prismatic beam shown in Section 4.2.

5.3 Continuous Prestressed Haunched Beam

The concept mentioned in the previous section is now applied to a continuous prestressed haunched beam as shown in Figure 125. The beam is prestressed with 3 parabolas, with radii R_1 and R_2. Tapered section is provided near the intermediate support. The cross-sectional analysis is performed at a distance of x_1 from the origin of the parabola. The mechanical scheme, with different loading is given in Figure 126.
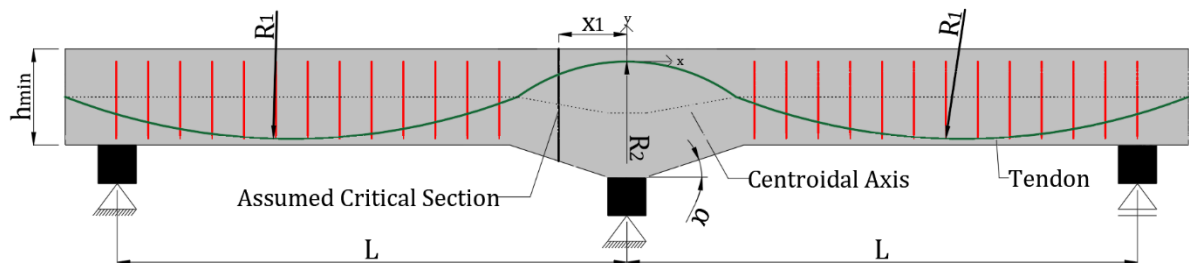
Figure 125 Continuous prestressed non - prismatic beam with parabolic tendons
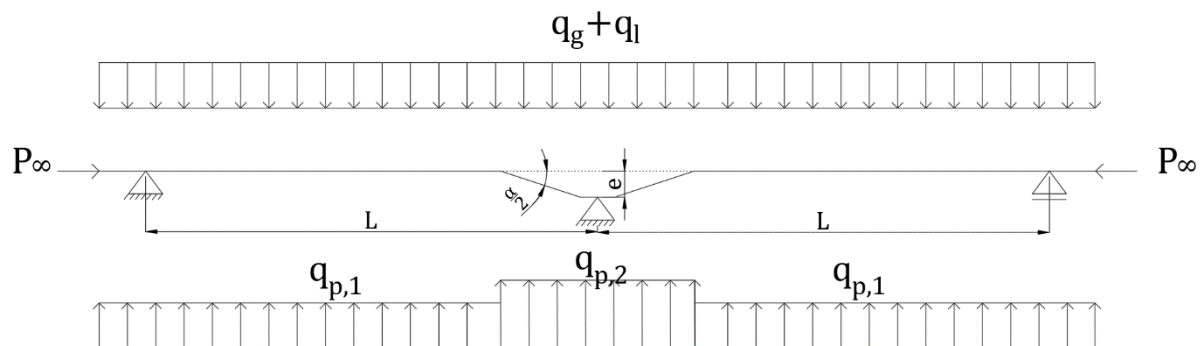
Figure 126 Static scheme for the beam shown in Figure 125

The beam is subjected to dead load (q_g) and live load (q_l). Other than the normal prestressing force P_∞, the beam is also subjected to curvature pressure given as $q_p = \dfrac{P_\infty}{R_i}$ acting throughout the length of the beam. The cross-section forces at the assumed critical section are given in Figure 127, where it is assumed that hogging moment is generated at the Ultimate Limit State. The force ΔP acts at an angle due to the parabolic layout of the tendon. This force is decomposed in the horizontal and the vertical direction. Due to the geometry of the beam, the concrete compressive force N_{cu} acts at the angle of taper 'α', which is further divided in the global direction as shown. The prestressing force P_∞ acts horizontally at the position of the centroidal axis, provided the bending moment due to the shift in the centroidal axis is considered.
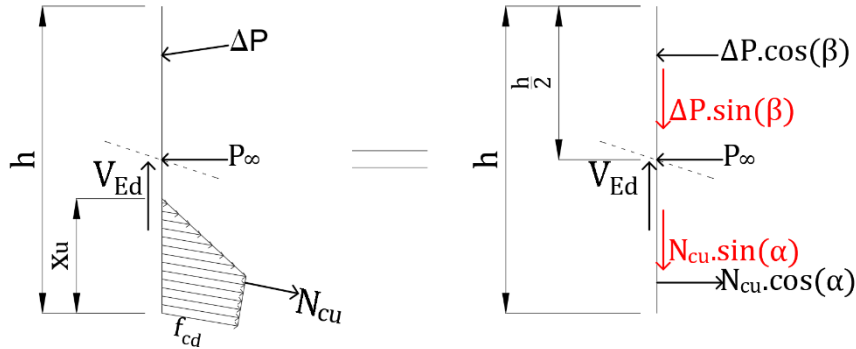
Figure 127 Cross - section forces in the critical section cut
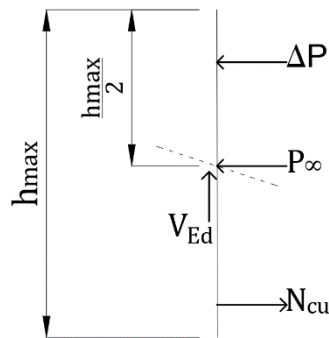
Figure 128 Cross-section forces for a cut at the intermediate support in Figure 125

If this cross-sectional analysis is to be performed exactly at the centre of the intermediate support, the cross-section forces are shown in Figure 128. The prestressing force P_∞ acts at the centre of the cross-section height, provided the equation of the applied bending moment is given as follows:

$$M_{Ed} = M_{g+l} - M_{pre} - P_\infty.e$$

where

$M_{g+l} =$ Bending Moment due to dead weight and live load

$M_{pre} =$ Bending Moment due to curvature pressure

$e =$ Eccentricity at the centre

The last term of the equation takes into account the moment due to the shift in the centroidal axis, which reduces the applied bending moment.

6   Errors while performing Cross-Sectional Analysis on Non-Prismatic Bridges

This chapter discusses different errors that engineers make in practice while performing cross-sectional analysis on non-prismatic bridge decks. The error in the cross-section results for different models are calculated for an existing bridge deck, Wolweg Bridge, and further discussed.

6.1 General Information – The Wolweg Bridge

The Wolweg Bridge is located near a village named Stroe, in the Gelderland province of The Netherlands. The construction of the bridge was completed back in 1965. The bridge is located on the A1 motorway, where the European Route E30 also follows. The bridge is a skew bridge as can be seen from Figure 129, with a skew angle of 51.5º.

Figure 129 Aerial photograph of the bridge [15]

The bridge has 2 deck, with three spans per deck as shown in Figure 129 and Figure 130. The length of the end decks is 10.5 m whereas the length of the middle deck is 13 m as shown in Figure 130. Tapered section is provided near the intermediate support to increase the shear capacity. The width of the deck is 20.8 m in the southern part, where the study is focused on. The zoomed in tapered section is given in Figure 131. Tapered section can also be seen in Figure 132 and Figure 133.
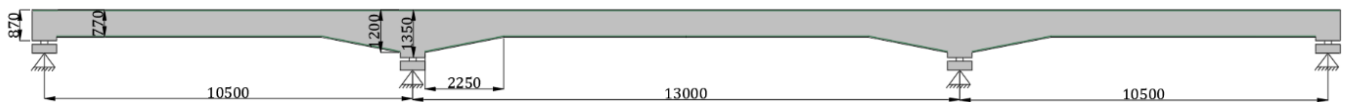
Figure 130 Deck dimensions
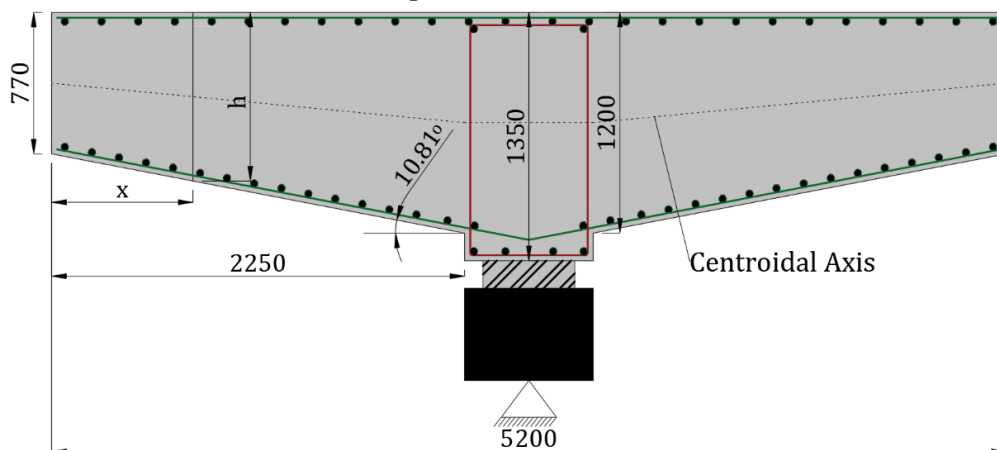
Figure 131 Tapered section of the deck

The height of the deck in the prismatic section is 770 mm whereas the maximum height in the tapered section is 1200 mm and that at the intermediate support is 1350 mm. The angle of taper is 10.81º. The length of the tapered zone is 2250 mm. To distribute the longitudinal reinforcement, the bridge deck was divided into 15 different zones as can be seen in Figure 134. In this study, the focus is on the tapered section of the deck i.e. either zone 4, 5 and 6 or

100

zone 10, 11 and 12. Reinforcement detailing is given in Table 50, Table 51, Table 52 and Table 53.

Figure 132 Zoomed in tapered section [15]

Figure 133 Tapered section at the intermediate support [15]
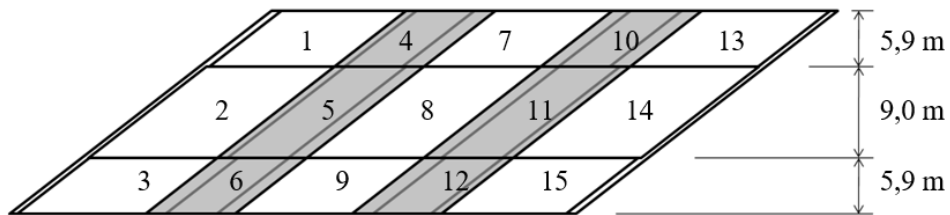
Figure 134 Lane and zone division in the bridge deck [15]

Table 50 Top reinforcement detailing

Zone number	Diameter (in mm)	Spacing (in mm)
4	40	139
5	40	159
6	40	139

Table 51 Bottom reinforcement detailing

Description	Diameter (in mm)	Spacing (in mm)
Zone 4, 5 and 6	19	275

Table 52 Concrete properties of the bridge deck

Description	Value	Unit
Characteristic Cube Compressive Strength	22	MPa
Characteristic Cylinder Compressive Strength (f_{ck})	19	MPa
Design Compressive Strength	12	MPa
Mean Compressive Strength	27	MPa
Mean Tensile Strength	2.11	MPa
Young's Modulus	27750	MPa

Table 53 Reinforcment properties of the bridge deck

Description	Value	Unit
Characteristic Yield Strength (f_{yk})	400	MPa
Design Yield Strength (f_{yd})	348	MPa

Due to the shape, these type of bridge deck has a non-linear layout of the centroidal axis along the length of the tapered deck as shown in Figure 131. Engineers, in practice, model these decks differently such that the centroidal axis remains straight. This is done by introducing taper or curve shape to the opposite side of the haunch. By doing so, the centroidal axis remains straight. The volume of concrete used is same but the structure is changed and this might change the cross-sectional results. The Wolweg Bridge was investigated by TNO in 2003 for the shear capacity [15]. While analysing the bridge deck, professionals at TNO modified the cross-section of the deck as shown in Figure 135 so that the centroidal axis remains straight. Cross-sectional analysis on the original deck and the modified deck is performed in this study and the results are discussed.
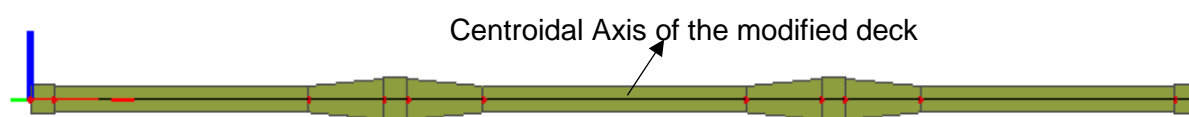
Figure 135 Modified section of the bridge deck [15]

6.2 Cross Sectional Analysis – Original deck

Figure 136 shows the cross-section analysis performed at a distance 'x' from the free end of the tapered section shown in Figure 131. F_{st} is the steel force due to top reinforcement which acts at a distance of 30 mm from the top fibre. F_{sb} is the steel force due to bottom reinforcement and $N_{cu,1}$ is the concrete compressive force, both of which acts at an angle 'α' with respect to the horizontal axis. Due to this inclination, these forces are decomposed in the horizontal and vertical component. The horizontal component is taken into account by the moment resistance with the given lever arms and the vertical component is included in the shear capacity or the applied shear force of the deck. Figure 136 shows that the vertical component of the inclined forces reduces the applied shear force or increase the shear capacity of the deck. This also confirms that providing a haunch at the intermediate support increases the shear resistance of the deck and is therefore advantageous for the structure. To calculate these vertical components, the use of horizontal equilibrium is made.

a. Upper Bound Shear Capacity

In this case, it is assumed that the reinforcements are yielded and concrete strength is equal to the design concrete compressive strength throughout the length of the tapered section.
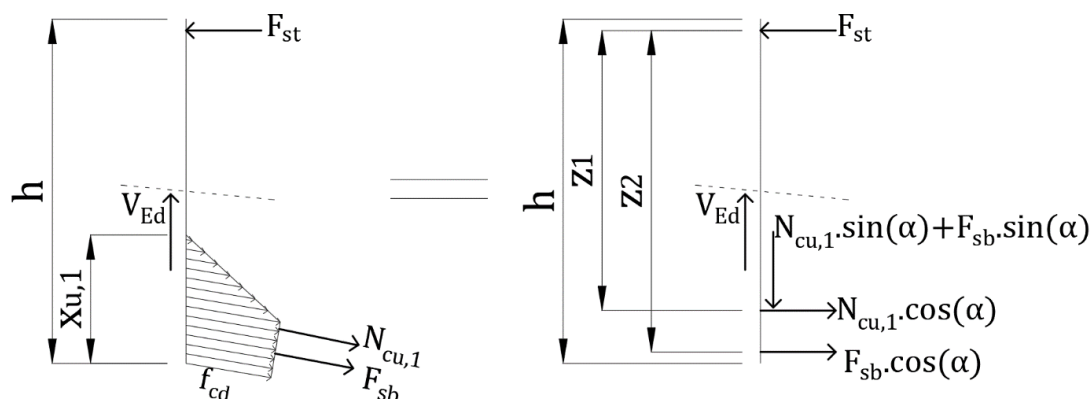
Figure 136 Cross-sectional analysis on the tapered section shown in Figure 131

102

The equation of horizontal equilibrium is given as follows:

$$F_{st} = (N_{cu,1} + F_{sb}).\cos(\alpha)$$

$$F_{st} = A_{st}f_{yd} = 62097.9 \text{ KN}$$

$$F_{sb} = A_{sb}f_{yd} = 7498.7 \text{ KN}$$

$\alpha = 10.81$ degrees

Hence $N_{cu,1} = 55721 \text{ kN} = \dfrac{3.f_{cd}.x_{u,1}.b}{4}$

The shear resistance contributed by concrete is calculated using the formula shown below,

$$V_{Rd,c} = 0.12.k.(100\rho_l f_{ck})^{\frac{1}{3}}.b.d$$

where,

$k =$ size factor $= 1 + \sqrt{\dfrac{200}{d}}$

$d =$ effective depth $= h - 30$

$\rho_l = \dfrac{A_{st}}{b.d}$

$A_{st} =$ Area of top reinforcement

$f_{ck} =$ Characteristic Cylinder Compressive Strength

The effective shear resistance is given by,

$$V_{Rd} = V_{Rd,c} + F_{sb}.\sin(\alpha) + N_{cu,1}.\sin(\alpha)................(6.01)$$

The moment resistance calculated at the point of application of top force is given as,

$$M_{Rd} = N_{cu,1}.\cos(\alpha).z_1 + F_{sb}.\cos(\alpha).z_2................(6.02)$$

where,

$z_1 = h - c - \dfrac{7.x_{u,1}}{18}$

$z_2 = h - 2.c$

$x_{u,1} =$ concrete compressive zone

$c =$ concrete cover

As it is a ULS check, the magnitude of both the vertical component would remain constant throughout the length of the tapered zone. Figure 137 shows the effective shear resistance variation, which is the upper bound shear capacity, along the length of the tapered deck. It can be seen that as soon as the tapered section begins, the concept of effective shear resistance comes into account which increases the capacity. This drastic increase is due to the assumption that the magnitude of cross-section forces are maximum throughout the length of the tapered deck. At the intermediate support of the tapered section, the height remains constant and therefore the shear resistance is constant as well. Due to the vertical component of the assumed inclined yielded forces, the shear resistance in the tapered section is almost 3 times the shear resistance of the prismatic segment. But John J. Orr et al. [11] proved in his study that it leads to overestimation or underestimation of shear capacity of the non-prismatic deck/beam, if it is assumed that the steel reinforcement is yielded throughout the length of the

beam. Therefore the vertical component should be calculated based on the applied bending moment at that section.

Figure 138 shows the bending moment variation along the length of the tapered bridge deck. The cross-section forces are constant, as it is a ULS check, and only the lever arm is increasing due to increase in the height of the cross-section. Therefore the bending moment resistance keeps on increasing along the length of the deck, with maximum at the intermediate support.
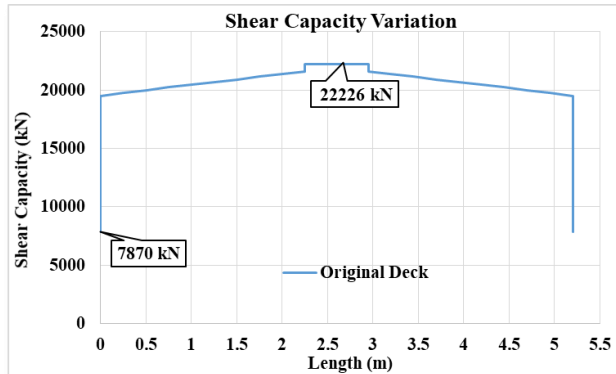
Figure 137 Shear resistance variation along the length of the original tapered deck
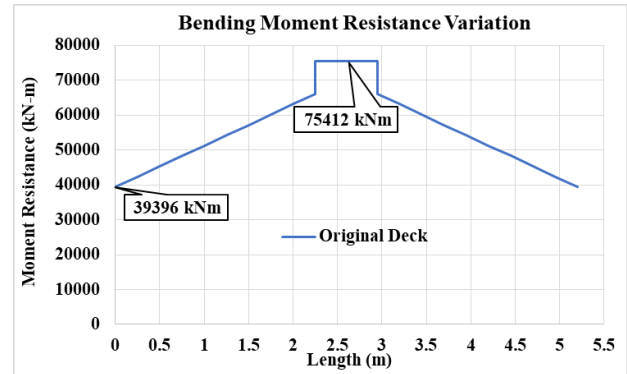
Figure 138 Bending moment resistance variation along the length of the original tapered deck

b. Lower Bound Shear Capacity

Figure 137 is the variation of the shear capacity of the deck based on the effective shear resistance concept and also on the assumption that the cross-section forces are maximum throughout the length of the tapered deck. This leads to overestimation of the capacity as evident from the jump in the plot. Therefore, a lower bound shear capacity is computed, which would be in effect after the construction stage. This is the capacity of the deck in the tapered zone which is the result of the dead load and the asphalt loading. A 1-D beam was modelled with a cross-section of 770 x 20800 mm^2, which are the dimensions of the prismatic deck, and was subjected to self-weight and asphalt loading as shown in Figure 139. The thickness of the asphalt was unknown and the author assumed a thickness of 0.12m [15]. The effect of the tapered section was taken into account by the varying self-weight near the intermediate support.
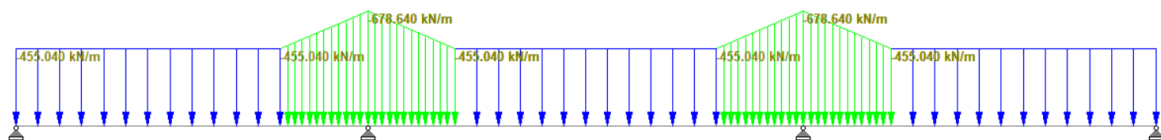
Figure 139 Bridge deck subjected to dead load
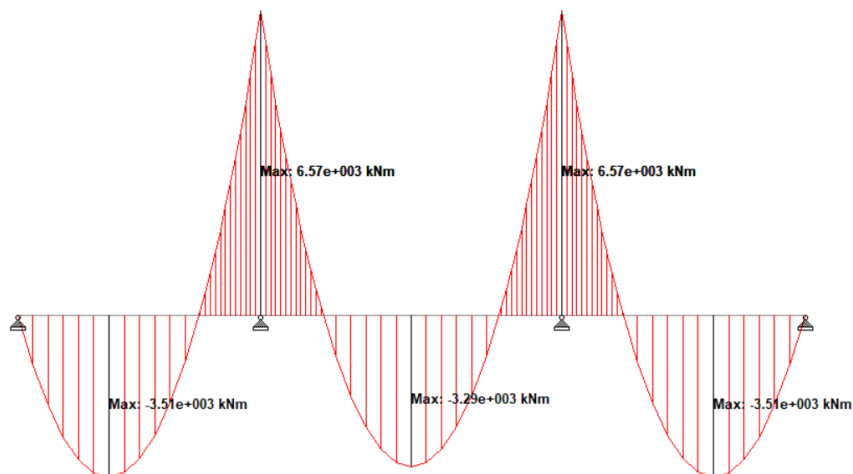
Figure 140 Bending moment diagram for the loading shown in Figure 139

104

Figure 140 gives the bending moment diagram for the static scheme shown in Figure 139. Note that the sign convention in the figure is different viz. negative bending moment is the sagging moment whereas positive bending moment is the hogging moment. The bending moment diagram in the haunch part varies, with maximum at the intermediate support and zero at the beginning of the haunch. The bridge deck has no internal or external prestressing. Traffic load would certainly increase the magnitude of hogging moment at the intermediate support. Truck point loads might decrease this magnitude, but that should be for a brief period as it is a moving load. Hence hogging moment is generated near the tapered section as expected. Now the applied bending moment at the intermediate support, due to the dead load and asphalt loading, is used to calculate the inclined compressive force that is generated at the bottom fibre. The vertical component of this inclined compressive force is then added to the shear resistance of concrete to create an envelope of the lower bound shear capacity as shown in Figure 141. This is the minimum capacity of the deck irrespective of the loading scenario.

Moment resisted due to the internal forces $= N_{cu,1}.\cos(\alpha).z =$ Applied Moment = 6570 kNm

$$z = \text{Lever arm} = d - \frac{x_s}{3}$$

$$\frac{x_s}{d} = -\alpha_e.\rho_l + \sqrt{(2.\alpha_e.\rho_l) + (\alpha_e.\rho_l)^2}$$

$$\alpha_e = \frac{E_s}{E_c}$$
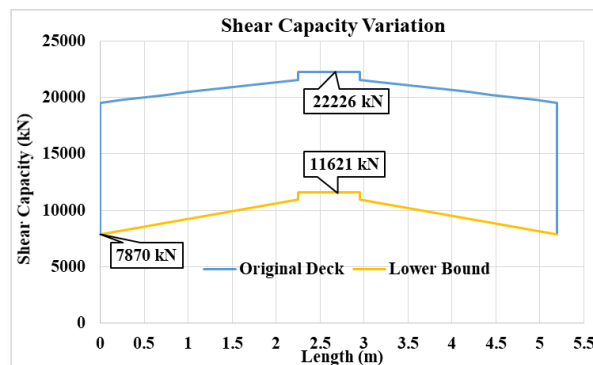
Figure 141 Lower Bound Shear Capacity

The maximum capacity in the lower bound envelope i.e. at the intermediate support is about 1.47 times that of the prismatic section. This capacity would be present irrespective of the external loading on the deck. The applied shear force at the intermediate support, due to the self-weight and asphalt loading, is 3250 kN which is much smaller than the shear capacity of the deck as can be seen from the curve. The professional at TNO calculated the applied shear force, at the haunch section, for different load combination and the critical value was approximately equal to 483.5 kN/m [15]. The maximum value of the lower bound shear capacity is equal to 558.7 kN/m, which is higher than the applied shear force. Note that this capacity is calculated based on the dead load and the asphalt loading. Traffic load would certainly increase this capacity.

6.3 Cross Sectional Analysis – Modified Deck

As mentioned earlier, engineers find it difficult to perform cross-sectional analysis on non-prismatic beam, mainly due to the non-linear layout of centroidal axis. In order to escape that, engineers change the cross-section of the beam such that the centroidal axis remains straight. The tapered slab deck shown in Figure 131, which has a non-linear layout of centroidal axis, is changed to double tapered deck shown in Figure 142, which has a linear centroidal axis. In order to keep the same volume of concrete in the "transformed" deck, the angle of taper is halved, the tapered section is introduced on the top side as well and the top reinforcement is

placed at an angle. Material parameters and the reinforcement detailing remains the same as shown in Table 50, Table 51, Table 52 and Table 53.
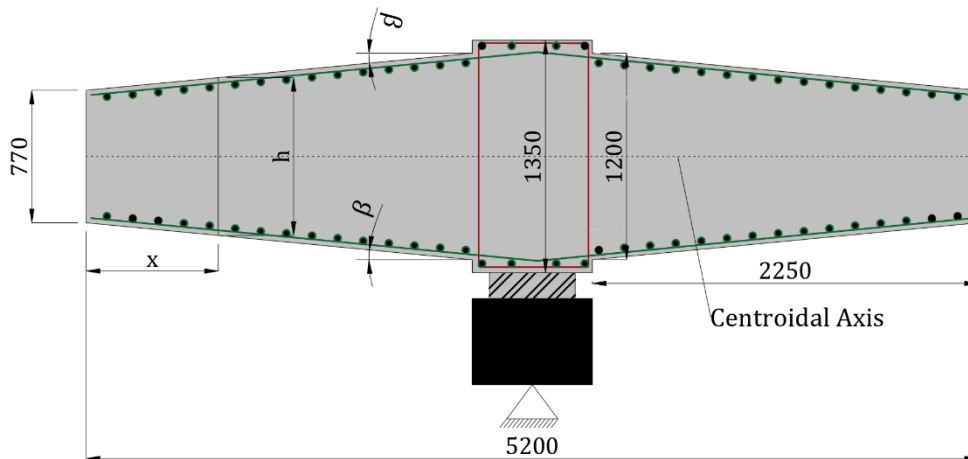
Figure 142 Modified tapered section of the deck
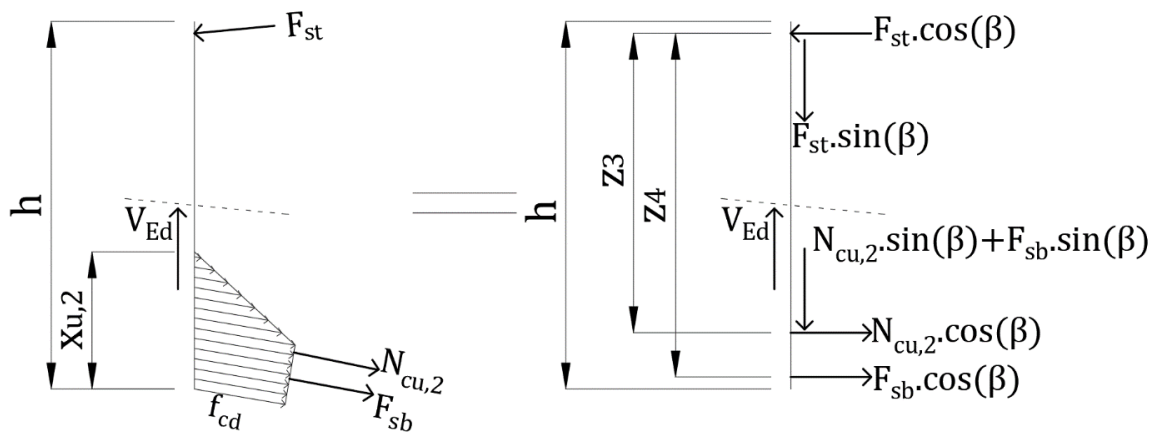
Figure 143 Cross-sectional analysis for the tapered section shown in Figure 142

Cross-sectional analysis is performed at a distance 'x' from the free end of the tapered section as shown in Figure 143. As the deck is modified, the angle β is equal to half of the angle α. Also, now the top reinforcement is placed at an angle. Therefore, the steel force due to the top reinforcement is acting at the angle β as well. Due to the shape, the concrete compressive force ($N_{cu,2}$) and the steel force due to the bottom reinforcement (F_{sb}) also acts at the angle β, with respect to the horizontal. All these forces are decomposed in the horizontal and the vertical direction. The horizontal component is used for equilibrium in the X-direction whereas the vertical component is considered in the shear capacity of the deck. In this case as well it is assumed that the cross-section forces are maximum throughout the length of the tapered deck.

Horizontal Equilibrium

$$F_{sb}.\cos(\beta) + N_{cu,2}.\cos(\beta) = F_{st}.\cos(\beta)$$

$$F_{sb} + N_{cu,2} = F_{st}$$

$$F_{sb} = 7495 \text{ kN}$$

$$F_{st} = 62067 \text{ kN}$$

$$N_{cu,2} = 54571.9 \text{ kN} = \frac{3.f_{cd}.b.x_{u,2}}{4}$$

The effective shear resistance is calculated using the formula,

106

$$V_{Rd} = V_{Rd,c} + F_{sb}.\sin(\beta) + N_{cu,2}.\sin(\beta) + F_{st}.\sin(\beta)................(6.03)$$

The differences in the formula of the effective shear resistance for the 'modified' (equation 6.03) and the actual deck (equation 6.01) is the term of the vertical component of the inclined top steel force (F_{st}) and the angle β. The formula for the shear resistance contributed by concrete is unchanged. The moment resistance is calculated using the following equation:

$$M_{Rd} = N_{cu,2}.\cos(\beta).z_3 + F_b.\cos(\beta).z_4................(6.04)$$

where,

$$z_3 = h - c - \frac{7.x_{u,2}}{18}$$

$$z_4 = h - 2.c$$

The equation of lever arm is changed in this case, as the horizontal equilibrium in a modified deck is different than that of an original deck. Figure 145 shows the shear capacity envelope for the modified deck, which is similar to the one shown in Figure 137. Table 54 gives the comparison of the upper bound shear capacity, for the original and modified deck at different intervals. The percentage error is negligible, with an average of 0.19%, and hence this type of modelling of the tapered section would still yield accurate shear resistance results.

Figure 144 shows the bending moment resistance along the length of the modified tapered section of the deck. Table 55 gives the comparison of the bending moment resistance for the original and the modified tapered section at regular intervals. From the table, the bending moment obtained in case of the modified tapered section is less than that of the original one, but the error is not more than 1% at every interval, which is acceptable.
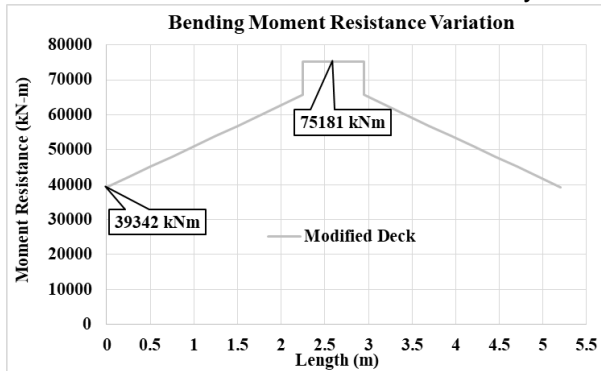
Figure 144 Bending moment resistance along the length of the modified tapered deck
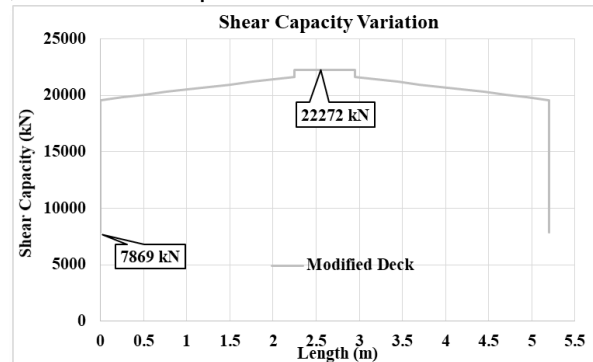
Figure 145 Shear capacity variation along the length of the modified tapered deck

Table 54 Comparison of shear capacity for the modified and original deck

Span (m)	V_{Rd} (Original section) (kN)	V_{Rd} (Modified section) (kN)	Error (%)
0	7869.31	7869.3	0.00
0	19515.95	19562.12	0.24
0.25	19764.48	19808.44	0.22
0.5	20001.4	20049.07	0.24
0.75	20238.8	20284.47	0.23
1	20471.3	20515	0.21
1.25	20699.2	20741.1	0.20
1.5	20922.9	20963	0.19
1.75	21142.7	21181	0.18

2	21358.7	21395.37	0.17
2.25	21571.3	21606.31	0.16
2.251	22226.27	22272.44	0.21
2.949	22226.27	22272.44	0.21
2.95	21571.3	21606.31	0.16
3.2	21358.7	21395.37	0.17
3.45	21142.7	21181	0.18
3.7	20922.9	20963	0.19
3.95	20699.2	20741.1	0.20
4.2	20471.3	20515	0.21
4.45	20238.8	20284.47	0.23
4.7	20001.4	20049	0.24
4.95	19758.7	19808.44	0.25
5.2	19515.95	19562.12	0.24
5.2	7869.31	7869.3	0.00
Average Percentage Error			0.19

Table 55 Comparison of bending moment resistance for the modified and original deck

Span (m)	M_{Rd} (Original section) (kN-m)	M_{Rd} (Modified Section) (kN-m)	Error (%)
0	39396	39342.29	-0.14
0.25	42360.26	42265.5	-0.22
0.5	45324.53	45188.7	-0.30
0.75	48288.8	48111.9	-0.37
1	51253	51035.1	-0.43
1.25	54217.32	53958.31	-0.48
1.5	57181.58	56881.51	-0.52
1.75	60145.85	59804.71	-0.57
2	63110.11	62727.92	-0.61
2.25	66074.38	65651.13	-0.64
2.251	75412.3	75181	-0.31
2.95	75412.3	75181	-0.31
2.95	66074.38	65651.13	-0.64
3.2	63110.11	62727.92	-0.61
3.45	60145.85	59804.71	-0.57
3.7	57181.58	56881.51	-0.52
3.95	54217.32	53958.31	-0.48
4.2	51253	51035.1	-0.43
4.45	48288.8	48111.9	-0.37
4.7	45324.53	45188.7	-0.30
4.95	42360.26	42265.5	-0.22
5.2	39396	39342.29	-0.14
Average Percentage Error			-0.42

6.4 Cross Sectional Analysis – Ignoring the inclination of Cross Section Forces

In Chapter 4 – Cross Sectional Analysis on reinforced non-prismatic beams, tapered beams were analysed and comparison between the experimental results, analytical results including the vertical component and analytical results excluding the vertical component was performed. It was seen that if the vertical component is not taken into account by the shear resistance of the beam, one might overestimate the capacity in case of negatively haunched beam and underestimate the capacity in case of positively haunched beams. To evade any complications, an error that engineers make is to ignore the vertical component, by applying the cross-section forces perpendicular to the cut and not at an angle. Consider the tapered section of the bridge deck shown in Figure 131. Figure 146 shows the cross-sectional forces, where the angle of inclination of the internal forces are ignored. This analysis is performed at a distance 'x' from the free end of the tapered section shown in Figure 131. Engineer applies the cross-section forces perpendicular to the cross-section cut. By doing so, one would underestimate the shear capacity, which was also shown in Chapter 4.
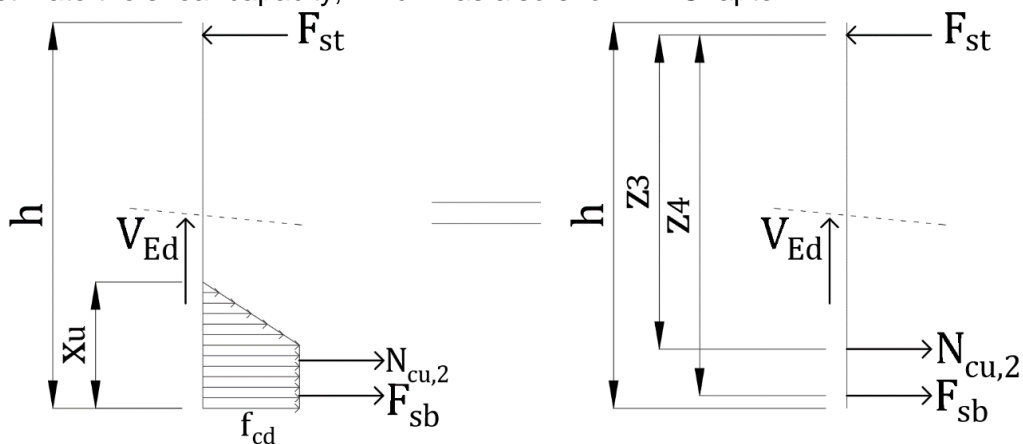
Figure 146 Cross - section analysis ignoring the inclination of forces

Horizontal Equilibrium

$$F_{st} = F_{sb} + N_{cu}$$

where,

$$F_{st} = 62067 \text{ kN}$$

$$F_{sb} = 7495 \text{ kN}$$

$$N_{cu,2} = 54572 \text{ kN}$$

The shear resistance of this section would be equal to the shear resistance contributed by the concrete. The Moment resistance is given as,

$$M_{Rd} = N_{cu,2} \cdot z_3 + F_{sb} \cdot z_4 \dots \dots \dots \dots (6.05)$$

In this case, the lever arms are equal to the one where the cross-section is modified (Section 6.3) as the equation of horizontal equilibrium in both these cases are the same. However, the equation of bending moment resistance is different as stated above.

Figure 147 and Figure 148 shows the variation of bending moment resistance and the shear resistance along the length of the tapered section respectively where the inclination of the cross-section forces are ignored. It can be seen that the shear capacity of the tapered section where the vertical component is ignored is much smaller than the upper bound shear capacity of the original deck or modified deck. The difference between the capacity obtained by ignoring the inclination of the cross-section forces and the lower bond shear capacity envelope, showed

in Figure 141, is about 1050 kN (50 kN/m). If the inclination of the cross-section forces are ignored, the capacity might just be equal to the applied shear force. The bending moment resistance obtained due to these cross-section forces are slightly higher than the one where the inclination is considered, which is logical as the reduction factor of the cosine of the angle of inclination is ignored.
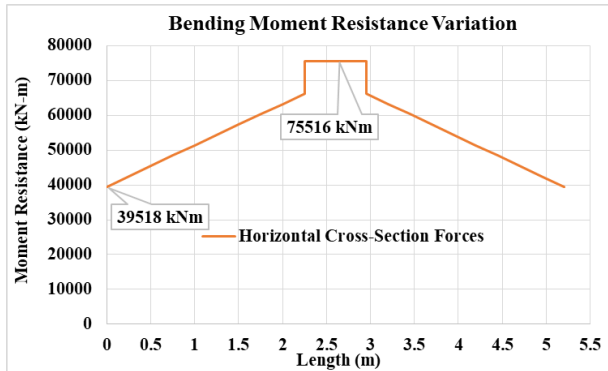
Figure 147 Bending moment resistance variation along the length of the tapered deck (ignoring inclination of forces)
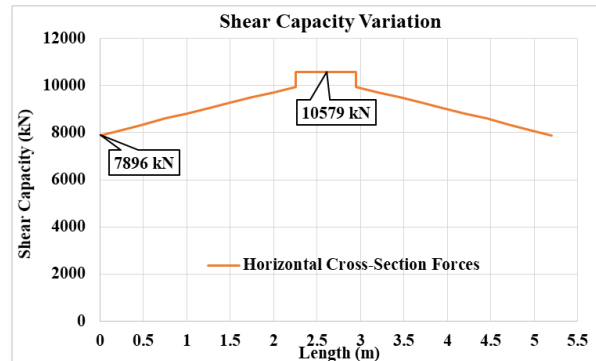
Figure 148 Shear resistance variation along the length of the tapered deck (ignoring inclination of forces)

6.5 Comparison of Cross Section Results

Figure 149 shows the bending moment resistance comparison for different models along the length of the deck. It can be concluded, that there is no difference in the bending moment resistance for the different models. This is due to the low reduction factor of the cosine of the angle of inclination, which creates negligible effect to the bending moment resistance.

Figure 150 shows the comparison of shear resistance between different models. The shear resistance variation for the original tapered deck and the modified tapered deck is identical. This is because in the modified deck – the angle of taper is reduced to half, tapered section is introduced in the top side and the steel force at the top is placed at an angle, eventually yielding the same result. It can also be seen that ignoring the vertical component leads to underestimation of the capacity. The lower bound shear capacity envelope is approximately 10% higher than the envelope where the inclination of the cross-section forces are ignored, which is due to the vertical component of the inclined compression chord.
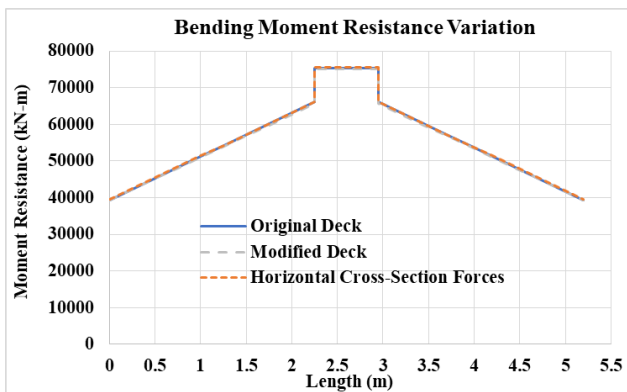
Figure 149 Bending moment resistance comparison for different models
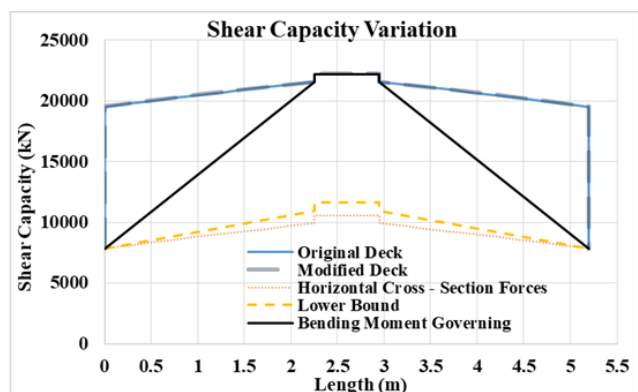
Figure 150 Shear capacity comparison for different models

In reality, the magnitude of the cross section forces are not maximum throughout the length of the tapered deck but only at the position where the applied hogging bending moment is maximum, which is at the intermediate support. The shear capacity variation for the load combination in which the bending moment is governing is also plotted in Figure 150 (black graph). In this case, the cross-section forces are maximum only at the intermediate support and varies linearly along the length of the tapered deck. It can be seen from the graph that the assumption of the magnitude of cross-section forces being maximum throughout the length of

the tapered deck leads to overestimation of the capacity as was shown by John J. Orr [11]. By assuming that the cross-section forces are maximum at the intermediate support, the capacity obtained (1068.55 kN/m) is much higher than the applied shear force. However this would still lead to overestimation of the capacity and the procedure to calculate the real shear capacity variation is given as follows:

I.   The load combination where the applied shear is governing in the bridge is considered and the applied bending moment along the tapered section is noted.
II.   The inclined cross-section forces are calculated, from the applied bending moment, and the vertical component of this force is further added to the shear capacity contributed by concrete to obtain the "Real Shear Capacity" envelope.

The procedure is similar to that mentioned in Chapter 4. The actual shear capacity envelope would be somewhere in between the "Bending Moment Governing" envelope and the "Lower Bound Capacity" envelope from Figure 150. The figure also shows different types of error an engineer might make while analysing the non-prismatic deck for the shear capacity such as:

I.   Assuming maximum cross-section forces throughout the length of the tapered deck
II.   Modifying the cross-section of the tapered deck
III.   Ignoring the inclination of the cross-section forces
IV.   Envelope of the load combination where the bending moment is governing.

6.6 Generalized Method

As shown from the previous section, the shear capacity of the original deck with a non-linear layout of centroidal axis is the same as that of a modified deck with a linear centroidal axis. A generalized model is proposed in this section which proves the same. Note that both these models are analysed in the Ultimate Limit State (ULS) and the behaviour of these two models might differ in the Serviceability Limit State (SLS).

6.6.1 Original Deck – Non Linear Layout of Centroidal Axis
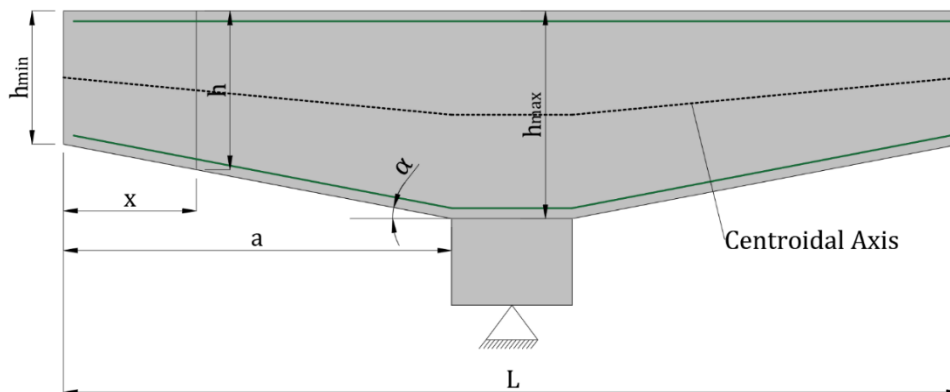
Figure 151 Original tapered deck near the intermediate support

Figure 151 shows a tapered deck with minimum height at the ends and maximum at the centre, with the angle of taper 'α'. The cross – sectional analysis is performed at a distance of 'x' from the free end of the tapered deck as shown in Figure 136. Horizontal Equilibrium is given as

$$F_{st} = \left(F_{sb} + N_{cu,1} \right) . \cos(\alpha) ....(6.06)$$

$$F_{sb} + N_{cu,1} = \frac{F_{st}}{\cos(\alpha)}$$

$$N_{cu,1} = \frac{F_{st}}{\cos(\alpha)} - F_{sb} ....(6.07)$$

$$N_{cu,1} = \frac{3f_{cd}b.x_{u,1}}{4}$$

$$x_{u,1} = \frac{4}{3f_{cd}b}.\left(\frac{F_{st}}{\cos(\alpha)} - F_{sb}\right)..........(6.08)$$

The vertical component of the inclined compression force and the steel force due to bottom reinforcement increases the shear capacity of the deck. The effective shear resistance equation is written as follows:

$$V_{Rd} = V_{Rd,c} + F_{sb}.\sin(\alpha) + N_{cu}.\sin(\alpha)$$

$$V_{Rd} = V_{Rd,c} + (F_{sb} + N_{cu}).\sin(\alpha)$$

$$V_{Rd} = V_{Rd,c} + F_{st}.\tan(\alpha)$$

For small angle of inclination, $\tan(\alpha) = \alpha$ (in radians)

$$V_{Rd} = V_{Rd,c} + F_{st}.\alpha..........(6.09)$$

The increase in the shear resistance of the original model is equal to the steel force due to the top reinforcement multiplied with the angle of taper, in radians. The moment resistance is given as:

$$M_{Rd} = N_{cu,1}.z_1.\cos(\alpha) + F_{sb}.\cos(\alpha).z_2..........(6.10)$$

$$z_1 = h - c - \frac{7.x_{u,1}}{18} = h - c - \frac{14}{27f_{cd}b}.\left(\frac{F_{st}}{\cos(\alpha)} - F_{sb}\right)$$

$$z_2 = h - 2.c$$

6.6.2 Modified Model – Linear Layout of Centroidal Axis

Figure 152 shows the double tapered deck with half of the angle of inclination of the original deck model. As the tapered section is introduced at the top as well, the volume of concrete in this deck is equal to that of the tapered original deck model. Cross-Sectional Analysis is performed at a distance of 'x' from the free end of the modified deck as shown in Figure 143, where $\beta = \frac{\alpha}{2}$. Horizontal Equilibrium is given by,
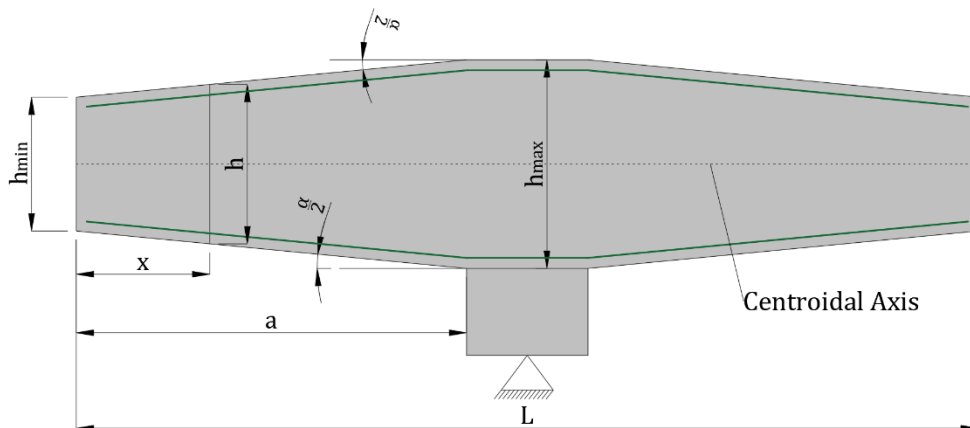
Figure 152 Modified double tapered deck

$$F_{st}.\cos\left(\frac{\alpha}{2}\right) = F_{sb}.\cos\left(\frac{\alpha}{2}\right) + N_{cu,2}.\cos\left(\frac{\alpha}{2}\right)$$

$$F_{st} = F_{sb} + N_{cu,2}..............(6.11)$$

$$N_{cu,2} = \frac{3f_{cd}b.x_{u,2}}{4}$$

$$x_{u,2} = \frac{4}{3f_{cd}b}.(F_{st} - F_{sb})\ldots\ldots\ldots(6.12)$$

The effective shear resistance is given by

$$V_{Rd} = V_{Rd,c} + F_{sb}.\sin\left(\frac{\alpha}{2}\right) + N_{cu,2}.\sin\left(\frac{\alpha}{2}\right) + F_{st}.\sin\left(\frac{\alpha}{2}\right)$$

$$V_{Rd} = V_{Rd,c} + (F_{sb} + N_{cu,2}).\sin\left(\frac{\alpha}{2}\right) + F_{st}.\sin\left(\frac{\alpha}{2}\right)$$

$$V_{Rd} = V_{Rd,c} + F_{st}.\sin\left(\frac{\alpha}{2}\right) + F_{st}.\sin\left(\frac{\alpha}{2}\right)$$

$$V_{Rd} = V_{Rd,c} + 2.F_{st}.\sin\left(\frac{\alpha}{2}\right)$$

For small angle of inclination, $\sin\left(\frac{\alpha}{2}\right) = \frac{\alpha}{2}$

$$V_{Rd} = V_{Rd,c} + F_{st}.\alpha\ldots\ldots\ldots(6.13)$$

The equation of the bending moment resistance which is calculated at the position of the top reinforcement is given as,

$$M_{Rd} = N_{cu,2}.\cos\left(\frac{\alpha}{2}\right).z_3 + F_{sb}.\cos\left(\frac{\alpha}{2}\right).z_4\ldots\ldots\ldots(6.14)$$

$$z_3 = h - c - \frac{7.x_{u,2}}{18} = h - c - \frac{14}{27f_{cd}b}.(F_{st} - F_{sb})$$

$$z_4 = h - 2c$$

It can be seen that the equation of shear resistance for the original deck (equation 6.04) is approximately equal to that of a modified deck (equation 6.08). The equation of Bending Moment Resistance for the original deck (equation 6.05) and the modified deck (equation 6.09) is slightly different and have different lever arms. But if the angle of inclination is not too large (less than 18°), the error in the bending moment resistance is small as can be seen from Table 55 and hence it can be ignored. From the above calculations, it can be said that the shear resistance of a deck, with non-linear centroidal axis, is almost equal to the shear resistance of a modified deck with linear centroidal axis, provided that the volume of concrete in use remains constant.

7 Conclusion and Recommendation

This chapter discusses the conclusion that are drawn from the results obtained in the previous chapters. On the work done, few recommendations are proposed for researchers to further explore the behavior of non-prismatic beams.

7.1 Conclusion

1. When the cross-sectional analysis is performed in a prismatic beam subjected to four point bending test, the cross-section results i.e. Bending Moment Resistance and Shear Resistance remain constant irrespective of whether the analysis is performed on a vertical cut or on an inclined cut. Both the detailed procedure and the simplified approach leads to a constant cross-section result in the prismatic beam. From the approaches it can be concluded that the results in a prismatic beam are independent of how the cross-section cut is made, as stated in the hypothesis.

2. In a negatively haunched beam, when the cross-section analysis is performed in the tapered zone, it was observed that the bending moment resistance obtained on an inclined cut, which is perpendicular to the centroidal axis with forces in the local direction is different than that obtained on a vertical cross-section cut with forces in the global direction. The detailed method and the simplified approach both proves the same and therefore it can be concluded that in a negatively haunched beam, the cross-section results depends on how the cross-section cut is built, not following the hypothesis. From the approaches it was seen that one would overestimate the bending moment resistance and correspondingly provide less amount of reinforcement if the analysis is performed on an inclined cut. However no experimental data is available to prove this outcome and therefore in negatively haunched beam it is recommended to perform a cross-section analysis on a vertical cut, until further research.
In positively haunched beam as well, the equation of bending moment resistance obtained on an inclined cross-section cut, which is perpendicular to the centroidal axis with forces in the local direction, is different when compared to the equation obtained on a vertical cut, with the forces in the global direction. In this case as well the cross-section results depends on how the cross-section cut is made. Therefore, in positively haunched beam as well it is recommended to perform a vertical cross-section analysis until some experimental data is available.

3. From the analysis of the limited experimental data, it can be concluded that in non-prismatic beam the vertical component of the inclined compression chord or tensile tie should be considered in the shear capacity equation. Moreover the capacity of such beam depends on the applied load. The procedure to calculate the shear resistance of the non-prismatic beams is given as follows:

    i. Determine the critical section in the non-prismatic beam. The critical section is defined as that section in the tapered zone where the shear resistance contributed by concrete or stirrup is less, compared to the other section of the haunch. Furthermore, the vertical component of the inclined cross-section forces has a maximum effect in case of negatively haunched beam and minimum assistance in case of positively haunched beam. Generally, in a negatively haunched beam, the critical section is at the vertex of the haunch near the loading point. On the other hand, in a positively haunched beam it is preferable to consider the section at a distance of h_{min} (minimum height) from the support/vertex depending on the beam.

    ii. The critical moment (M_{cr}) and the critical force (P_{cr}), above which non-linearity begins for the given section, are calculated as follows:

$$M_{cr} = f_{ctm,fl} \cdot W$$

$$P_{cr} = \frac{M_{cr}}{x}$$

$f_{ctm,fl} = $ Flexural tensile strength

$W = $ Section Modulus

$x = $ Distance of the critical section from the support

iii. To calculate the horizontal component of the inclined cross-section forces, lever arm is required which is determined using the following equations:

$$\frac{x_s}{d} = -\alpha_e \cdot \rho_l + \sqrt{2 \cdot \alpha_e \cdot \rho_l + \left(\alpha_e \cdot \rho_l\right)^2}$$

$$\alpha_e = \frac{E_s}{E_c} = $$ Ratio between elastic modulus of steel to that of concrete

$$\rho_l = \frac{A_{sb}}{b.d} = $$ Reinforcement ratio

$$z = d_{eff} - \frac{x_s}{3} = $$ Lever arm

$x_s = $ Height of the compressive zone

iv. Once the critical force and the lever arm are known, the horizontal component of the inclined force for a given load can be calculated using moment equilibrium. The vertical component is calculated subsequently and is added or subtracted from the shear resistance, which is contributed due to concrete and stirrups. This is done for every load increment and the failure of the beam occurs when the effective shear resistance is less than the applied load.

An example to calculate the shear capacity of non-prismatic beam is shown in Table 56. The critical section, which is at a distance 'x' from the support, is predicted and the critical force (P_{cr}), lever arm (z) and the shear capacity contributed by concrete ($V_{Rd,c}$) and stirrups ($V_{Rd,s}$) are calculated. As soon as the applied load is greater than the critical force (P_{cr}), cracking occurs and both the components of the inclined cross-section forces (H_i and V_i) are determined. The shear resistance (V_{Rd}) is calculated, by adding or subtracting the vertical component of the inclined cross-section forces (equation 4.09). As the capacity of the beam depends on the applied loading, failure of the beam occurs when the effective shear resistance ($V_{Rd,c} + V_{Rd,s} \pm V_{26}$) is less than the applied load ($P_{cr} + 26$).

Table 56 An example to calculate the shear resistance of non - prismatic beam

Load (kN)	Horizontal Component in kN (H_i)	Vertical Component in kN (V_i)	Effective Shear resistance in kN (V_{Rd})	Condition
1	0	0	$V_{Rd,c} + V_{Rd,s}$	No Failure
$P_{cr} + 1$	H_1	V_1	$V_{Rd,c} + V_{Rd,s} \pm V_1$	No Failure
$P_{cr} + 10$	H_{10}	V_{10}	$V_{Rd,c} + V_{Rd,s} \pm V_{10}$	No Failure
$P_{cr} + 20$	H_{20}	V_{20}	$V_{Rd,c} + V_{Rd,s} \pm V_{20}$	No Failure
$P_{cr} + 25$	H_{25}	V_{25}	$V_{Rd,c} + V_{Rd,s} \pm V_{25}$	No Failure
$P_{cr} + 26$	H_{26}	V_{26}	$V_{Rd,c} + V_{Rd,s} \pm V_{26}$	Failure

Applied Moment = Moment resisted by internal forces

$$H_i.z = \left(P_{cr} + i\right).x$$

$$H_i = \frac{\left(P_{cr} + i\right).x}{z}$$

$$V_i = H_i.\tan\left(\alpha\right)$$

P_{cr} = Critical Load

x = Distance of the critical section from the support

H_i = Horizontal component of the inclined cross-section force

V_i = Vertical component of the inclined cross-section force

α = Angle of taper

i = Load increment after the critical force

Shear Capacity = $P_{cr} + 25 / V_{Rd,c} + V_{Rd,s} \pm V_{25}$

One of the setback of the above procedure is the assumption that the lever arm remains constant throughout the load increment. The change in the lever arm depends on the strain in the concrete at the critical section. If the strain in the concrete is less than 1.75‰ (for concrete class is less than or equal to C50/60) the lever arm remains unchanged but this might not always be the case. However, negligible effect in the lever arm is observed even if the strain in the concrete at the critical section enters the constant part of the bilinear concrete constitutive compression model given in Figure 3.4 of the Eurocode 1992-1-1 [1] (or Figure 57). Hence the analytically calculated shear capacity of all the beams would be more or less the same.

When the above procedure is applied to the available experimental data, it was seen that the analytically calculated shear capacity, where the vertical component is taken into account by the shear resistance, complies well with the experimental results confirming the hypothesis. The mean and the standard deviation for the ratio between experimental results to the analytical results for different types of beams is given in Table 57.

Table 57 Mean and standard deviation for different types of beams

Type of beam	Ratio between experimental to analytical including vertical component		Ratio between experimental to analytical excluding vertical component	
	Mean	**Standard Deviation**	**Mean**	**Standard Deviation**
Prismatic beam	1.04	0.2	-	-
Negatively haunched beam	0.98	0.24	0.64	0.19
Positively haunched beam	1.09	0.36	1.43	0.59

From the above table it can be concluded that one would overestimate the shear capacity of the negatively haunched beam and underestimate the capacity of the positively haunched beam if the vertical component of the inclined internal force is ignored. The table also proves that the vertical component of the inclined cross-section forces should be considered in the shear capacity equation, validating the equation 4.09. In case of a positively haunched beam, better results are obtained if the critical section is considered at a distance of h_{mean} (($h_{min}+h_{max}$)*0.5) from the support/vertex rather than considering at a distance of h_{min} from the support/vertex.

4. From the experimental data it was seen that excess volume of concrete does not always provide higher capacity and less amount of concrete does not always lead to a lower capacity. Using concrete smartly such as the case of double cantilevered haunched beam tested by Macleod et al. [6] will provide desirable and better results.

5. When a cross-section analysis is performed in a prestressed haunched beam, the prestressed force P_∞ is applied horizontally at the center of the cross-section height. Furthermore the equation of the applied bending moment is changed by an amount equal to the prestressing force P_∞ multiplied with the eccentricity. This eccentricity is due to the variation of centroidal axis along the length of the beam. Once the non-prismatic beam is prestressed, the tendons act as reinforcement and the procedure to calculate the shear capacity of non-prismatic prestressed beam remains the same. Note that in case of a prestressed prismatic beam, it might be that the cross-section force ΔP acts at an angle, due to the tendon profile, leading to a vertical component and effecting the shear resistance of the beam. This effect might be critical when the section is considered near the support as tensile splitting is the governing failure mode.

6. In practice engineers make different errors while performing cross-sectional analysis of haunched concrete bridges, mainly because of the non-linear layout of centroidal axis. The haunched decks are modified such that the centroidal axis remains linear, with the same volume of concrete in use. Although this does not affect the shear capacity and bending moment resistance of the deck, but these results are obtained at Ultimate Limit State (ULS) and the structural behavior might differ in Serviceability Limit State (SLS). Another simplified method that engineers prefer is to ignore the inclination of the cross-section forces, underestimating the capacity in most cases. Moreover the assumption that the shear capacity envelope is obtained by considering the load combination where the bending moment is governing also leads to overestimation of the resistance. The shear capacity of the deck should be calculated based on the bending moment that occurs for the governing load combination with respect to shear force.

7.2 Recommendations

1. The result from this study shows that in a non-prismatic beam the vertical component of the inclined force should be considered in the shear capacity, however all the beams tested were short with a maximum span of 3 m. When the span of the non-prismatic beam is long, this inclusion might significantly affect the shear capacity, as the magnitude of the cross-section forces is quite large as is evident from Figure 150. Further study on the shear capacity and structural behavior of long non-prismatic beam can be done in this regard. A conservative approach in long non-prismatic beams is to increase the shear capacity by 0.5 times the vertical component of the inclined compression chord or tensile tie which was suggested by Nghiep [9]. This can also be further validated.

2. Strut Action was observed in almost every non-prismatic beam that was experimentally tested, with a pronounced effect in short beams. Due to this strut action, the shear capacity of the beam increases significantly as is seen in the beam specimen tested by Chenwei et al. [8]. A study that emphasizes on the reasoning behind the occurrence of strut action in non-prismatic beam would be quite useful to not only predict the shear capacity but also to understand its effect on such beams. The study can also focus on whether this type of mechanism occurs in long curved bridges or not.

3. When an inclined cross-sectional analysis was performed on the tapered side of a negatively haunched beam, it was observed that the amount of reinforcement required is less as compared to a vertical cross-section cut. Using both these approaches, negatively haunched beams can be experimentally tested and the difference between the estimated load bearing capacities can be further noted. From the results a conclusion can be drawn about which of the two approaches i.e. inclined cut or vertical cut gives the best estimation of the load bearing capacity.

Appendix A

While performing cross-section analysis on an angled cut, different approaches were considered, compared to that discussed in Chapter 3 and Chapter 4, where the cross-sectional results are not constant. Some of them are discussed here. These cross-sectional analysis are performed in the constant bending moment zone of the prismatic beam shown in Figure 49.

1) No reduction of compressive force.
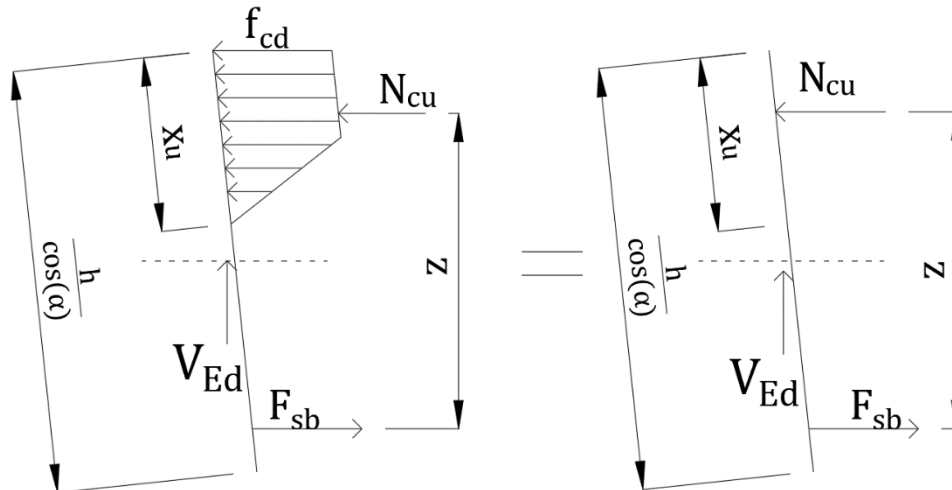
Figure 153 Cross-section forces on an inclined cut without the reduction of concrete compressive force

Figure 153 shows the stress distribution on an angled cut in a prismatic beam. The cross-section forces are similar to Figure 53 – except the reduction of the concrete compressive force. Bending Moment Resistance is calculated as shown below,

$$\sum H = 0$$

$$N_{cu} = F_{sb} \ldots\ldots\ldots (A.01)$$

$$N_{cu} = \frac{3.f_{cd}.b.x_u}{4} \ldots\ldots\ldots (A.02)$$

$$x_u = \frac{4.F_{sb}}{3.f_{cd}.b} \ldots\ldots\ldots (A.03)$$

From the above formulation, the equation of the inclined compression zone (equation A.03) is equal to that when the cross-section analysis is performed on a vertical cut, with the vertical compression zone (equation 3.03). The bending moment resistance is given as follows,

$$M_{Rd} = F_{sb}.z$$

$$z = d_{eff} - \frac{7.x_u.\cos(\alpha)}{18} = d_{eff} - \frac{14.F_{sb}.\cos(\alpha)}{27.f_{cd}.b}$$

$$M_{Rd} = F_{sb}.\left(d_{eff} - \frac{14.F_{sb}.\cos(\alpha)}{27.f_{cd}.b} \right) \ldots\ldots\ldots (A.04)$$

The inclined compressive zone is first decomposed in the vertical direction and then the lever arm is calculated. From the above formulation, it proves that if the compressive force is not reduced then the equation of the bending moment resistance (equation A.04) is not equal when the analysis is performed on a vertical cross-section cut (equation 3.04).

2) Decomposition of Shear Resistance

As the analysis is performed in the zone of no applied shear force (V_{Ed}), the applied shear force (V_{Ed}) from the analysis is replaced by the shear resistance (V_{Rd}) as shown in Figure 154.
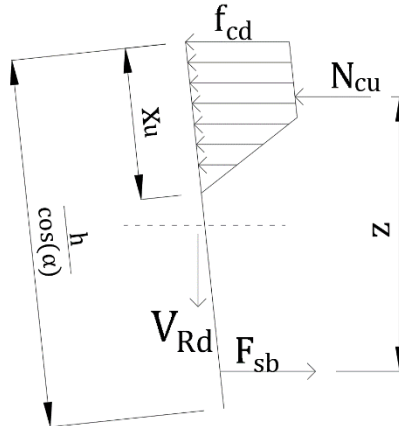
Figure 154 Cross-section forces with shear resistance

In this approach the shear resistance was assumed to be a cross-section force and is decomposed in the local direction (parallel and perpendicular direction) as shown in Figure 155
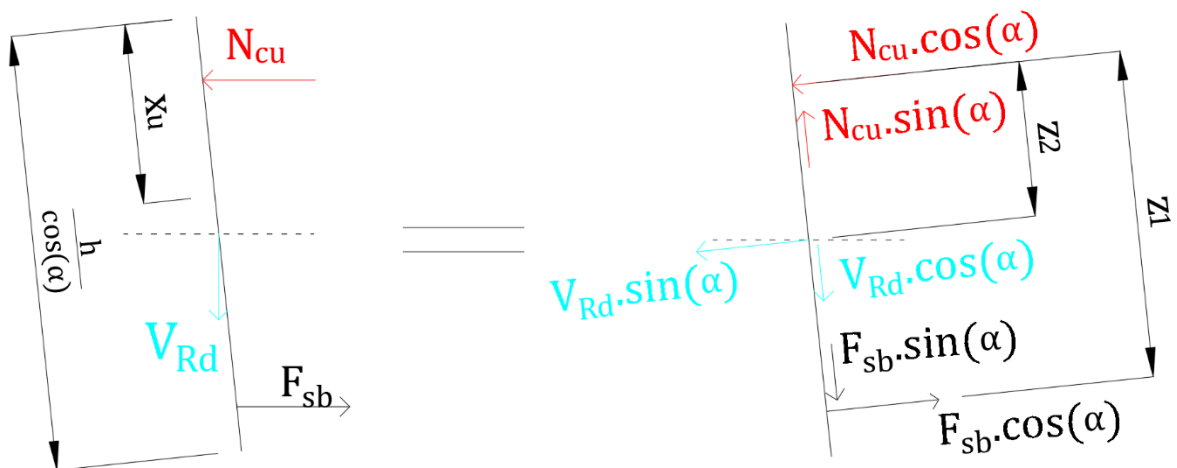
Figure 155 Decomposition of all the cross-section forces including the shear resistance

Horizontal equilibrium equation is given as follows,

$$F_{sb}.\cos(\alpha) = V_{Rd}.\sin(\alpha) + N_{cu}.\cos(\alpha)..............(A.05)$$

$$N_{cu} = F_{sb} - V_{Rd}.\tan(\alpha)$$

$$N_{cu} = \frac{3.f_{cd}.b.x_u}{4}$$

$$x_u = \frac{4.(F_{sb} - V_{Rd}.\tan(\alpha))}{3.f_{cd}.b}..............(A.06)$$

The equation of the inclined compressive zone (equation A.05) is completely different than the one showed in previous approaches. The bending moment resistance, due to the cross-section forces in the perpendicular direction, is given as follows

$$M_{Rd} = F_{sb}.\cos(\alpha).z_1 + V_{Rd}.\sin(\alpha).z_2$$

$$z_1 = \frac{d_{eff}}{\cos(\alpha)} - \frac{7.x_u}{18}$$

$$z_2 = \frac{h}{2.\cos(\alpha)} - \frac{7.x_u}{18}$$

$$M_{Rd} = F_s.\cos(\alpha).\left(\frac{d_{eff}}{\cos(\alpha)} - \frac{7.x_u}{18}\right) + V_{Rd}.\sin(\alpha).\left(\frac{h}{2.\cos(\alpha)} - \frac{7.x_u}{18}\right) \dots\dots\dots(A.07)$$

The equation of the bending moment resistance is completely different. The component of the shear resistance, acting in the perpendicular direction, increases the bending moment resistance which is not constant anymore. These different approaches leads to major error and should be avoided.

References

[1] T. E. Union, "Eurocode 2: Design of concrete structures - Part 1-1: General rules and rules for buildings," Brussels, 2004.

[2] A. Committee, "Building code requirement for structural concrete and commentary," ACI, 2004.

[3] "fib Model Code for Concrete Structures," Ernst & Sohn - A Wiley Brand, Berlin, Germany, 2010.

[4] W. K. R. N. Daejoong Kim, "Arch Action in Reinforced Concrete Beams - A Rational Prediction of Shear Strength," *ACI Structural Jounrnal,* vol. 96, no. 4, pp. 586-593, July-August 1999.

[5] E. E. S.Y. Debaiky, "Behavior and Strength of Reinforced Concrete Haunched Beams in Shear," *ACI Journal,* pp. 184 - 194, May-June 1982.

[6] A. H. I.A. MacLeod, "Shear Strength of Haunched Beams without Shear Reinforcement," *ACI Structural Journal,* vol. 91, no. 1, pp. 79-89, November - December 1994.

[7] G. Stefanou, "Shear Resistance of Reinforced Concrete Beams with Non-Prismatic Sections," *Engineering Fracture Mechanics,* vol. 18, no. 3, pp. 643-666, 1983.

[8] K. M. a. J. N. Chenwei HOU, "Shear Failure Mechanism of Reinforced Concrete Haunched Beams," *JSCE,* vol. 3, pp. 230-245, 2015.

[9] V. H. Nghiep, "Shear Design of Straight and Haunched beams," Hamburg, 2011.

[10] H. I. A.-A. O. M. G.-C. Arturo Tena-Colunga, "Behavior of reinforced concrete haunched beams subjected to static shear loading," *Engineering Structures,* vol. 30, pp. 478-492, 2008.

[11] T. J. I. A. P. D. M. E. John J. Orr, "Shear behavior of non-prismatic steel reinforced concrete beams," *Engineering Structures,* vol. 71, pp. 48-59, 2014.

[12] G. C. A. Paglietti, "Remarks on the current theory of Shear Strength of Variable Depth Beams," *Open Civil Engineering Journal,* vol. 3, pp. 28-33, 2009.

[13] J. a. C.R.Braam, CIE 4160 - Prestressed Concrete, Delft : Delft University of Technology, April 2018.

[14] C. B. a. E. C. Nasreddin El-Mezaini, "Analysis of Frames with Non-Prismatic Members," *Journal of Structural Engineering,* vol. 117, no. 6, pp. 1573 - 1592, 1991.

[15] I. G. a. D. v. d. V. Ir.J.M.Zwarthoed, "Viaduct in de A1 over de Wolweg bij Stroe KW 32F-103," Rijkswaterstraat, Delft/Utrecht, 2010.